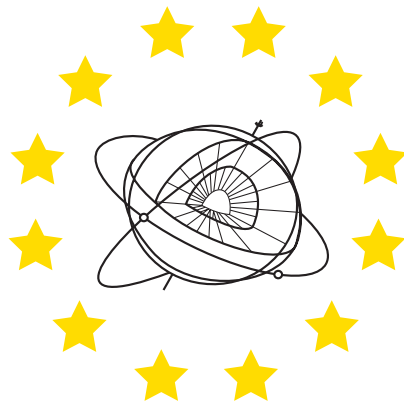


MINISTERE DE LA CULTURE

Cahiers
du Centre Européen
de Géodynamique
et de Séismologie

Volume 30



Proceedings of the Workshop:

Induced Seismicity

November 15-17, 2010
Hotel Hilton
Luxembourg
(Grand-Duchy of Luxembourg)

Edited by Joachim Ritter and Adrien Oth

Luxembourg 2010

Proceedings of the Workshop:

INDUCED SEISMICITY

November 15-17, 2010

Hotel Hilton
Luxembourg
Grand-Duchy of Luxembourg

Organized by
The European Center for Geodynamics and Seismology (ECGS)

Supported by

European Center for Geodynamics and Seismology (ECGS)
Ministère de la Culture
Fonds National de la Recherche de Luxembourg (FNR)
The Council of Europe (EUR-OPA)
Landesforschungszentrum Geothermie – Baden Württemberg (KIT)
Forschungskollegium Physik des Erdkörpers (FKPE)
Musée National d'Histoire Naturelle (MNHN)



Scientific Committee:

N. Cuenot (EEIG Heat Mining, France)
Bernard Dost (KNMI, The Netherlands)
Stephan Husen (ETH Zürich, Switzerland)
Manfred Joswig (Univ. Stuttgart, Germany)
Adrien Oth (ECGS, Luxembourg)
Joachim Ritter (KIT, Germany)
Serge Shapiro (Freie Univ. Berlin, Germany)

Local Organizing Committee:

A. Oth (ECGS, Luxembourg)
C. Galassi (ECGS, Luxembourg)
G. Celli (ECGS/MNHN, Luxembourg)
E. Buttini (ECGS/MNHN, Luxembourg)

Edited by:

Joachim Ritter and Adrien Oth
Luxembourg - 2010

Workshop organized and Proceedings published
with the support of

MINISTERE DE LA CULTURE



FONDS NATIONAL DE LA RECHERCHE



ACCORD PARTIEL OUVERT

en matière de prévention, de protection et d'organisation des secours
contre les risques naturels et technologiques majeurs

du **CONSEIL DE L'EUROPE**



**LANDESFORSCHUNGSZENTRUM GEOTHERMIE
BADEN-WÜRTTEMBERG (KIT)**



ISBN N° 978-2-91989-709-4

Centre Européen de Géodynamique et de Séismologie

Musée National d'Histoire Naturelle
Section Astrophysique et Géophysique, Luxembourg

Foreword

This issue of the Cahiers du Centre Européen de Géodynamique et de Séismologie (Proceedings of the European Centre for Geodynamics and Seismology - ECGS) is devoted to the *ECGS-FKPE Workshop on Induced Seismicity*. The workshop was organised by the Luxembourg ECGS and the German FKPE (Forschungskollegium Physik des Erdkörpers e.V. - Research Association of the Physics of the Earth's Interior). The Workshop deals with ground shaking due to human activities on and inside the Earth such as mining, water reservoirs, dams, tunnel construction, etc. The impacts of *induced seismicity* on society range from annoying minor ground displacements or shaking to frightening ground motion and even damage. For example, earthquakes induced by dam operations led to destruction, waste water pumping into the Earth led to alarming shaking in several regions (e.g. Denver and the Paradox Valley, USA) and mining-induced shaking regularly causes minor damage in affected regions world-wide.

Currently, *induced seismicity* receives enormous attention worldwide. This interest is due to (1) recent advancement in exploiting geothermal energy, (2) the concept of storing fluid CO₂ inside the Earth in the context of mitigating climate change and (3) the increase in the number of mining operations to exploit the Earth's natural resources.

(1) Geothermal energy is a viable option for a CO₂-free renewable base-load energy source. An earthquake swarm induced by development of enhanced geothermal reservoirs, called deep heat mining in Switzerland, occurred in Basel (Switzerland) in 2006. Several earthquakes with local magnitudes reaching $M_L=3.4$ were generated by massive water injection of 11,566 m³ (11.57 tonnes) at a depth of 5,000m and caused cracking in buildings and anxiety and anger in the population. In the end, this induced seismicity caused the multi-million Euro project to be cancelled. In Landau (SW Germany) earthquakes with local magnitudes as high as $M_L=2.7$ due to reservoir testing were measured; the surface shaking also caused anxiety and protests. In southern Germany the threat of *induced seismicity* is delaying and may even stop geothermal development thus posing a serious threat to investments worth several 100 million Euros. Induced seismicity curtailed water injection to sustain reservoir pressure in part of the Geysers reservoir (California). Similar problems are known from different areas within Europe.

(2) The widely discussed technology of storage of CO₂ in the underground (CCS: carbon capture and storage), by injecting it at depths of several kilometres, is a probable future cause of induced seismic events. The main goal of CCS technology is to pump gigatons of fluid CO₂ into the underground in order to keep it away from the atmosphere where it may contribute to global warming. However *induced seismicity* due to the injection of fluid CO₂ is not completely understood. In this case seismic events may even influence the sealing of the CO₂ underground reservoirs.

(3) Damaging mining-induced *seismicity* stopped the coal mining in the Saarland area (SW Germany) and similar problems are known from many other sites.

Induced seismicity is associated with nearly all sources of energy in Europe: oil and gas fields, coal mines and water reservoirs, thus impacting the future energy supply from all conventional sources. To deal with the problem of induced seismicity, we must carry out research to understand the mechanisms of how man-made stress changes at depth interact with the ambient physical conditions in the reservoir, which

are unknown until the reservoir is accessed by drilling. Therefore, we urgently need more data, physical theories and case studies to get a better handle on *induced seismicity*. Beside the negative effects due to *induced seismicity*, there are also benefits: microseismicity provides the main information that we have about our reservoirs. Most models on the dimension of the reservoir or fracturing in the reservoir are deduced from seismological data including induced seismicity. It is interesting to note that the oil industry has begun to monitor reservoir seismicity “passive seismics” whose main sources are mostly induced events. In Germany, the FKPE initiated a working group on *induced seismicity* that is also a co-organiser of this workshop.

The aim of the ECGS-FKPE Workshop on „Induced Seismicity“ is to bring together leading scientists that work in the field of *induced seismicity*, and we are happy that about 50 scientists from 13 countries registered for this meeting. Leading researchers from different scientific institutions will present their latest results. This overview of new research results and physical principles will form a basis for the following sections of the workshop. The section on monitoring will also include experts from state surveys that are actually confronted with measuring and interpreting induced seismic events. Discussions and exchange of ideas are a major and integral part of the workshop. The TAIS (Triggered and Induced Seismicity) initiative was invited to include their expertise in the workshop and to develop close ties between the involved scientists. The TAIS Working Group is a part of IASPEI Commission on Seismological Observation and Interpretation.

Approved counter measures against *induced seismicity* are still an unsolved problem that needs more experiments and theoretical understanding. Therefore, reported case studies and more dedicated experimental research are important issues, because such studies are based on real data and experience.

We thank the Ministère de la Culture, the Fonds National de la Recherche (FNR), the Council of Europe and the Landesforschungszentrum Geothermie at the Karlsruhe Institute of Technology for financial support. Many thanks also go to C. Galassi and G. Celli (ECGS) for their invaluable support during the organization of the workshop.

Joachim Ritter and Adrien Oth

October 2010

ECGS-FKPE Workshop

INDUCED SEISMICITY

Program

MONDAY NOVEMBER 15 2010

09:00 – 09:30 Registration, Welcome

Morning session

09:30 – 10:10 Shapiro, S. (**keynote**)

Towards quantifying the seismogenesis of fluid injections in rocks

10:10 – 10:30 Wenzel, F., A. Barth, C. Langenbruch, and S. A. Shapiro

Occurrence probability and earthquake size of post shut-in events in geothermal projects

10:30 – 10:50 Plenkers, K., D. Schorlemmer, G. Kwiatek, and the JAGUARS research group

On the potentials and limitations of a seismic network's sensitivity when monitoring induced seismicity

10:50 – 11:10 Coffee break

11:10 – 11:50 Deichmann, N., and K. F. Evans (**keynote**)

Injection-induced seismicity – lessons learned and open questions

11:50 – 12:10 Kraft, T., N. Deichmann, and K. F. Evans

Detailed imaging of the Basel EGS reservoir – high-precision relocation and focal mechanisms of the induced microseismicity

12:10 – 12:30 Bethmann, F., N. Deichmann, and P. M. Mai

Attenuation measurements from borehole and surface recordings for induced earthquakes in the city of Basel, Switzerland

12:30 – 14:00 Lunch

Program

Afternoon session 1

- 14:00 – 14:20 Blascheck, P., M. Häge, and M. Joswig
First results of nanoseismic monitoring at geothermal sites
- 14:20 – 14:40 Mena, B., S. Wiemer, and C. Bachmann
Performance testing of forecasting models developed for induced seismicity due to enhanced geothermal systems
- 14:40 – 15:00 Schmidt, B., B. Rogulic, and J. Ritter
Relationship between reduced injection rates and reduced induced seismicity – 3 years of field data from the commercial geothermal power plant Landau (Germany)

Monday Poster Session

- 15:00 – 15:30 Poster introductions (3 slides / max. 5 min per poster)
- 15:30 – 16:30 Poster session and coffee break

Afternoon session 2

- 16:30 – 17:10 Cuenot, N. (keynote)
Induced microseismic activity at the Soultz-sous-Forêts EGS site: Main scientific results obtained in different experimental conditions
- 17:10 – 17:30 Calo', M., C. Dorbath, N. Cuenot, F. Cornet, and A. Genter
The contribution of the Local Earthquake Tomography in the EGS geothermal reservoir of Soultz-Sous-Forêts (France) during hydraulic stimulations
- 17:30 – 18:00 General discussion

Debate 1

- 18:00 – 19:00 Wording conventions for induced seismicity; Communicating with the public

TUESDAY NOVEMBER 16 2010

Morning session

- 09:00 – 09:40 Husen, S., E. Kissling, and A. van Deschwenden (**keynote**)
Induced earthquakes during the construction of the Gotthard basetunnel, Switzerland: Hypocenter locations and source parameters
- 09:40 – 10:00 Contrucci, I., E. Klein, N.-T. Kao, and P. Bigarre
Micro-seismic and leveling monitoring of a solution mining cavern collapse
- 10:00 – 10:20 Bischoff, M., L. Fischer, S. Wehling-Benatelli, R. Fritschen, T. Meier, and W. Friederich
Spatio-temporal characteristics of mining induced seismicity in the eastern Ruhr-area
- 10:20 – 10:40 Kwiatek, G., K. Plenkers, G. Dresen, and the JAGUARS research group
Scaling relations of induced seismicity in picoscale: A case study from Mponeng deep gold mine, South Africa
- 10:40 – 11:00 Coffee break
- 11:00 – 11:40 Fischer, T., A. Guest, and V. Vavryčuk (**keynote**)
Shear and tensile earthquakes caused by fluid injection
- 11:40 – 12:00 Bohnhoff, M., and M. D. Zoback
Oscillation of fluid-filled cracks triggered by degassing of CO₂ due to leakage along wellbores
- 12:00 – 12:30 General discussion
- 12:30 – 14:00 Lunch

Afternoon session 1

- 14:00 – 14:40 Dahm, T., S. Hainzl, D. Becker, and the DINSeis working group (**keynote**)
How to discriminate induced, triggered and natural seismicity

Debate 2

- 14:40 – 15:30 How to discriminate between natural and induced seismicity?

Tuesday Poster Session

- 15:30 – 16:30 Poster session and coffee break

Afternoon session 2

- 16:30 – 17:10 Dost, B., D. Kraaijpoel, T. van Eck, and F. Goutbeek (**keynote**)
Observing and analyzing seismicity at gas production fields in the Netherlands
- 17:10 – 17:30 Kononov, A. V., and S. B. Turuntaev
Induced seismicity due to hydrocarbon production in the North-Eastern part of Sakhalin island: Weak motion monitoring and further prospects
- 17:30 – 18:30 Presentation of the TAIS (Triggered and Induced Seismicity) working group
- 19:00 Conference dinner

WEDNESDAY NOVEMBER 17 2010

Morning session

- 09:00 – 09:20 Oye, V., H. N. Gharti, D. Kühn, and A. Braathen
Microseismic monitoring of fluid injection at the Longyearbyen CO₂-Lab, Svalbard
- 09:20 – 09:40 Turuntaev, S. B., E. I. Eremeeva, and E. V. Zenchenko
Laboratory study of temporal-spatial peculiarities of microseismicity spreading due to pore pressure change
- 09:40 – 10:00 Groos, J., and J. R. R. Ritter
Seismic noise: A challenge and opportunity for seismological monitoring in densely populated areas
- 10:00 – 10:40 General discussion
- 10:40 – 11:00 Coffee break
- 11:00 – 11:40 Joswig, M. (**keynote**)
Recent alternatives in seismic monitoring of geothermal sites

Debate 3

- 11:40 – 12:30 Which new techniques and technologies can we expect in the future?
- 12:30 – 14:00 Closing remarks and lunch
- 14:00 – Departure of participants

POSTERS

1. Akopian, S. Ts., and E. A. Popov
Monitoring induced seismicity based on seismic entropy method
2. Braun, T., J. Heinicke, and T. Dahm
The difficulty to distinguish natural and human related seismicity in a complex tectonically active area
3. Lindenfeld, M., G. Rumpker, and M. Kracht
Microseismic monitoring: A proposed study in the Upper Rhinegraben and experiences from the East African Rift System
4. Moldoveanu, T., K.-P. Bonjer, and M. Pecingine
Aspects concerning seismicity analyses of the Vidraru – Arges (Romania) dam area
5. Plenefisch, T., U. Wegler, M. Keyser, and E. Wetzig
Monitoring of microseismic activity around the GenSys deep geothermal drilling site, Hannover (Germany)
6. Turuntaev, S. B., and O. Yu. Melchaeva
Non-linear analysis of seismic regime response to electromagnetic powerful source actions
7. Wegler, U., and C. Bönnemann
Project MAGS – Microseismic Activity of Geothermal Reservoirs
8. Zahran, H. M., Sy. El-Hadidy, and Kh. Yosef
Recent earthquake activity at Haradh region, western Saudi Arabia
9. Godey, S., and R. Bossu
How to better discard non tectonic events from seismicity catalogues?
- 10./11./12. FKPE working group posters

List of Participants

ACHAUER Ulrich
Université de Strasbourg
EOST - IPG
5, rue René Descartes
F-67084 Strasbourg
France
ulrich.achauer@unistra.fr

AKOPIAN Samuel
Earthquake Prediction Centre "Geoquake"
Bolshaya Pereyaslavskaya St. 52 Str. 1, 63
129110 Moscow
Russia
sakopian@yandex.ru

BACHMANN Corinne
ETH Zuerich
Swiss Seismological Service
Sonneggstrasse 5
CH-8092 Zurich
Switzerland
banu.sanli@sed.ethz.ch

BARTH Andreas
Karlsruhe Institute of Technology
Geophysical Institute
Hertzstrasse 16
D-76187 Karlsruhe
Germany
a.barth@kit.edu

BECHET Georges
Musée National d'Histoire Naturelle
25, rue Münster
L-2160 Luxembourg
Luxembourg
georges.bechet@mnhn.lu

BETHMANN Falko
ETH Zürich
Swiss Seismological service
Sonneggstrasse 5
CH-8092 Zürich
Switzerland
bethmann@sed.ethz.ch

BISCHOFF Monika
Ruhr-Universität Bochum
Institut für Geologie, Mineralogie und Geophysik
NA 3/172
D-44780 Bochum
Germany
monika.bischoff@ruhr-uni-bochum.de

BLASCHECK Patrick
Universität Stuttgart
Institute of Geophysics
Azenbergstr. 16
70174 Stuttgart
Germany
patrick.blascheck@geophys.uni-stuttgart.de

BOHNHOFF Marco
GFZ German Research Centre for Geosciences
Geomechanics and Rheology
Telegrafenberg
D-14473 Potsdam
Germany
bohnhoff@gfz-potsdam.de

BONATZ Manfred
GeoObservatorium Odendorf
Wilkenstrasse 49
D-53913 Swisttal
Germany
geo.bonatz@t-online.de

BÖNNEMANN Christian
Central Seismological Observatory,
Federal Institute for Geosciences and Natural
Resources
Stilleweg 2
D-30655 Hannover
Germany
christian.boennemann@bgr.de

BRAUN Thomas
Istituto Nazionale di Geofisica e Vulcanologia
Osservatorio Sismologico
Via U. Della Faggiuilla 3
I-52100 Arezzo
Italy
thomas.braun@ingv.it

List of Participants

BURG Helena
Fonds National de la Recherche (FNR)
6, rue Antoine de Saint-Exupéry
L-1017 Luxembourg
Luxembourg
helena.burg@fnr.lu

BUTTINI Eric
Musée National d'Histoire Naturelle
25, rue Münster
L-2160 Luxembourg
Luxembourg
eric.buttini@ecgs.lu

CALO' Marco
EST University of Strasbourg
5 rue René Descartes
F-67084 Strasbourg
France
calo@unistra.fr

CELLI Gilles
Musée National d'Histoire Naturelle
19, rue Josy Welter
L-7256 Walferdange
Luxembourg
gilles.cell@ecgs.lu

CONTRUCCI Isabelle
INERIS
DRS/AS2G
Ecoles des mines de Nancy, Parc de Saurupt
F-54000 Nancy
France
isabelle.contrucci@ineris.fr

CUENOT Nicolas
EEIG Heat Mining
Route de Sultz
F-67250 Kutzenhausen
France
cuenot@sultz.net

D'OREYE Nicolas
Musée National d'Histoire Naturelle
19, rue Josy Welter
L-7256 Walferdange
Luxembourg
ndo@ecgs.lu

DAHM Torsten
University of Hamburg
Institute of Geophysics
Bundesstrasse 55
D-20146 Hamburg
Germany
torsten.dahm@zmaw.de

DEICHMANN Nicholas
ETH Zürich
Swiss Seismological service
Sonneggstrasse 5
CH-8092 Zürich
Switzerland
deichmann@sed.ethz.ch

DOST Bernard
KNMI
Seismology Department
Wilhelminalaan 10 i
NL-3732GK De Bilt
The Netherlands
dost@knmi.nl

FEIDER Michel
Administration des Services de Secours
1, rue Robert Stümper
L-2557 Luxembourg
Luxembourg
michel.feider@secours.etat.lu

FISCHER Tomas
Faculty of Science, Charles University Prague
Albertov 6
12843 Praha 2
Czech Republic
fischer@natur.cuni.cz

FRITSCHEN Ralf
DMT Gmbh & Co KG
Exploration & Geosurvey Division
Am Technologiepark 1
D-45307 Essen
Germany
ralf.fritschen@dmtd.de

GALASSI Corine
ECGS - European Center for Geodynamics and
Seismology
19, rue Josy Welter
L-7256 Walferdange
Luxembourg
corine.galassi@ecgs.lu

List of Participants

GAUCHER Emmanuel
Karlsruhe Institute of Technology
Geothermics
Adenauer Ring 20B
D-76131 Karlsruhe
Germany
emmanuel.gaucher@kit.edu

GROOS Jörn
Karlsruhe Institute of Technology
Geophysical Institute
Hertzstrasse 16
D-76187 Karlsruhe
Germany
joern.groos@kit.edu

HORALEK Josef
Institute of Geophysics, Academy of Sciences of
the Czech Republic
Department of Seismology
Am Technologiepark 1
14131 Prague 4
Czech Republic
jhr@ig.cas.cz

HUSEN Stephan
ETH Zürich
Swiss Seismological service
Sonneggstrasse 5
CH-8092 Zurich
Switzerland
husen@sed.eths.ch

JECHUMTALOVA Zuzana
Institute of Geophysics, Academy of Sciences of
the Czech Republic
Department of Seismology
Am Technologiepark 1
14131 Prague 4
Czech Republic
zs@ig.cas.cz

JOSWIG Manfred
Universität Stuttgart
Institute of Geophysics
Azenbergstr. 16
70174 Stuttgart
Germany
manfred@m-joswig.de

KONOVALOV Aleksey
Far Eastern Branch of Russian Academy of
Sciences
Institute of Marine Geology & Geophysics
Nouka Street 1B
693022 Yushno-Sakhalinsk
Russia
konovalov@imgg.ru

KÖNIG Matthias
RWE DEA AG
Exploration Germany
Flamingoweg 1
D-44139 Dortmund
Germany
matthias.koenig@rwe.com

KRACHT Matthias
Hessisches Landesamt für Umwelt und Geologie
Hessischer Erdbebendienst
Rheingastr. 186
D-65203 Wiesbaden
Germany
Matthias.Kracht@hlug.hessen.de

KRAFT Toni
ETH Zürich
Swiss Seismological service
Sonneggstrasse 5
CH-8092 Zurich
Switzerland
kraft@sed.ethz.ch

KWIATEK Gregor
GFZ German Research Centre for Geosciences
Geomechanics and Rheology
Telegrafenberg
D-14473 Potsdam
Germany
kwiatek@gfz-potsdam.de

LASOCKI Stanislaw
Institute of Geophysics, Polish Academy of
Sciences
ks. Janusza 64
01-452 Warsaw
Poland
lasocki@igr.edu.pl

LINDENFELD Michael
Goethe University Frankfurt
Institute of Geosciences
Altenhoferallee 1
D-60438 Frankfurt
Germany
lindenfeld@geophysik.uni-frankfurt.de

MELCHAYEVA Olga
Russian Academy of Sciences
Institute of Geosphere Dynamics
Leninsky prosp., d.38, k.1
119334 Moscow
Russia
malchaeva@gmail.com

List of Participants

MOLDOVEANU Traian
S.G. Geotec Consulting Srl
Geophysics and Engineering Seismology
1bis, Bvd Lacul Tei - Sector 2
Bucharest
Romania
trm.geohazard@yahoo.com

ORLECKA-SIKORA Beata
Institute of Geophysics, Polish Academy of
Sciences
ks. Janusza 64
01-452 Warsaw
Poland
orlecka@igf.edu.pl

OTH Adrien
ECGS - European Center for Geodynamics and
Seismology
19, rue Josy Welter
L-7256 Walferdange
Luxembourg
adrien.oth@ecgs.lu

OYE Volker
NORSAR
Earthquakes and Environment
Gunnar Rander Vei 15
2007 Kjeller
Norway
volker@norsar.no

PAVLOU Kiriaki
University of Athen
Geology and Geoenvironment
Panepistimioupoli, Ilissia
Athens
Greece
kpavlou@geol.uoa.gr

PLENEFISCH Thomas
BGR Bundesanstalt für Geowissenschaften und
Rohstoffe
Geozentrum Hannover
Stilleweg 2
D-30655 Hannover
Germany
plenefisch@sdac.hannover.bgr.de

PLENKERS Katrin
Karlsruhe Institute of Technology
Geophysical Institute
Hertzstrasse 16
D-76187 Karlsruhe
Germany
katrin.plenkers@kit.edu

RITTER Joachim
Karlsruhe Institute of Technology
Geophysical Institute
Hertzstrasse 16
D-76187 Karlsruhe
Germany
joachim.ritter@kit.edu

RIVALTA Eleonora
University of Hamburg
Institute of Geophysics
Bundesstrasse 55
D-20146 Hamburg
Germany
eleonora.rivalta@zmaw.de

RÜMPKER Georg
Goethe Universität Frankfurt
Facheinheit Geophysik
Altenhöferallee 10
D-60438 Frankfurt am Main
Germany
ruempker@geophysik.uni-frankfurt.de

SCHARES Nico
Les Services du Géomètre
Ville de Luxembourg
1-3, rue du Laboratoire
L-1911 Luxembourg
Luxembourg
nschares@vdl.lu

SCHMIDT Bernd
Landesamt für Geologie und Bergbau Rheinland-
Pfalz
Landeserdbebendienst Rheinland-Pfalz
Emy-Roeder-Strasse 5
D-55129 Mainz
Germany
bernd.schmidt@lgb-rlp.de

SHAPIRO Serge
Freie Universität Berlin
Geophysics
Malteserstrasse 74-100
D-74100 Berlin
Germany
shapiro@geophysik.fu-berlin.de

TURUNTAEV Sergey
Russian Academy of Sciences
Institute of Geosphere Dynamics
Leninsky prosp., d.38, k.1
119334 Moscow
Russia
turunt@postman.ru

List of Participants

WEGLER Ulrich
BGR Bundesanstalt für Geowissenschaften und
Rohstoffe
Geozentrum Hannover
Stilleweg 2
D-30655 Hannover
Germany
wegler@sdac.hannover.bgr.de

YOUSSEF Salah
Saudi Geological Survey
P.O. Box 54141
21514 Jeddah
Saudi Arabia
salah_elhadidy53@yahoo.com

YOSEF KHALID
Saudi Geological Survey
P.O. Box 54141
21514 Jeddah
Saudi Arabia
yousef.KH@sgs.org.sa

ZAHRAN Hani
Saudi Geological Survey
P.O. Box 54141
21514 Jeddah
Saudi Arabia
zahran.hm@sgs.org.sa

SECTION I

ABSTRACTS

(sorted following first author's surname)

Monitoring induced seismicity based on seismic entropy method

S.Ts. Akopian and E. A. Popov

Earthquake Prediction Centre "GeoQuake", Moscow.

The proposed method of monitoring and prediction of earthquakes based on seismic entropy is practically applied to different regions of the world since 2007. The method allows monitoring and induced seismicity. In 1993, for a quantitative description of seismic processes in real media Akopian introduced the physical parameters of the density of states and entropy, and as the quantum - an elementary micro earthquake. It was shown that these processes occur within a specific volume of the lithosphere, called Seismic System (SS). To identify the SS calculated the integral of total seismic energy released in the volume of the geological media and its logarithm – entropy. These parameters are always increasing over time and contain information about the SS as a whole. The system is considered to be definite if it satisfies the law of seismic entropy production. Each earthquake with a magnitude less than the threshold is accepted as a natural indicator of the external impact on the system - earthquake-indicator. The law of seismic entropy production - regularity between the total energy of earthquake-indicators, released in seismic cycles, and the energies of strong earthquakes which end these cycles. Introduction to basic micro earthquake – the quantum, and the new parameters allowed transferring the description of real processes in a mathematical plane, which is expressed in the construction of energy and track diagrams. The choice of quantum depends on the size of SS and the tasks that solve seismologists. Predicted magnitude based on the law of entropy production corresponds to the energy of earthquakes generated and accumulated by geological structure for many years. Traditional magnitude (determined from records of seismic waves), may contain the influence of fluids, artificial and human-induced factors in the focal zone, which can strengthen or on the contrary weaken the intensity of earthquake. A comparison of earthquake magnitudes by the method of seismic entropy with traditional magnitudes, defined by seismological networks can identify a fluid, technogenic component in the preparation of earthquake. It found that on the north of Sakhalin occurs a certain strengthening of the force of tectonic earthquakes due to natural variations hydrocarbon fluids. Preparation of the earthquake is depicted by step trajectory, which ultimately falls into the attractor and ends strong earthquake. Track diagram makes it possible to forecast the different manifestations of seismicity before the strong earthquake. Fig.1 shows schematically the simplest attractor for hypothetical SS and different versions for approaching the tracks. Evidently from the figure, in what cases it is possible to observe foreshock activity, seismic swarms and calms, the induced seismicity. If the track is below the attractor, then the earthquake-indicator can raise track. Thus if the track falls into the local region of instability of any element of the system, then strong earthquake there can be excited. Such earthquake-indicators will be a trigger for strong earthquakes. In contrast to the foreshocks they can be removed from the focal zone of strong earthquakes; however, the distance of this trigger mechanism is limited by the framework of system. The method of seismic entropy revealed a trigger mechanism of the recent earthquake in Baja California on April 4, 2010, M=7.2. Earthquake-indicator of December 30, 2009, M=5.8 near Mehikalli raised track, it fell into a zone of instability of the Laguna Salada fault, where occurred after three months strong earthquake. On the basis of hindsight shown that the catastrophic 1988 Spitak earthquake in Armenia could be the

trigger. Focal zone of the Spitak earthquake was weakened Akhuryan reservoir, which was commissioned in 1983. In small reservoirs, in contrast to large, throughout the season are large fluctuations in water level variations in pore pressure, which in adverse seismo-tectonic conditions can be fatal. At present the world we revealed more than 100 SS and subsystems with sizes from 20 km to 3000 km with the threshold magnitudes from 5.5 to 8.5. Monitoring and forecast of strong earthquakes in all these systems in real time and examples of triggering earthquakes can be seen on our site www.geoq.ru.

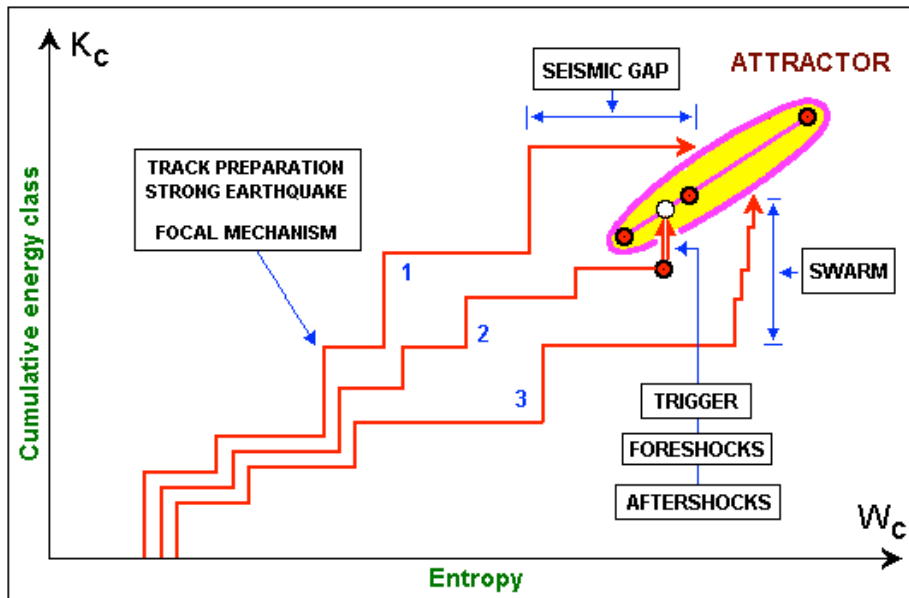


Figure 1. The simplest seismic attractor and options approach tracks.

Attenuation measurements from borehole and surface recordings for induced earthquakes in the city of Basel, Switzerland.

Falko Bethmann¹, Nicholas Deichmann¹ and P. Martin Mai²

¹ Swiss Seismological Service, Institute of Geophysics, ETH Zurich, NO, Sonneggstrasse 5, 8092 Zurich, Switzerland

² Division of Physical Sciences and Engineering, Building No.1 (UN 1550), Office No 3111, Level 3, 4700 King Abdullah University of Science and Technology, Thuwal 23955-6900, Kingdom of Saudi Arabia

Source parameter determinations of earthquakes are often contaminated by reverberation and attenuation of high frequencies close to the earth's surface. Also results from shallow boreholes are often inconclusive because waveforms can be severely contaminated by downward reflected phases. Investigations of deeper borehole recordings for induced earthquakes underneath the city of Basel, Switzerland revealed that attenuation (Q) at greater depths is also significant. We therefore investigate attenuation of sediments of 2.5 km thickness using recordings of 195 induced events that were obtained during and after the stimulation phase of a reservoir underneath the city of Basel for a Deep Heat Mining Project in 2006 and 2007. The data set is ideally suited to estimate Q as all events are confined to a small source volume and were recorded by a dense surface network of 92 stations as well as 6 borehole sensors at 2.7 km, 1.2 km, 553 m, 542 m, 500 m and 317m depth. The deepest borehole sensor is positioned inside the crystalline basement at hypocentral distances as low as 2.2 km allowing us to measure Q for frequencies of up to 250 Hz for signal to noise ratios greater than five. We apply three different methods to estimate Q . First we use a standard spectral ratio technique to obtain Q independent of frequency. We then compare Q to a frequency dependent $Q(f)$ using a two station method that delivers a Q estimate at all frequencies and as a third measure we estimate Q in the time domain, by folding signals of a deep station with a Q -operator and compare the folded signal to recordings of a shallower station. We find the sediments of Basel highly attenuating also at deeper depths. At 500 m depth we obtain a Q as low as 50 and at 1200 m depth we obtain a Q of 100. All three methods deliver similar values for Q . The frequency dependent $Q(f)$ exhibits an increase in Q towards higher frequencies. We also find attenuation of similar value using either P- or S-wave for the analysis.

Spatio-temporal characteristics of mining induced seismicity in the eastern Ruhr-area

M. Bischoff¹, L. Fischer², S. Wehling-Benatelli¹, R. Fritschen³, T. Meier² and W. Friederich¹

¹ Ruhr-Universität Bochum,

² Christian-Albrechts-Universität zu Kiel,

³ DMT GmbH & Co. KG

Seismicity in the tectonically inactive Ruhr area is induced by deep coal mining. Since 1983 the seismicity has continuously been monitored by the Ruhr-University Bochum. About 1000 seismic events with $0.7 \leq M_L \leq 3.3$ are located every year. About 30 seismic events per month exceed $M_L \geq 1.2$ and can be recognized by people living close to the mining activity. This results in considerable public interest in mining induced seismicity.

Between June 2006 and July 2007 seismicity of a single longwall in Hamm was continuously monitored by a dense seismic network. About 7500 seismic events with $-1.7 \leq M_L \leq 2.0$ are located. Epicenters cluster in the region of active mining with sharp boundaries that trace the borders of the longwall. Hypocentral depths are mainly between 1200 and 900 m and thus up to 100 m below and 200 m above the active mining. This pattern implies that the observed seismicity is a direct answer to stresses induced by the ongoing mining. This is supported by the migration of epicenters with the advance of mining at about 100 m/month from southwest to northeast at an azimuth of 60° . For 90% of the epicenters the horizontal distance to the longwall face is less than 60 m.

Furthermore, spatial clusters of seismic activity are observed within distances up to 500 m to the longwall. Here, the layout of former longwalls may have led to areas of enhanced stresses. Where rocks at higher levels have been untouched by previous mining the gravitational load is increased compared to regions where mined areas lie on top of each other. Especially border regions are prone to enhanced seismicity.

Fault mechanisms of selected events of the most prominent spatial clusters are analyzed. A total of 105 fault plane solutions is determined from the polarities of P-onsets and polarization of S-waves. In general, two types of fault mechanisms are observed. Firstly, the mechanism of events accompanying mining activity at the longwall face is characterized by steeply dipping, near vertical fault planes that strike parallel to the longwall face. Displacement is in direction towards the goaf and P-axes are oriented at an azimuth of 60° , which is equal to the direction of face advance. The second type of events mainly occurs at clusters at larger distances up to 500 m. These events can be described by vertical P-axes corresponding to gravitational load and variable azimuths of the T-axes. Here, load-bearing structures may fail when additional stresses are induced by active mining.

Nearly identical seismograms are observed for events of our dataset. Thus, we quantitatively define seismic clusters by waveform similarity. Cross-correlation matrices are calculated for each station using all events with available P-onsets and a weighted sum of the coefficients of the respective seismogram components. Cross-correlation matrices are sorted so that events that are similar to the same subset of events are separated from other subsets. Clusters are defined by visual inspection.

Clusters of events with common properties have been identified, e.g. clusters of events with different locations or with similar locations but different magnitude ranges.

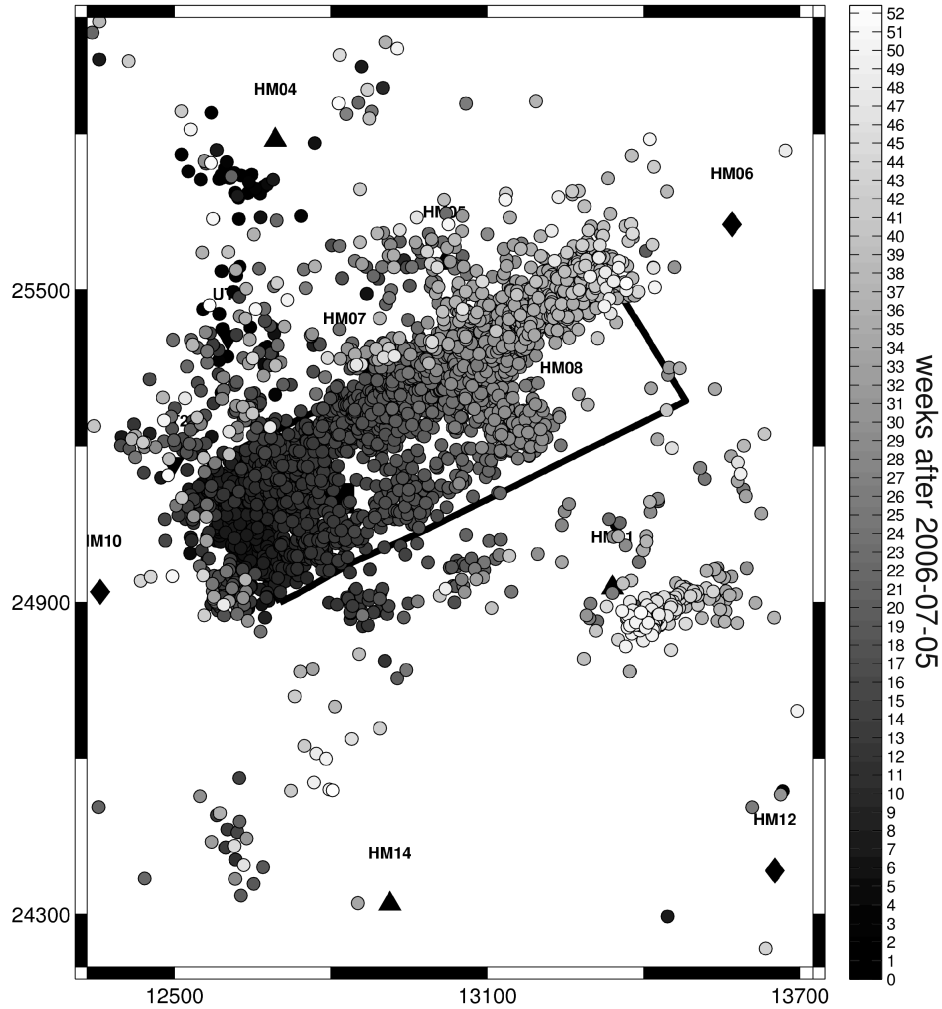


Figure. 1. Locations of seismic events between July 2006 and July 2007. Origin time is denoted in grayscale. Most epicentres are confined to the mined area and move with the advancing longwall face. Some events may also occur at some hundred meters distance from the longwall.

First results of nanoseismic monitoring at geothermal sites

Patrick Blascheck, Martin Häge and Manfred Joswig

Institute for Geophysics, Universität Stuttgart

The method of nanoseismic monitoring, presented in the talk of Manfred Joswig (see Manfred Joswig: Recent alternatives in seismic monitoring of geothermal sites), as a seismic microscope can detect weak earthquakes of magnitude $M_L = -2.0$ and lower. To verify the location accuracy, a reference network had to be found in order to compare these low energy earthquakes.

Geopower Energy Limited set up a microseismic network near Basel to seismically monitor the construction of a geothermal plant where also the seismic information of the SED regional network is available. The Hot-Dry-Rock method was used to increase the fissures via artificial stimulation by hydraulic fracturing. Six borehole seismometers in a depth of 317 m to 2740 m were installed and represent an excellent reference for our surface based array. Our measurements were carried out with two small arrays (SNS - seismic navigating system) deployed on the surface from the 6th of December 12:45 UTC to the 8th of December 9:30 UTC 2006 with a samplerate of 400 Hz. A SNS consists of a central 3-component seismometer and in a distance of about 100 m and an angle of 120° three 1-component seismometers. They were deployed at a distance of 2.1 km (SNS1) and 4.8 km (SNS2) to the borehole (see figure 1).

20 Events in a magnitude range from $0.7 \leq M_L \leq 2.2$ detected with the networks were chosen to test our accuracy. In order to be able to compare all networks, the velocity model of the SED, which is based on a 3D tomography was supposed to be used. For our evaluation the program *Hypoline* was used. This program can only deal with 2D models and therefore these have been extracted from the existing 3D model. Due to inconsistencies with the velocity model and the results from the SED showing that their locations wouldn't increase the accuracy, only the borehole seismometer data was used. The results are shown in figure 1. The average location difference is 770 m in the horizontal and 360 m in the vertical direction. A systematical displacement can be observed to the different velocity models.

The same events have been reinvestigated using the master event technique. These results were compared to the results of Deichmann et al (2007) using the master event technique as well and the results of Kahn (2008) using the double difference algorithm. All methods show the same northnorthwest-southsoutheast distribution of the hypocenters. The average displacement difference compared to Deichmann et al is 420 m in x and 110 m in y direction, compared to Kahn 110 m in x and 110 m in y direction.

Further evaluation will determine the magnitude of completeness. The extension of the investigated 20 events will allow a statistical approach to verify the Gutenberg-Richter scale and to compare these results to other nanoseismic monitoring campaigns. First results will be presented.

Abstracts

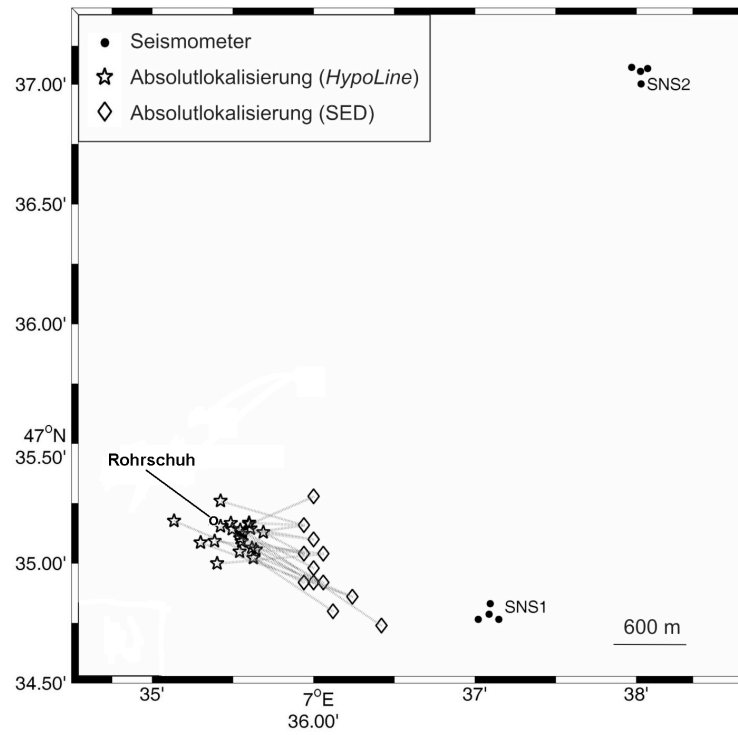


Figure 1: Comparison of the location results.

Oscillation of fluid-filled cracks triggered by degassing of CO₂ due to leakage along wellbores

Marco Bohnhoff^{1,2} and Mark D. Zoback¹

¹ Department of Geophysics, Stanford University

² Helmholtz Centre Potsdam GFZ German Research Centre for Geosciences

We present evidence for a seismic source associated with degassing CO₂ during leakage along two wellbores instrumented with arrays of downhole seismometers. More than 200 microseismic events were detected in direct vicinity of the monitoring wells. The observed seismic waves are dominantly P waves and tube waves, with no (or extremely weak S) shear waves. The waveforms of these events indicate extremely rapid amplitude decays with distance across the arrays, consistent with the seismometers being in the near field of the seismic source. The frequency characteristics, first-motion polarities and S to P amplitude ratios suggest a single force source mechanism. Because the seismic arrays were located at the depth where the density of ascending CO₂ changes most rapidly, it appears that the transition of CO₂ from supercritical fluid to gas triggers an oscillation of fluid-filled cavities and fractures very close to the wellbores in which the monitoring arrays were deployed. In many aspects, the observed waveforms show a striking similarity to those modeled for degassing processes below volcanoes. We suggest that the single force represents bubble growth and resulting oscillations in cement cavities between the steel casing of the well and the rock adjacent to the wellbores and/or within fractures in the rock just outside the wellbores.

The difficulty to distinguish natural and human related seismicity in a complex tectonically active area

Thomas Braun¹, Jens Heinicke² and Torsten Dahm³

¹ Istituto Nazionale di Geofisica e Vulcanologia, Seismological Observatory, Arezzo

² Sächsische Akademie der Wissenschaften zu Leipzig, Office TU Bergakademie Freiberg,

³ Institut für Geophysik, Universität Hamburg

Human operations, such as mining, fluid production and the construction of a barrier lake in a tectonically active area can play an important role of triggering seismic events. An interesting area to study those phenomena is the northern part of the Upper Tiber Valley, which is characterized by the presence of a Low Angle Normal Fault, the so called Alto Tiberina Fault (ATF). The recent seismic activity of this fault line reflects the geodynamic behaviour in the regional stress field. Close to this fault zone, a deep borehole PSS1 is located which will be reopened at the end of 2010 to extract CO₂. This will lead to a change in the hydraulic equilibrium in this region with potential consequences for the overall local geodynamics. Crustal deformation and microseismicity could be induced by the extraction. Fluid pressure changes and their influence to the hydraulic conduits up to the natural fluid emissions sites (mofettes) will be investigated as part of an active controlled forcing experiment on this fault. Further human activities like mining industry and the filling of water reservoirs influence the local stress field. The derivation of natural and human induced seismicity can be improved by a comprehensive analysis.

Scientific studies of the influence of human activity to the geodynamic processes on site

The Upper Tiber Valley is situated in the northern part of the Central Apennines and is setting of a number of geological phenomena typical for volcanic areas, like CO₂ degassing, moderate earthquakes ($M \leq 6$) and a strong microseismicity. The major part of the recorded seismicity can be associated to a Low Angle Normal Fault (LANF) – the so called Alto Tiberina Fault (ATF), but some of the recorded seismograms show signals similar to those recorded on active volcanoes. In the vicinity of the ATF human activity provides a number of candidates, capable to influence the seismic release in the area:

- a huge barrier lake with a dam height of 52 m and a water holding capacity more than 150 million m³ is directly situated on the ATF and is characterized by seasonal water level oscillation of up to 12 m.
- a cement plant, quarries and decommissioned mines present in the area are in the direct vicinity of epicentres of tornillo-like seismograms and episodes of non-volcanic tremor.
- CO₂ extraction – also this candidate influence the local stress regime: with the original scope to find methane, between 1982 to 1984 a perforation well has been sunk to a depth of 4800 m at a distance of about 5 km from the Montedoglio-Lake, the so called PSS well. Instead of finding methane, carbon dioxide has been encountered, with the consequence, that the borehole was closed and sealed. In 2004 the well has been reopened and prepared for a future commercial use of carbon dioxide by a company that will start with continuous extraction from December 2010 on.

Since 2003 many field experiments (gas flux measurements, different seismic network and array configurations, webcam etc) have been carried out to monitor the different geophysical phenomena. Interesting in the near future will be the controlled extraction of CO₂ and its influence on the seismicity.

Human related influences, as realized by the activities of cement plants, quarries or mines may produce interesting seismic signals, but will not directly have an impact on the mechanical behaviour of an active fault system. However, water level changes in a huge barrier lake, as the Montedoglio-Lake, or long term CO₂-extraction from the Upper crust have the capability to directly influence the local stress field. A large scale field experiment gives us the opportunity to study the overall influence of human activity at this LANF.

Beginning from December 2010, the user of the CO₂ reservoir will re-open the PSS borehole and plans to produce 5 tons per hour of reservoir gases for commercial usage and trading. This production will lead to a pore pressure change and slow depletion of the reservoir formation, similar to many other gas fields under production. Since production volumes and pore pressure changes are relatively well known, we will consider the local depletion-induced stress changes on the ATF and in the surrounding rock as driving forces to the system. We consider the geodynamic response of the ATF as result of a pore pressure perturbation by crustal fluids which influence the static stress regime in the reservoir.

The contribution of the Local Earthquake Tomography in the EGS geothermal reservoir of Soultz-Sous-Forets (France) during hydraulic stimulations

M. Calo¹, C. Dorbath², N. Cuenot³, F. Cornet⁴ and A. Genter³

¹ Institut de Physique du Globe de Strasbourg, IPGS - UMR 7516, CNRS et Université de Strasbourg (EOST), 5 rue René Descartes, F- 67084 Strasbourg

² IRD-UR154 (LMTG) - EOST Institute. 5 rue René Descartes, F- 67084 Strasbourg

³ GEIE, Route de Soultz, BP 40038, F-67250 Kutzenhausen, France.

⁴ EOST, 5 rue René Descartes 67084 Strasbourg cedex, France

In July 2000 a stimulation test was performed in the GPK2 well of the Enhanced Geothermal System (EGS) site of Soultz-Sous-Forêts (Alsace, France). During the stimulation an intense micro-seismic activity has been detected and recorded by downhole and surface seismic stations. Previous studies have shown temporal changes of the physical properties in the reservoir during the fluid stimulations through the results of a 4D seismic tomography obtained by dividing the induced seismicity into chronological sub-sets of a constant number of events (Cuenot et al, 2008). We present here the results of new 4D tomographies relative to this stimulation experiment. The velocity models have been obtained by rearranging the sub-sets in the light of the injection parameters. To obtain the final velocity model we applied the double-difference tomographic method (Zhang and Thurber 2003) and the WAM post processing (Calo' et al., 2009).

The applied tomographic method (tomoDD plus WAM) together with the subset selection matching with the changes of the injection parameters played a fundamental role to obtain representative descriptions of the temporal evolution of the velocity variations in geothermal fields.

The new models give clearer insights on the temporal changes of the velocities and show that their evolution is not strictly related to the induced seismicity. Our tomographies show low velocity anomalies aligned along the main strikes of the pre-existing structures and moving during the stimulation test. During the fluid injection the stress field changed in the time and space domains accommodating the strains with seismic and probably also with aseismic displacements. Indeed velocity anomalies are also detected in regions that were not-seismic during the stimulation. Therefore, the volumes where sudden changes of the velocities occurred should be mainly interpreted as the expression of transient stress conditions and not as regions affected directly by the injected fluids. In this study we show how the improved tomographic models are fundamental to describe velocity and seismic structures not clearly visible previously, with the conventional seismic imaging. The resolution and the reliability of the proposed method could make the Local Earthquake Tomography a practical tool for the characterization and exploration of a geothermal reservoir.

References

- Calò, M., Dorbath, C., Luzio, D., Rotolo S.G., and D'Anna, G., 2009, Local Earthquakes Tomography in the southern Tyrrhenian region: geophysical and petrological inferences on subducting lithosphere. Subduction Zone Dynamics Series: Frontiers. in Earth Sciences., XX, doi: 276-10.1007/978-3-540-87974-9.
- Cuenot, N., Dorbath, C. & Dorbath, L., 2008. Analysis of the microseismicity induced by fluid injection in the Hot Dry Rock site of Soultz-Sous-Forêts (Alsace, France): implications for the characterization of the geothermal reservoir properties, Pure appl. Geophys., 165, 1–32.
- Zhang, H., and Thurber, C.H., 2003, Double-difference tomography: The method and its application to the Hayward fault, California. Bulletin of the Seismological Society of America, v. 93, p. 1175-1189.

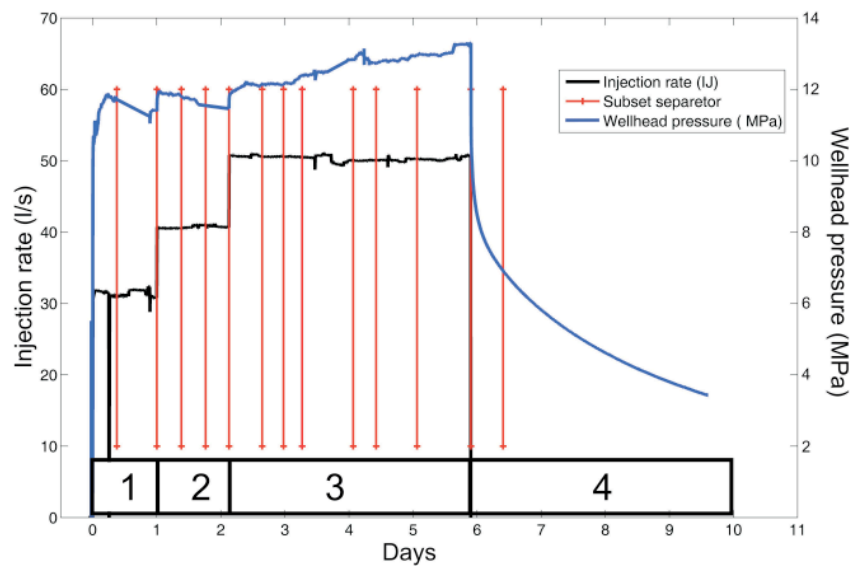


Figure 1. Hydraulic parameters of the stimulation of GPK2 (2000): wellhead pressure (blue) and flow rate (black). The whole time period enclosing the recorded seismic data set has been separated into 14 subsets (red) matching with the changes of the hydraulic parameters.

Abstracts

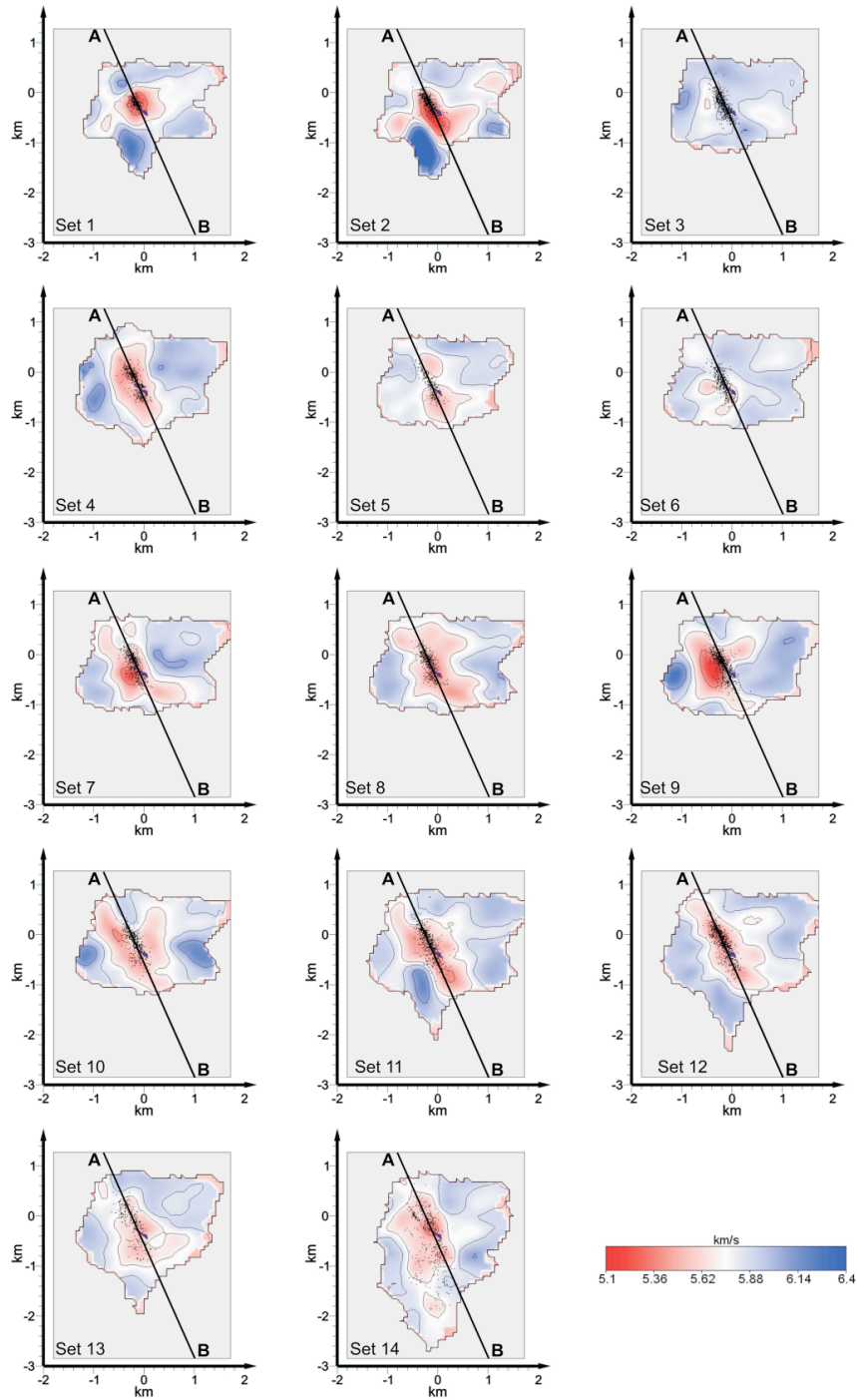


Figure 2. Temporal evolution of the P-wave seismic velocity model at a depth of 4.6 km during the stimulation test of GPK2. The black dots are the events used for the computation of each picture. The images display only the well resolved part of the models ($DWS > 10$).

Micro-seismic and leveling monitoring of a solution mining cavern collapse

I. Contrucci, E. Klein, N-T. Cao and P. Bigarre

INERIS, Institut National de l'Environnement Industriel et des Risques, Ecoles des Mines de Nancy, Parc de Saurupt, 54000 Nancy

To improve our understanding in large scale ground failure phenomenon induced by old underground mining works, a field experiment was undertaken by the partners of GISOS¹ in collaboration with the SOLVAY mining company: a solution mine was instrumented in 2004 previously to its collapse which was triggered in February 2009, as part of the mining scheme. This solution mine is located in the Lorraine salt basin, at Cerville-Buissoncourt southwards from Nancy, France. To monitor the cavern collapse, a permanent monitoring system was set up (Figure 1). This comprises a SYTGEM multi-parameter system featuring high resolution microseismic (5 1D geophones, 4 3D geophones, 40-1000 Hz) linked to ground surface monitoring (tacheometer and GPS high resolution measurements). The important amount of data transmitted for on-line processing offered daily insight of the evolution of the geological system.

The early signs of unstable evolution were detected by high resolution microseismic monitoring during spring 2008: a shift in microseismic background regime as well as recurrent microseismic episodes were associated to a general process of rock failure due to the cavern growing upwards. This was accompanied by a few episodes of massive roof falls, with no ground surface movement detected. During a second and last stage of evolution that lasted three days, the cavern collapse was triggered by brine pumping. Three main microseismic regimes were then observed, each being well correlated with changes in both the surface subsidence rate and the brine level in the cavern (Figure 2). The first peak of activity, due again to massive roof falls below the Beaumont dolomite bed, also initiated the brittle rupture of this bed. The second and major peak of activity marked its rapid and energetic failure; it also corresponded to an acceleration in the subsidence rate. The last peak of activity, a few hours later, weaker in terms of number of events and energy released, signed the final collapse.

The complete dataset confirms the major role of the Beaumont dolomite bed in the site stability. Besides, if the preliminary analysis of the microseismicity patterns right before the general collapse, confirms that the acceleration in the microseismic activity follows a power law, it also shows that the b-value is a complex marker in such context. Even though local falls of b-value well correlate, as expected, to local increases in microseismic energy release, it seems inappropriate to use it for forecasting purposes: over a short period of time, several b-value decreases are observed while a continuous pumping regime is applied to the system (Figure 2). So, apparent b-value variations don't show clear precursory pattern, as observed in other case-study. Nevertheless, further investigations over the different stages of evolution of the cavern, including the collapse period, are needed to confirm this preliminary result.

¹ Groupement d'Intérêts Scientifique sur l'Impact et la Sécurité des Ouvrages Souterrains, which is a scientific consortium including INERIS, BRGM and INPL

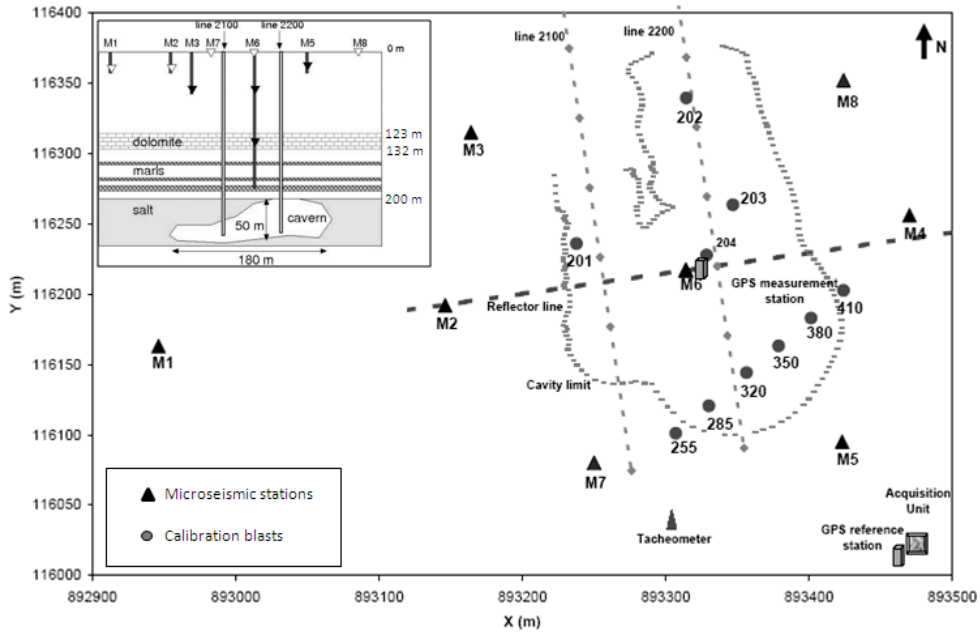


Figure 1 : Location map showing the layout of the high resolution microseismic monitoring network and the ground surface movement measurement system (RTK GPS and tacheometer). The insert illustrates a cross section of the instrumentation, where the extension of the salt cavern is represented as well as the geological structure and the elevation of the microseismic network, especially the M6.3, located in the dolomite banc at around 125 meters depth. Dotted line represent the cavern border as known in 2005.

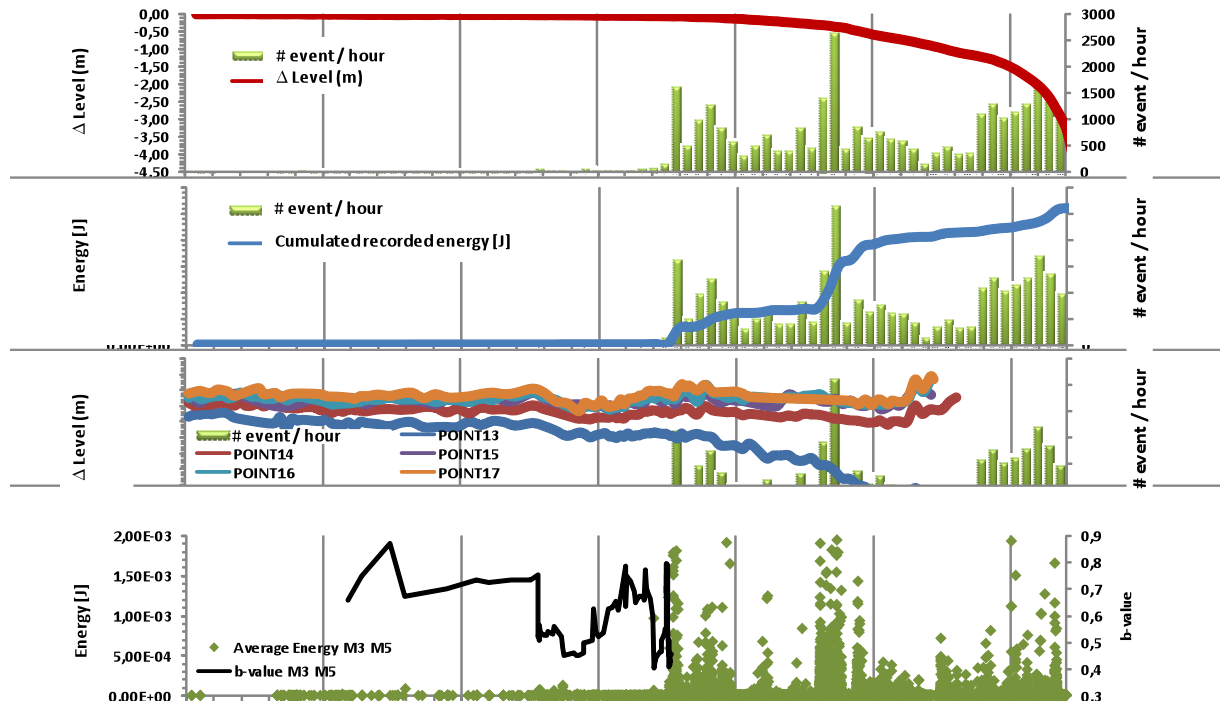


Figure 2 : Between 10th and 13th February 2009 : a) number of microseismic events recorded on site and GPS measurements; b) number of microseismic events recorded and cumulative energy recorded; c) number of microseismic events recorded and tacheometer leveling; d) recorded energy per event and b-value before the main activity.

**Induced microseismic activity at the Soultz-sous-Forêts EGS site:
Main scientific results obtained in different experimental conditions.**

Nicolas Cuenot

GEIE "Exploitation Minière de la Chaleur" / EEIG "Heat Mining", Route de Soultz, BP 40038, 67250 Kutzenhausen, France

Monitoring of the induced microseismic activity at the Soultz geothermal site has been performed for more than 20 years. During the development of the project, many different hydraulic tests were conducted: hydraulic and chemical stimulations, circulations with or without pumps. The seismological data recorded during these experiments have given a unique opportunity to study the development of induced seismicity in different hydraulic conditions and slightly different geological and tectonic contexts, as both a shallow (~3.5 km depth) and a deep reservoir (~5 km depth) were developed.

Monitoring is performed with 2 seismological networks:

- A deep network, which is composed of 5 stations, 4 installed in 1500 m deep boreholes and 1 in a 2200 m deep borehole. Both 4C accelerometers and 3C geophones are used.
- A surface network, which is composed of 9 stations. 3C and 1C (vertical) seismometers are installed.

Induced microseismicity is mainly related to hydraulic stimulations. The most intense activity and the strongest earthquakes occurred during these tests. 3 hydraulic stimulations were performed in the shallow reservoir (1993: well GPK1; 1995 & 1996: well GPK2), during which several thousands of microearthquakes were induced (largest observed magnitude: 1.9). 4 stimulation tests were then performed into the deep reservoir: the borehole GPK2 was stimulated in 2000, GPK3 in 2003 and GPK4 twice in 2004 and 2005. The recorded induced microseismic activity was much larger than during the stimulations of the shallow reservoir. Moreover the strongest earthquakes ever recorded at Soultz occurred during the stimulations of the deep reservoir: several earthquakes of magnitude larger than 2 were induced, mainly in the shut in period. The strongest one reached a magnitude of 2.9 during the stimulation of GPK3 in 2003. It was felt by a part of the population (as well as several other earthquakes of magnitude larger than 2), leading to unwanted nuisances and some complaints. Several chemical stimulations were also performed in the deep wells. The induced microseismicity was much lower than during hydraulic stimulations and no large event was induced.

One of the major concerns is the seismicity induced during circulation tests, as the results observed in these conditions could give important information about the seismic behaviour of the reservoir when the power plant will be fully in operation. In every circulation tests a moderate activity was recorded. This behavior was observed in different experimental settings (artesian or pump-assisted circulation; 2, 3 or 4 wells involved; different durations). Variations of the microseismic activity were often linked with variations of hydraulic parameters (increase/decrease of circulation flow rate, failure of a production pump, shut in). Some rare earthquakes reached a magnitude higher than 2, which were often also linked with some perturbations of the hydraulic parameters.

Abstracts

The huge seismological database recorded at Soultz has been the basis of many research studies, which aim at a better understanding of the hydro-mechanical processes that are involved in the generation of induced seismicity. Several modeling studies were able to reproduce the development of induced seismicity. These studies were mainly focused on hydraulic stimulations. Analysis of the seismological data allowed also getting structural information about the fracture network which constitutes the geothermal reservoir. In the frame of the future continuous exploitation of the power plant, an effort should be made on the better understanding of the seismic response of the reservoir under circulation conditions.

How to discriminate induced, triggered and natural seismicity

Torsten Dahm¹, S. Hainzl², Dirk Becker¹ and the DINSeis* working group

¹ Universität Hamburg

² Helmholtz Centre Potsdam, GFZ German Research Centre for Geosciences

* DINSeis (D**isc**rimination between **I**nduced and **N**atural **S**eismicity)

Man-made operations such as mining, fluid withdrawal or injection, drilling and hydro-fracturing, or impounding reservoir filling, have impact the stress, pore pressure, fluid migration and strain in the sub-surface. Earthquakes occurring in spatial and temporal proximity to such operations are immediately under suspicion to be triggered or induced. The discrimination between natural, triggered or induced earthquakes is a difficult task, and clear rules and scientific methods are not well established or commonly accepted. The code of current practice to distinguish the possible causes of the earthquakes is not quantitative and is differently applied for different specific cases. It often leads to long and difficult questions of general liability. This situation has a negative drawback for private and public claimants and for the companies performing the operations. The planning and the estimation of an earthquake-related compensation risk is difficult to be made.

This DINSeis working group aims to review the current state of practice and to develop scientific and geophysical-based recommendations how to assess the earthquake discrimination problem. The approach relies on the observation of seismicity before, during and after the operation and includes models of stress and stress and pore pressure perturbations. Different information shall be considered in a probabilistic manner. The talk aims to present the theoretical frame of the probabilistic approach and to describe the modules that need to be implemented in the near future.

Injection-induced seismicity – lessons learned and open questions

Nicholas Deichmann¹ and Keith F. Evans²

¹ Swiss Seismological Service, Sonneggstrasse 5, 8092 Zürich, Switzerland

² Engineering Geology, ETH Zürich, Sonneggstrasse 5, 8092 Zürich, Switzerland

Induced or triggered seismicity (here taken to mean the same) is a recognised hazard in practically all engineering endeavours where stress or pore pressure in the Earth's crust are altered. This can be taken as a reflection of the realisation that has dawned in the past 20 years that the Earth's crust generally supports high shear stress levels and is often close to failure. Historically, the most damaging events, which in some cases have even caused numerous fatalities, are associated with the impoundment of reservoirs. However, earthquakes of sufficient size to threaten material damage to localities have also been associated with mining activity, long-term fluid withdrawal wells, and long-term fluid injection wells. There are also several incidences where periods of heavy rainfall have triggered seismicity.

Recently, the phenomenon of injection-induced seismicity received considerable media attention when water injection into granite at 5 km depth during the development of an Engineered Geothermal System (EGS) beneath the Swiss city of Basel resulted in the generation of a ML 3.4 earthquake. The purpose of the injection was to raise the pore pressure in the granite, thereby reducing the shear strength of fractures and fracture zones and promoting their localised shear failure. The shearing of the rough interfaces of the fractures forces them to dilate and increase their hydraulic permeability. In this way, the bulk permeability of the granite is increased so that water can be circulated through the rock and the heat extracted. The shearing movement generates earthquakes or microearthquakes, depending upon the scale of the failure, whose location can be mapped to obtain an image of the geometry of pressure diffusion within the reservoir. Such information is vital for targeting subsequent wells drilled to complete the circulation system. Shear failure activated through weakening of fractures and faults by increased pore pressure is the mechanism underlying most incidences of injection- and rainfall-induced seismicity. The pore pressure increase above ambient that is required to initiate shearing is invariably lower than required for conventional hydrofracturing operations, often substantially so, and may be less than a megapascal, reflecting the tendency for high shear stress levels in the crust.

Long-term injection of fluid generally carries a higher risk of inducing felt or damaging events than short-term injection, such as in EGS stimulation operations, since the volume of rock in which pore pressure is disturbed is expected to be larger. The largest events generally recognised as having been induced by injection fall into this category (ML 5.5 at Rocky-Mountain Arsenal; ML 4.3 at Paradox Valley). For similar reasons, the disturbed volume is also limited for balanced circulation of geothermal systems, where the produced fluid is re-injected into the same reservoir several hundred meters away. The presence of permeable structures such as faults or fracture zones will complicate the flow field. Thus, even for balanced systems, pressure perturbations can migrate greater distances along such structures, which are of greatest concern from the hazard point of view. A case in point are the subset of 'hydrothermal'-type geothermal systems that exploit the natural permeability of faults by drilling wells to intersect them. In these systems, injection and production wells

may be several kilometres apart, and the flow between the wells will occur primarily through the natural fault systems. There have been a few recent examples of these systems where felt but not damaging earthquakes have been induced by the operation of such systems (e.g. Unterhaching near Munich, Landau in the Rhinegraben).

In EGS projects, the massive 'stimulation' injections used to create permeability in the reservoir typically last for only 1-2 weeks. Such injections have routinely been performed at EGS sites since the early 70s. Given this, it is perhaps surprising that the seismic hazard associated with these operations has only recently become an issue. In large part this is because the massive fluid injections of early projects, whilst generating abundant microseismicity, did not produce events large enough to disturb the local population. Examples include the projects at Fenton Hill in New Mexico (up to 4.2 km depth; maximum ML 1.5), Rosemanowes in Cornwall, UK (2.2 km; max. ML 2.0), Hijiori in Japan (1.8-2.2 km; max. ML 2.4), Bad Urach, Germany (3.5-4.5 km; max. ML 1.8) and Soultz (3.5 km; max. ML 2.0). It is only recently that events approaching or exceeding ML 3.0 have occurred during or shortly after injections at Soultz (4.5-5.0 km; ML 2.9), Cooper Basin - Australia (4.2 km; ML 3.7) and Basel (4.7-5.0; ML 3.4). Greater depth may be a factor in promoting larger magnitudes, but it is not the only factor, since injections at the Fenton Hill and Urach EGS sites were also deep yet no felt events were generated, and injections at 6.0 and 9.0 km in the KTB main hole yielded a max. ML of 1.5.

The maximum magnitudes generated through EGS stimulation operations to date are comparable to or smaller than the largest events recorded for other types of induced seismicity. This fact alone, whilst very relevant, does not in itself satisfy public concern about the seismic risk posed by geothermal operations. Whilst it is important that the hazard be recognised and steps taken to mitigate it, it is equally important to place it into perspective. Seismic risk has not halted reservoir impoundment, mining, oil or gas extraction, or liquid waste injection. As with these other economic activities, the complete elimination of risk for EGS development and operation is not possible. This fact should be accepted. Nevertheless, it is incumbent upon us to find ways of assessing the risk, and develop practices that minimise it.

Mandatory monitoring of geothermal sites, whether they be EGS or hydrothermal, is certainly recommended. However, what is really needed by the stakeholders (including local populations) in all operations that involve the injection of fluids is the development of means to estimate the seismic risk. It is sensible to distinguish between risk estimation prior to drilling, and risk assessment after drilling when there is the possibility to directly study the seismic response to injection.

Risk estimation prior to drilling is difficult, because much of the needed information is not yet available. Once an exploration well has been drilled, it is possible to perform trial injections and analyse, perhaps in real-time, the attributes of the microseismicity that is produced, such as moment-frequency relations. This greatly enriches the information that is available for seismic hazard assessment and may be a very fruitful approach that does not depend upon parameters of physical models that are difficult to quantify in advance.

Observing and analyzing seismicity at gas production fields in the Netherlands

B. Dost, D. Kraaijpoel, T. van Eck and F. Goutbeek

Royal Netherlands Meteorological Institute, KNMI, P.O.Box 201, 3730 AE De Bilt, the Netherlands

In 1986 seismicity started in the northern part of the Netherlands, which was regarded aseismic. Early studies showed in 1993 that these events could be caused by gas production in the region and in 1995 the region was instrumented with a borehole network, designed to detect $M > 1.5$ events in the region. Later, this network was extended with accelerometers. Until summer 2010 over 650 events have been recorded and located, with magnitudes $-0.5 < M_l < 3.5$.

Nearly all locations seem to be connected to faults within existing gas fields. However, errors in the locations are large (0.5-1 km in horizontal dimensions, at least 2 km in vertical dimension) and therefore the connection could only be assumed. In two cases relative locations could be computed, due to highly correlated waveforms, reducing the location error. In one case this was combined with a downhole microseismic survey, showing a high correlation between the location of microseismic events ($M_l < -1$) and larger events ($M_l > 1$).

Another approach to improve the location is to try to explain details of the complex waveforms. We started by looking at the influence of a 1 km thick salt layer in the Groningen field, just above the reservoir. In this high velocity layer strong conversion phases are produced and we are investigating how these can be used to constrain depth.

Source mechanisms could only be calculated of a few of the larger events. Both the borehole seismograph and acceleration network data are used. The larger fields, like the Groningen field, shows normal faulting, while smaller fields show reverse faulting. The mechanism is essential as input for geomechanical modeling of the reservoirs.

In the Netherlands a seismic hazard analysis of the induced seismicity is required as part of the permitting. Therefore, the KNMI started this analysis in an early stage and regularly provides updates. These studies are open to the public and do require a careful explanation to non-experts. All aspects will be discussed.

Shear and tensile earthquakes caused by fluid injection

Tomáš Fischer¹, Alice Guest² and Václav Vavryčuk³

¹ Charles University in Prague, Faculty of Science, Czech Republic

² ESG Solutions, Geomechanical Interpretations, Canada

³ Institute of Geophysics, Academy of Science of the Czech Republic

Fluid injection into the rock formation is often accompanied by induced seismicity. This is routinely utilized in the exploitation of hydrocarbons and geothermal energy. The induced seismic events make injection audible, which makes possible to use methods of seismology to localize the fluid flow and to determine parameters of the stimulated or newly created fractures. However, in some cases, namely in the geothermal projects, the seismic activity exceeds acceptable level and may invoke concern of the population. A better design of fracturing operations and their more effective realization requires a deeper understanding of the physical processes accompanying the hydraulic fracture stimulations and also the more effective utilization of the information provided by seismic monitoring.

It has been assumed for many years that pure shear events accompany the fracturing operations. The microseismic data were routinely inverted for the double-couple (DC) component of the focal mechanism and the non-double-couple (non-DC) components were usually neglected, because the data were not of sufficient quality required for a reliable determination of full moment tensors (Nolen-Hoeksema and Ruff, 2001; Rutledge and Phillips, 2003; Vavryčuk, 2007). However, few recent studies using high-quality data (e.g. Šílený et al. 2009; Baig and Urbancic 2010; Julian et al., 2010) indicate that the non-DC moment tensors become a more frequent case. The non-DC moment tensors can be, for example, interpreted that besides shear faulting also tensile faulting caused by crack opening can take place. Therefore, a deeper understanding of the relation between resolved moment tensors and physics of the fracturing processes becomes necessary.

In the first part of this study we focus on the interplay between the state of stress, fracture network geometry and fluid injection characteristics. A common clue to the elevated fluid pressure is the presence of

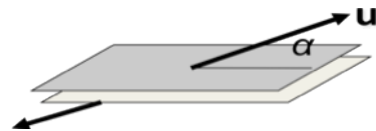


Figure. 1. The schematic model of tensile earthquake; the slip vector is deviated from fault plane by α .

opening of the fault, which results from the tensional effective normal stress acting on the fault plane. We use the non-linear Mohr-Coulomb failure criterion to resolve the stress components along the fracture in the extensional regime. We argue that the pure tensile events striking parallel to S_{Hmax} are very unlikely in the presence of natural fractures. In contrast, all fractures that are deviated from S_{Hmax} show a combined shear plus tensile faulting, which is clearly the reason why the focal mechanisms constrained to the double-couple solution have been successfully determined for many injection-induced seismic datasets. Assuming the Griffith's failure envelope, the tensile events can occur for fractures trending within 22.5° of σ_1 and for small differential stress only. The low shear traction of tensile events implies also their small stress drops. We show that different non-DC components in the injection-induced seismicity in Soultz-sous-Forêts and Cotton Valley can be explained by

different orientations of stimulated natural fractures and different differential stress in the targeted formations.

In the second part of our study we use synthetic moment tensors to better understand the type of faulting as defined by the source type plot of Hudson (1989). The composite shear-tensile fault model of Julian et al. (2010) fails in some cases to give an interpretation of the observed source mechanisms. Therefore, we use the model of tensile earthquakes of Vavryčuk (2001, see Fig. 1). In this model, the slip vector deviates from the fault surface, which results in observing a full moment tensor comprising the DC as well as the non-DC components. In the source type plot, this model projects into a line connecting +crack and -crack coordinates if a Poissonian solid is fractured (Fig. 2). However, extreme Poisson constants are required to obtain faulting of the dipole or volumetric type. In general, the tensile earthquake model allows only for CLVD and ISO components of the same sign. A composite source that can be interpreted as a sum of both tensile earthquake and explosion on a single fault or as a deformation of a volume consisting of pre-existing faults of various orientation is required to obtain a variability of observations.

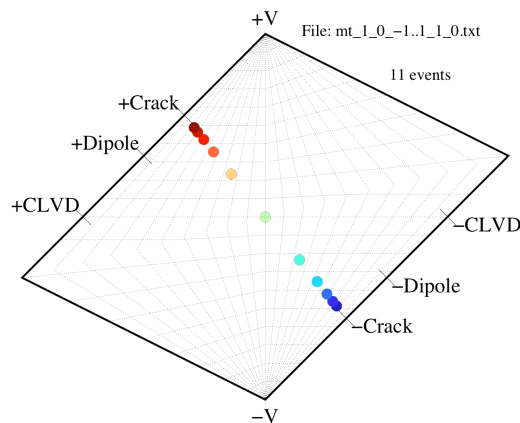


Figure. 2. The source type plot of a tensile earthquake with the angle α in the interval from -45° to 45° .

In conclusion we find that the probability of the occurrence of non-DC earthquakes depends also on the magnitude of deviatoric stress and on the existence of natural fractures and their orientation. We show that simultaneous shearing and opening is a plausible model for understanding observed source mechanisms of many injection-induced events.

References

- Baig A. and Urbancic T., 2010. Microseismic moment tensors: A path to understanding frac growth. The Leading Edge, March 2010, 320-324.
- Hudson, J. A., R. G. Pearce, and R. M. Rogers, Source type plot for inversion of the moment tensor, J. Geophys. Res., 94, 765–774, 1989.
- Julian, B. R., G. R. Foulger, F. C. Monastero, and S. Bjornstad, 2010. Imaging hydraulic fractures in a geothermal reservoir, Geophys. Res. Lett., 37, L07305.
- Nolen-Hoeksma, R. C. and Ruff J.R., 2001. Moment tensor inversion of microseisms from the B-sand propped hydrofracture, M=site, Colorado. Tectonophysics, 336, 163-181.
- Rutledge, J. T., and W. S. Phillips (2003), Hydraulic stimulation of natural fractures as revealed by induced microearthquakes, Carthage Cotton Valley gas field, east Texas, Geophysics, 68, 441–452.
- Šílený, J., D.P. Hill, D. P., L. Eisner, L., and F.H. Cornet, F. H., 2009, Non-double-couple mechanisms of microearthquakes induced by hydraulic fracturing, J. Geophys. Res., 114, B08307.
- Vavryčuk, V., 2001. Inversion for parameters of tensile earthquakes. J. Geophys. Res., 106, No. B8, 16.339-16.355.

How to better discard non tectonic events from seismicity catalogues?

Stéphanie Godey and Rémy Bossu

European-Mediterranean Seismological Centre (EMSC), Bruyères-le-Châtel, France

To provide an accurate image of the seismicity useful for seismic hazard assessment, it is crucial to properly identify the different type of events. Not all seismic events are earthquakes. Rock bursts, quarry blasts, explosions are also detected by seismic networks and without proper identification they are reported in seismic catalogues and pollute the image of the seismicity. It can, in turn, affect the computation of seismic hazard assessments.

Event type identification relies on the information provided by the local networks. However, data policies are very different. One network may properly identify a non tectonic event and not distribute it while, the neighbouring country was not able to identify it and provide data which will be seen as a seismic event. Moreover, discrimination methodologies are heterogeneous. Specific waveform analysis is pursued in some networks while others institutes are in contact with the mining companies.

The EMSC has contacted the network operators in order to have an image of the current status of their discrimination policy, aiming to discuss and to improve the event identification. We have gathered discrimination methods and policies. We have also collected lists of known quarries location and list of explosions. In this presentation, we review the results and the difference among regions.

Based on the Euro-Med Bulletin 1998-2008, we show the uncertainties in some regions and how event type identification can be inconsistent. We also present how, over 10 years, we have been able to improve non tectonic event identification in collaboration with the local networks.

While the main goal of this presentation is to review the different problems and inconsistencies encountered, solutions and common procedures still need to be achieved in the seismological community. A dedicated working group will be created and we would like to collect the opinions and ideas of the different actors dealing with non tectonic seismicity.

Seismic noise: A challenge and opportunity for seismological monitoring in densely populated areas

Jörn Groos and Joachim R.R. Ritter

Geophysical Institute, Karlsruhe Institute of Technology (KIT)

Several of the new techniques using the deep underground, such as geothermal power plants or CO₂ sequestration, have to be installed in densely populated areas to be economically successful. Geothermal power plants need access to the district heating network to efficiently use the low-temperature heat remaining after power production. Therefore, even weak and non-destructive induced earthquakes became a serious problem for operators of geothermal power plants as such events are felt by many residents. This provokes a loss of acceptance for the new technologies in the local population. The potential application of CO₂ sequestration struggles with similar problems as large coal power plants are also installed in densely populated areas. A transparent and comprehensive (seismological) monitoring of new interventions in the underground is crucial to get and keep the public acceptance.

Seismological monitoring in cities and densely-populated areas is a challenging task due to the complexity of the man-made seismic noise wave field. Especially the important identification of the small events which are unnoticeable for humans is made difficult by numerous other man-made sources of seismic energy such as traffic and industry. Man-made seismic signals are the dominant source of seismic energy in the frequency range of interest above 1 Hz. A good knowledge and understanding of the seismic noise wave field in densely populated areas is important for the successful planning and operation of seismological monitoring networks. Especially the identification of suitable measuring sites is important as the installation of entire networks in boreholes is hardly possible for economic or practical reasons. Furthermore, the reliable identification of small earthquakes requires a good knowledge of the local seismic noise wave field besides other parameters (e.g. velocity structure, etc.).

We present a statistical classification scheme in the time domain to quantify and characterise automatically the seismic noise wave field. The character of seismic noise (e.g. Gaussian distributed or dominated by single transient signals) is represented by only six noise classes. This approach allows us to easily visualise the seismic noise properties (amplitude and statistical properties). Furthermore, it provides a reduced dataset from broadband seismic waveforms to analyse temporal and spatial changes of seismic noise conditions.

We use this new classification scheme in combination with a spectral time-frequency analysis to demonstrate the most important properties of the urban seismic noise wave field especially in the frequency range important for seismological monitoring. We select representative seismological measurements in the city of Bucharest, Romania, and in the vicinity of geothermal power plants in south-western Germany for our discussion of the seismic noise wave field in large cities and densely populated areas.

Induced earthquakes during the construction of the Gotthard basetunnel, Switzerland: Hypocenter locations and source parameters

S. Husen¹, E. Kissling² and A. von Deschwenden¹

¹ Swiss Seismological Service, ETH Zurich, Sonneggstrasse 5, CH 8052 Zurich, Switzerland.

² Institute of Geophysics, ETH Zurich, Sonneggstrasse 5, CH 8052 Zurich, Switzerland.

Between the years 2005 to 2007 a series of induced earthquakes occurred in the vicinity of the multi-purpose section MFS Faido. The MFS Faido is part of the Gotthard basetunnel, which is currently being constructed in Switzerland. It is located near the village of Faido in the Ticino in the southern Alps of Switzerland. Local geology of the MFS Faido is dominated by the Leventina and Lucomagno gneisses, which are part of the Penninic gneiss zone. Furthermore, a local fault system was detected during construction of the MFS Faido. The fault system cuts the tubes of the MFS Faido at an angle of 15° ; the dip was estimated at about 80° . The brittle Leventina gneiss is located to the east of the fault zone, whereas the more ductile Lucomagno Gneiss is located to the west of the fault zone.

The earthquakes were recorded at a dense local seismic network that was installed and operated by the Swiss Seismological Service (SED) on behalf of the Gotthard Alptransit AG, the building owner of the Gotthard basetunnel. The network consisted of 12 stations arranged in two rings centered on the MFS Faido with 2-3 km and 6-10 km in diameter, respectively; two stations were installed directly in the MFS Faido. Stations were equipped with short-period seismometers (Lennartz LE-3D 1s) and strong motion sensors (Kinometrics EpiSensor ES-T). Data were recorded using Nanometrics Taurus digitizers and transmitted to SED in real-time. In total, 112 earthquakes were recorded between October 2005 and August 2007. Local magnitudes M_L ranged from -0.9 to 2.4. The largest earthquake ($M_L=2.4$) occurred on March 25, 2006. It was felt by the local population in nearby villages. Seismicity was highest from October 2005 to December 2006, with peaks of activity in December 2005, March 2006, and May 2006. Some of the earthquakes could be associated with local rock bursts in the MFS Faido, although no clear correlation between rock burst and earthquake activity was found. Earthquakes showed a high degree of waveform similarity and 12 families of very similar waveforms could be identified. Whereas 10 of these 12 families consisted only of 2-4 events per family, two families consisted of 9 and 16 events, respectively.

In order to study the processes that lead to the series of induced earthquakes we computed high-precision hypocenter locations using non-linear probabilistic and double-difference location techniques. We further computed moment magnitudes, source corner frequencies, and associated rupture radii for 53 earthquakes out of the 112 earthquakes. Absolute hypocenter locations were obtained using local P-wave velocities that were calibrated using an explosion in the MFS Faido. Relocation of the explosion indicated a location accuracy of 75 m in epicenter and 250 m in focal depth. Relative hypocenter locations were computed for all earthquakes with at least 8 P-wave observations using double-difference earthquake location (hypoDD). Source corner frequencies and moment magnitudes were computed by inverting the Fourier spectra of horizontal averaged S-wave recordings at the surface stations. Due to quality constrains (signal-to-noise ratio, number of stations) source corner frequencies and moment magnitudes could only be computed for 53 earthquakes. By assuming a

circular rupture model, rupture radii are computed using the obtained source corner frequencies. The determined moment magnitudes range from 0.4 to 2.5 and source corner frequencies range from 3 Hz to 12 Hz; associated rupture radii range from 50 m to 170 m.

Our results show that the induced earthquakes located at a distance of about 100-200 m of the MFS Faido. They occurred to the northeast of the fault zone within the brittle Leventina gneiss. Relative hypocenter locations of the two largest earthquake clusters suggest two parallel fault zones with overlapping rupture patches. The two fault zones are separated by 150 m and have a strike in NW-SE direction, which is in good agreement with the observed strike of the mapped fault system in the MFS Faido. Our results favor a model, in which earthquakes were induced due to local stress redistributions. These stresses were caused by the excavation of the MFS Faido and concentrated in the brittle Leventina gneiss to the northeast of the fault zone. Stress concentrations were then released by rupture of small patches along pre-existing fractures. These fractures are part of the mapped fault system in the MFS Faido.

Recent alternatives in seismic monitoring of geothermal sites

Manfred Joswig

Institute for Geophysics, Universität Stuttgart

Seismic monitoring at deep geothermal sites should (I) determine the potential increase of earthquakes by induced seismicity, and (II) map fracture growth during stimulation for EGS sites. The first task is routinely performed by surface networks while the increased demands of location accuracy for the second task usually require geophone borehole installations.

In this talk we will present recent alternatives of seismic monitoring systems for both tasks. In task (I), the seismic hazard monitoring, any increase must be determined relative to the historic level of background seismicity, i.e., the natural seismicity of the region prior to any subsurface modifications. This natural seismicity is well described in its statistics of occurrence by the Gutenberg-Richter relation. It states that the number of events increases by factor 8 to 10 if the seismic monitoring is extended to the next lower class of magnitudes. For example, if three events per year are observed at completeness threshold M_c 1.0, then in average one event every other day is recorded by M_c -1.0. Sensitivities that low can be reached by 'Nanoseismic Monitoring' (NM), an approach developed for nuclear arms control of CTBTO where minor aftershocks of a potential underground nuclear explosion must be detected and located even weeks after the blast. Utilizing small array surface installations and sophisticated signal processing tools, NM acts as seismic microscope to resolve weak events down to the ambient seismic noise level. Several field tests of NM in recent years yielded typical sensitivities for earthquake location of M_L -2.0 in 3 km distance. Applied to geothermal sites, NM promises to derive first estimates of background seismicity within weeks, instead of years by seismic monitoring of standard local networks.

For task (II) of hydrofrac mapping, NM comes to the limits of sensitivity. Still, a master-event technique of relative hypocenter location yields spatial resolution in the range of 10 m, sufficient for preliminary determination of fracture planes. This makes NM a cost-effective alternative to standard borehole installations. Just another, more powerful approach of surface-based monitoring is 'Passive Seismic' (PS). Originally, this technique comes from oil exploration where active seismic resolves subtle details of underground structure by large-scale stacking and migration of thousands of traces. Utilizing this asset of many-station-layouts, PS can resolve and locate the radiation of seismic energy well below the ambient noise level.

Standard seismic networks, NM, and PS will be compared by quality of location results, operation efforts, and achieved monitoring threshold.

Induced seismicity due to hydrocarbon production in the north-eastern part of Sakhalin Island: Weak motion monitoring and further prospects

A. V. Konovalov¹ and S. B. Turuntaev²

¹ Institute of Marine Geology & Geophysics of FEB RAS, Yuzhno-Sakhalinsk, Russia

² Institute of Geosphere Dynamics of RAS, Moscow, Russia

Over last decade there was an intensive development of oil and gas industry in the Sakhalin Island. Main number of the offshore oil and gas fields in the north-eastern part of the island are located in the vicinity of tectonic active faults. Over last two decades about 10 earthquakes with magnitude $M \geq 5$ occurred in this tectonic active area, in particular the catastrophic 1995 Neftegorsk Earthquake (M_W 7.2).

Many types of seismic events associated with oil and gas production, referred to in general as induced or triggered earthquakes, have been recognized or hypothesized over the past decades. There are many cases for which a connection between unusual seismicity and oil and gas production activities has been suggested in the scientific literature [Segall et al., 1994; Adushkin et al., 2000, Suckale, 2009;]. The seismic response to oil and gas production is highly variable from field to field. Some scientists [McGarr et al., 2002] assume that it is only speculative problem considering the possible connection between major hydrocarbon production and large earthquakes at midcrustal depths. Nevertheless, it is important to monitor seismic activity to advance scientific understanding of this phenomenon as it relates to oil and gas production.

Detailed seismological observations by permanent seismic local network were started in 2006, September in the north-eastern part of Sakhalin Island. Six seismic stations were equipped by KS-2000/SP short-period seismometers and SMART-24R recorders produced by Geotech Instruments, Dallas, Texas, USA. The seismic equipment was installed in the proximity to the Sakhalin-1 and Sakhalin-2 offshore production areas. The main objective of the local seismic network is to monitor and assess the potential effects of hydrocarbon production on the seismic activity.

SEISAN software [Havskov, Ottemoller, 2000] is applied for earthquake data processing. Unified database of registered seismic events and waveforms has been created. More than 500 seismic events with local magnitude $M_L \geq 1.0$ have been localized from 2006, September to 2010, March. Significant number of earthquake clusters including microearthquakes is related to mane active faults in the Northern Sakhalin and associated with a natural background seismicity corresponding to the regional tectonic stresses.

Over last five years a few moderate earthquakes occurred in the proximity to the offshore Piltun Astoskhskiye field, which is developing since 1999: 2005.06.12 M_W 5.6, 2005.09.05 m_b 4.1, 2009.08.22 m_b 4.8 (according NEIC). It seems like unusual seismicity pattern and is currently discussed among seismologists in terms of triggered seismicity due to hydrocarbon production [Tikhonov, 2010]. The summarized key arguments, which seem reasonable, are the following:

1. Time interval: level of seismic activity increases 10-20 years after beginning the oil and gas field development.
2. Spatial distribution: triggered earthquakes occur in the proximity to the oilfield production areas.
3. Frequency magnitude relation: variation of b-value.

We have analyzed the spatial-temporal and frequency magnitude distributions of seismicity according to the seismic monitoring data from 2006 to 2010 and regional catalogue from 1905 to 2005. The comparison of results showed that earthquake source distribution in the magnitude range $2 \leq M \leq 4$ is characterized by stable level of seismic activity at Northern Sakhalin including offshore oilfield production areas and may be considered as natural background seismicity. There is no significant activation of small to moderate earthquakes in examined areas.

It should be noted that activation of moderate earthquakes with magnitude greater than 4 over last two years is related to seismogenic areas at distances more than 100 km away from oilfield production areas. It cannot be associated with induced or triggered seismicity. This phenomenon should be probably described in terms of natural seismicity activation in 2009-2010 at a whole northern part of the island. Authors hope that further continuous monitoring of seismicity using dense seismic networks over the next decades will allow us to determine physical aspects of induced seismicity phenomenon.

Detailed imaging of the Basel EGS reservoir - high-precision relocation and focal mechanisms of the induced microseismicity

Toni Kraft¹, Nicholas Deichmann¹ and Keith F. Evans²

¹ Swiss Seismological Service at ETH-Zurich, Sonneggstrasse 5, 8092 Zurich, Switzerland

² Engineering Geology, ETH-Zurich, Sonneggstrasse 5, 8092 Zurich, Switzerland

The Deep Heat Mining project in Basel, Switzerland, was one of the first purely commercially oriented Enhanced Geothermal System (EGS) projects. Beginning on 2 December 2006, water was injected into a 5 km deep well with increasing flow rates. Because of strongly increased seismic activity, which included a ML2.7 event, injection had already been stopped a few hours prior to a ML3.4 event that occurred on 8 December 2006. This earthquake rattled the local population and received international media attention. Slight nonstructural damage has been claimed by many homeowners, with a damage sum of US\$7 million. Bleed-off of the injection well was initiated about 1 hour after the ML3.4 event, and hydrostatic down-hole pressure was reached within 4 days. Since then, the seismicity slowly decayed. Three additional earthquakes with $ML > 3$ were felt 1–2 months after bleed-off. More than 2 years later, sporadic seismicity inside the stimulated rock volume is still being detected by the down-hole instruments. A risk analysis came to the conclusion that similar minor, but perceived seismicity is likely to occur during the lifetime of a plant in this particular seismotectonic setting. Based on these findings the city council of Basel has decided to abort the project.

Here, we report on latest results of the analysis of the induced earthquake sequence which is one of the most densely monitored deep fluid-injections in the world. The seismic monitoring system consisted of six borehole seismometers near the injection well and of up to 30 seismic surface stations in the Basel area. The network is to a large part operational until today.

Considerable improvement of the hypocenter locations was achieved by refinement of arrival-time picks and subsequent relocation. First, highly similar events were grouped by a cluster analysis based on broad-banded waveform cross-correlation. The clusters represent groups of events that have nearly identical hypocenters and focal mechanisms. Based on this assumption we can estimate the location accuracy of the original catalog (Geothermal Explorers Ltd.) to range between 100-200m. In a second step, we improve the P and S arrival-time picks in a semi-automatic procedure by taking advantage of the waveform similarity within the clusters and the improvement of the signal-to-noise ratio by stacking. Finally, we relocate the strongest event of each cluster using the double-difference technique and apply a master-event technique to relocate the individual cluster members with respect to these events. The results indicate an improvement of the location accuracy by a factor of 10 and a reduction in the geometric complexity of the earthquake cloud.

Based on P-onset polarities, focal mechanisms of the 49 strongest events were derived. Based on relative hypocenter locations, the ML3.4 mainshock was identified as dextral strike-slip motion on a steeply dipping WNW-ESE striking fault. Overall, the observed focal mechanisms agree with what would be expected from both the in-situ stress observations and the stress field derived from the previously known natural seismicity. Although some of the focal mechanisms show signs of non-double-couple

components with a volume change, overall the results are compatible with shear failure on pre-existing faults.

To extend the moment tensor analysis to small events, that have only been recorded on the down-hole instruments, we have included relative amplitude information of P and S-onsets into the inversion. The derived focal mechanisms of events within each cluster are consistent, but their overall diversity suggests small-scale stress heterogeneity or the activation of non-optimally oriented faults.

Scaling relations of induced seismicity in picoscale: A case study from Mponeng deep gold mine, South Africa

G. Kwiatek¹, K. Plenkens^{1,2}, G. Dresen¹ and JAGUARS Research Group

¹ Helmholtz Centre Potsdam - GFZ German Research Centre for Geosciences

² Now at: Karlsruhe Institute of Technology KIT

One of the major questions in seismology is whether the faulting mechanisms of large and small earthquakes, as well as the fractures observed in laboratory experiments involves different physics (*Prieto et al., JGR 2004*). Namely, the question arises whether $M_w 7$, $M_w 0$ and $M_w -4$ events may be simply scaled by some factor. The idea of the self-similarity of earthquakes down to very small ruptures would be of practical importance for natural earthquakes as well as for induced seismicity and rockburst hazard estimates. This is because if we would know the source parameters of seismic events resulted from analysis of laboratory fracture experiments or analysis of microseismicity, we could easily extrapolate these values to those expected for larger and more devastating seismic events.

Studies of earthquake scaling relations involve analysis of magnitude-frequency Gutenberg-Richter distribution as well as comparison of static and dynamic source parameters such as seismic moment, source radius and radiated energy. Currently, the most promising results originate from analysis of micro- and nanoseismicity with magnitudes ranging $-2 < M_w < 2$. This type seismicity is obviously rarely recorded in natural environment due to the requirement of high-sensitivity local seismic networks. However, the deep mining as well as the exploitation of geothermal reservoirs allows for seismic monitoring of hazardous areas and investigation of the physical properties of induced seismicity using very sensitive seismic networks.

To study the scaling relations in nano- and picoscale ($-5 < M_w < -1$) we installed the high-sensitivity seismic network in Mponeng mine, South Africa (*Nakatani et al. SRL 79, 2*). The network, composed of one 3-component accelerometer (sensitivity from 50 Hz to 25 kHz) and 8 acoustic emission sensors (sensitivity from 700Hz to 200kHz) is located at a depth of 3543 m and covers the limited volume of approx. 300 x 300 x 300 m. The acoustic emission sensors were calibrated in-situ relative to the 3-component accelerometer and used to extend the catalogue to extremely small magnitudes ($M_w > -5$, source size of a few cm)

We investigated the magnitude-frequency Gutenberg-Richter relation for two major datasets:

1. Post-blasting activity during working days, located more than 80 m from the network. The dataset consisted of 4979 events
2. Aftershock sequence of a $M_w 1.9$ event that occurred ~30 m from our network. The final number of events analyzed equal to 9444 events.

Both datasets were thoroughly reviewed in order to remove false locations and man-made signals (drilling, debris removal). We found both datasets follow the Gutenberg-Richter frequency-magnitude relationship with no visible deviation from self-similar behavior of seismicity between $M_w -4.4$ and -1.9 for the aftershock sequence and between -3.5 and -1.5 for the post-blasting dataset. We estimated the magnitude of

completeness of selected subsets as low as -4.5 for the aftershock sequence and -3.4 for the post-blasting activity. Differences in magnitude of completeness were attributed to geometrical spreading, attenuation and site effects.

The self-similarity of earthquake occurrence relation encouraged us to analyze the source properties on piceoearthquakes in greater details. Using the calibrated acoustic emission sensors and accelerometer we estimated the source radii and radiated energies for subsets of aftershock and post-blasting datasets described earlier. The high-quality analysis of source properties was limited to 17 kHz due to the upper limit of accelerometer's frequency response which was used to calibrate acoustic emission sensors. We observed strong influence of attenuation and local geological and engineered structures on calculated source parameters. We used the spectral ratio method introduced by Imanishi&Ellsworth (*GRL 31, 2004*) to remove the propagation effects and account for the complicated travel paths and attenuation.

The calculated values of M_W ranged from -1.0 to -4.1 with corner frequencies 0.5-17kHz (source size from 10 m to a few centimeters). We observed a constant static stress drop release around 10MPa. This indicates the preservation of the self-similarity of rupture process within analyzed magnitude range. The values of E_S/E_P ratio suggests the dominance of shear type faulting events. The apparent stress ranged 0.5 MPa-50 MPa and it seems to be slightly dependent of seismic moment. The observed underestimation of energy and apparent stress may be attributed to data selection and the limited frequency band considered in our study.

Microseismic Monitoring: A Proposed Study in the Upper Rhinegraben and Experiences from the East African Rift System

M. Lindenfeld¹, G.Rümpker¹ and M. Kracht²

¹ Goethe University, Frankfurt, Germany

² Hessisches Landesamt für Umwelt und Geologie (HLUG), Wiesbaden, Germany

The northern parts of the Upper Rhinegraben exhibit enlarged temperature gradients compared to adjacent areas. Geothermal maps show a maximum with temperatures exceeding 120°C in 2000 m depth in the Rhine-Main area. Several geothermal drilling projects are planned in this region starting within the next years. Seismic monitoring is important to assess the influence of deep-heat mining on earthquake activity. It is well known that the Upper Rhinegraben shows seismic activity. Historic accounts report an earthquake swarm in this area between October 1869 and February 1871 which consisted of more than 2000 felt shocks, 190 of which had intensity IV and more. However, since that time no further macroseismic swarm events have been felt in this area. We intend to install a network of about 12 seismometers to monitor the microseismic activity prior and during the planned drilling activities. With improved localization methods (e.g. double difference algorithm) and determination of source parameters such as magnitude and fault mechanism we want to establish a comprehensive data base of the natural seismicity in the area.

The proposed study will benefit from our previous experience in monitoring microearthquakes of the East African Rift System (EARS). The University of Frankfurt has been operating seismic networks in the western branch of the EARS close to the Border between Uganda and the D.R.Congo for a number of years. Here, we located more than 800 earthquakes per month with local magnitudes ranging from 0.5 to 5.1. Vertical sections show, that towards the rift valley the focal depths range from 10 to 20 km, whereas the hypocentres go as deep as 30 km at the eastern rift shoulder. This is in good agreement with Moho-depths derived from receiver functions and implies that all of these events are located within the crust. However, we also located a cluster of 7 events that exhibit an anomalous depth of about 60 km. We can confidently locate these earthquakes within the mantle lithosphere beneath the rift. According to our present knowledge these are the deepest events so far observed within the EARS and the African Plate. We think that magmatic impregnation processes associated with dyke propagation into the mantle lithosphere may be a realistic cause for seismic radiation at the observed depth. P-wave polarities were used to determine fault plane solutions. Nearly all source mechanisms reveal normal faulting with strike directions more or less parallel to the rift axis and extension forces perpendicular to it. Crustal earthquakes northeast of the Rwenzori area are relocated with a double-difference algorithm to improve the spatial resolution of seismicity pattern. Several event clusters in the vicinity of the Fort Portal volcanic field form pipe-like structures with vertical extensions of 3 to 6 km and diameters of 1 to 2 km. In this region the rifting process is probably still in an early stage. The structures possibly indicate magmatic feeding channels through the crust that originate from the heated and impregnated lithospheric mantle.

Performance testing of forecasting models developed for induced seismicity due to enhanced geothermal systems

Banu Mena, Stefan Wiemer, and Corinne Bachmann

Swiss Seismological Service, ETH Zurich, Sonneggstrasse 5, 8092 Zurich, Switzerland.

In Basel, Switzerland a geothermal cogeneration pilot plant is being developed. The area at the southeastern margin is characterized by an increased heat flow and is known as a seismically active area. A refined micro-seismic monitoring system has been installed prior to drilling wells for visualizing micro-seismic activity before, during, and after hydraulic stimulation. The hydraulic stimulation process in well Basel-1 was stopped after six days when high seismic activity built up with magnitudes up to 2.7. Four hours after shut in a seismic event of M3.4 has been recorded, coinciding with the start of the bleeding off to hydrostatic.

A number of methods have been proposed to model seismicity due to enhanced geothermal systems (EGS), based on statistical and physical approaches. Here, we compare the forecasting performance of some of these models in a pseudo-prospective sense for the Basel EGS induced seismicity. We utilized the statistical models developed by Bachmann et al. (2010) where the focus of modeling the rates of the micro-seismicity is on two statistical models (Reasenberg and Jones, 1989; Hainzl and Ogata, 2005). In addition, we applied the physics based method of Shapiro et al. (2010), which relates the event probability to the pore pressure perturbation. Our models involve various combinations of free and fixed parameters for each of these methods. We follow similar approach as in Bachmann et al. (2010) for the updating strategy of the free parameters, the forecasting time bins, and the completeness magnitude. We performed a quantitative model performance evaluation using a likelihood test (Schorlemmer et al., 2007). The performance evaluation tests allow us to set the limitations of different models, besides their forecasting performance. We show that we can model well the seismicity rates using both approaches, however the physics based method of Shapiro et al. (2010) performs slightly better for the Basel sequence. On the other hand, it has the limitation of the total forecasting time since it cannot be used after the fluid injection is stopped.

Aspects concerning seismicity analyses of the Vidraru – Arges (Romania) dam area

Traian Moldoveanu¹, Klaus-Peter Bonjer² and Mircea Pecingine³

¹ S.C. Geotec Consulting SRL, Bucharest, Romania

² formerly with the Geophysical Institute, KIT, Germany

³ S.C. Hidroelectrica SA, Filiala S.H. Curtea de Arges, Romania

The Vidraru – Arges dam is located in a seismically active region of the Romanian Carpathian mountains. The initial filling of the reservoir started in 1965. The maximum height of the water level is 167 m and a maximum volume of $465 \times 10^6 \text{ m}^3$ water can be stored. The reservoir is operated at water levels between 100 and 150 m. The seismic hazard of the reservoir site is determined by the strong intermediate-depth earthquakes of the Vrancea zone (epicenter distances are about 140-183 km) and also of the local seismic activity of the nearby Fagaras and the Campulung focal areas (epicenter distances are about 20-40 km).

One of the strongest and well studied local earthquakes occurred on January 26, 1916 near the village of Cumpăna village, which is situated at the tail of the Vidraru reservoir at a distance of 15 km from the dam. The source parameters are: $T_0=07:37:55$ (UT), $M_S=6.5$, $I_0=VIII$ (MSK), focal depth $h=20$ km. On-scale records of the Goettingen Seismic Observatory (Germany) are presented as example below.

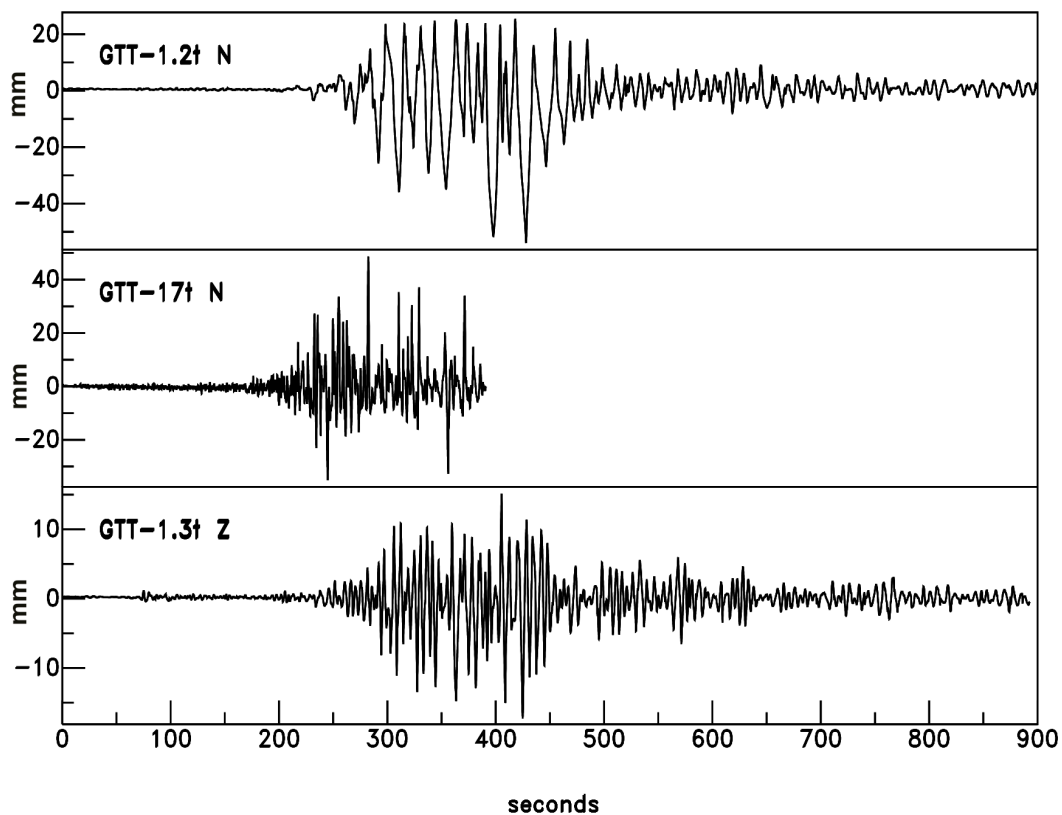


Figure 1. Fagaras-Earthquake of January 26, 1916: Wiechert-recordings of Goettingen station(epicentral distance: 11.5 degrees)

The seismic history of the dam area clearly renders a well-marked periodicity of the strong local earthquakes: 84-86 years for $I_0 > VII$ and 170-175 years for $I_0 > VIII$.

The seismic surveillance of the Vidraru-Arges dam and reservoir started in April 1975. On an average, 74 earthquakes with magnitudes between $+0.5 < M < 3.5$ are observed per year. The epicenter distribution shows a random pattern, i.e. no alignments or concentrations of foci are recognizable. Focal depths are mostly concentrated around 10 km. The comparison of the temporal changes of the seismic activity and the variation of the water level reveals that the seismic activity increases shortly after the water level decreases down to a relative minimum of about 100m. Intriguingly, the seismic activity drops down when the reservoir level reaches the maximum height. If the earthquakes are associated with a thrust regime, the repeatedly observed change in the seismic activity may be attributed on one hand to a stabilization of the seismic regime by increasing the load through filling the reservoir and on the other hand by a destabilization, i.e. triggering the activity by unloading the reservoir.

However, there is no evidence of thrust faulting in the lake area and, controversially, a composite fault-plane solution shows nearly pure normal faulting. To increase the reliability of the determination of the focal parameters in the close vicinity of the reservoir and to resolve the (apparent) discrepancy concerning these two observations, a seismic survey with 10 mobile seismic stations was performed over a period of two months. The analyses of that collected data set as well as of the seismological data, which were recorded during 35 years of continuous seismic monitoring at Vidraru – Arges dam, reveal the following:

- the existence of a correlation between the number of local shocks (with $(t_s - t_p) < 5$ seconds; epicentral distances ≤ 40 km) and the variation of the water level of the reservoir;
- the number of the local shocks increased in the periods when the level of the lake decreased (1508 shocks), and decreased when the level of the lake increased (1082 shocks);
- the confirmation of a remarkable microseismic activity in the proper reservoir area as well as in the surroundings up to about 8-25 km from the reservoir.

The seismic data, obtained during the 35 years of seismic surveillance, contribute to the refinement of the seismic hazard assessment and are used for the seismic computation of the periodically performed checking of the reservoir dam.

Microseismic monitoring of fluid injection at the Longyearbyen CO₂-Lab, Svalbard

Volker Oye¹, Hom Nath Gharti¹, Daniela Kühn¹ and Alvar Braathen²

¹ NORSAR, Gunnar Randers vei 15, 2007 Kjeller, Norway

² The University Centre of Svalbard, UNIS

The Longyearbyen CO₂ storage lab project addresses the problem to turn Svalbard into a CO₂ neutral community. The project has now reached the stage to demonstrate and study and monitor sub surface CO₂ storage over time. The construction of the Longyearbyen CO₂ storage lab will start as soon as the geometry of the reservoir has been determined. Liquids other than CO₂ have been used in this initial phase (water, brine, gel). The reservoir below Longyearbyen is considered physically open (no closure) and, therefore, will likely experience drift of the injected CO₂ plume towards the North East, through gradual mixing and expulsion of saline groundwater. This offers a unique opportunity for studying the behavior of CO₂ in subsurface saline aquifers. A number of monitoring wells will be drilled for this purpose. Attention is paid to the distance of approx. 15 km from the injection site where the reservoir appears at the surface. This fact and others will be considered in reservoir geo-models and subsequent flow simulations, which will predict flow in the reservoir and substantiate the odds for CO₂ leakage.



Figure 1: left: Installation of the 5-level 3C-geophone string at the CO₂ lab. Right: deployment of borehole seismometers at 12 m depth, well within the permafrost.

In August 2010 a fluid injection experiment has been carried out at the CO₂ lab and a microseismic monitoring network has been deployed close to the injection well. The network consists of a 5-level string of 3-component geophones in a vertical observation well, with 50m distance between the instruments and a maximum depth of 296 meters. In addition, three shallow boreholes of 12 m depth have been drilled at about 500 m distance to the injection well in order to provide more accurate microearthquake locations. The deep borehole had an inner diameter of only 67 mm, therefore we decided to use small 15 Hz geophones for the deployment and sampled at 1000 Hz. All 24 channels of the geophones were connected to a GEODE digitizer and a PC, which is connected to a fast internet connection, sending data in real-time to NORSAR where the data is automatically processed.

The data processing includes standard filtering, detection and association of phases using STA/LTA and beamforming methods, respectively. P- and S-wave onsets are estimated by filtering with an autoregressive model and subsequent application of the

AIC criterion. The localization is generally conducted with the iterative master event method (Oye and Roth, 2003). Different location methods using envelop stacking (e.g. Gharti et al. 2010) will also be considered for selected periods where additional data from seismic lines are available.

We have also started to investigate temporal changes in migrated seismic sections, which might be due to large-scale CO₂ injection. For this task we introduce new functionalities within NORSAR's SeisRoX software that can perform 4D seismic modelling. We will then correlate the results from the microearthquake locations with the 4D seismic modelling results and potentially with real 4D seismic data, if available.

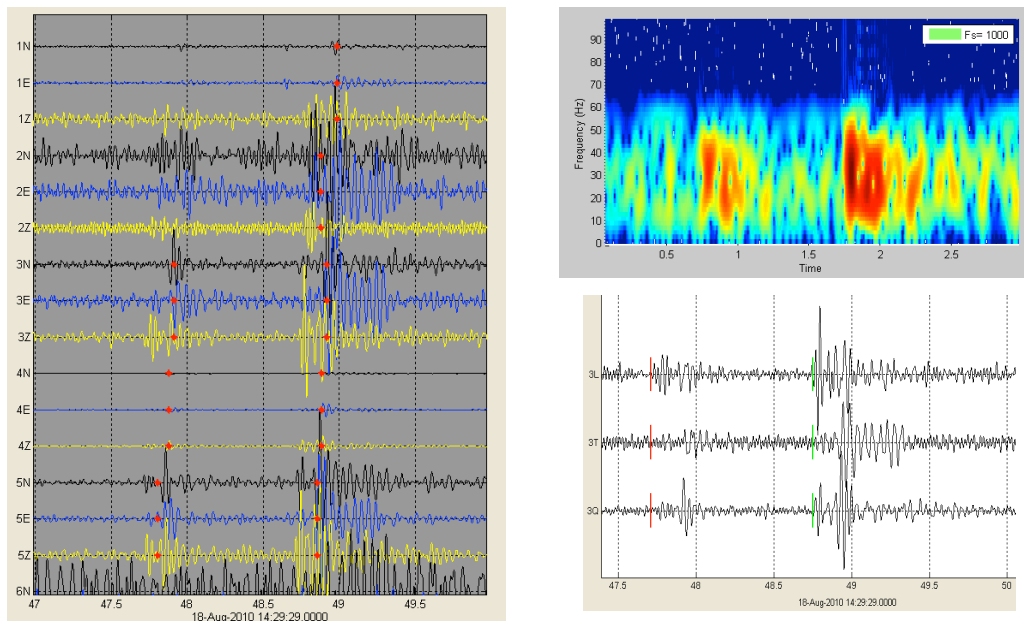


Figure 2: left: Example of two microearthquakes that follow up quickly after each other (about 1 sec) recorded on the 5 downhole geophones. Right: Spectrogram of the vertical trace of geophone 3 showing dominant frequency content from 10 to 60 Hz for both events. The lower figure shows the seismograms rotated into the local ray coordinate system. The red and green bar show the P-wave onsets of the first and second event, respectively.

References

- Gharti, H. N., V. Oye, M. Roth, D. Kühn, 2010. Automated microearthquake location using envelope stacking and robust global optimization, *Geophysics* 75, MA27 (2010); doi:10.1190/1.3432784.
 Oye, V., Roth, M., 2003. Automated seismic event location for hydrocarbon reservoirs, *Computers & Geoscience*, 29, 851-863.

Monitoring of microseismic activity around the GeneSys deep geothermal drilling site, Hannover (Germany)

T. Plenefisch, U. Wegler, M. Keyser and E. Wetzig

Federal Institute of Geosciences and Natural Resources (BGR), Stilleweg 2, 30655 Hannover, Germany

In the framework of the GeneSys-project (Generated Geothermal Systems) a borehole was drilled at the Geozentrum Hannover down to a depth of 3900 m. The aim of the project is to extract geothermal energy from one single borehole to heat the buildings of the Geozentrum. The borehole is drilled in mid-triassic sandstone formations of the Northern German Basin.

Collaterally to the drilling and the upcoming heat production phase BGR has installed a seismic network around the drilling hole to monitor and analyze possibly induced seismic micro-events, especially induced by the fracking activities which are planned in the beginning of 2011. Altogether, the network consists of 13 seismometers or geophones respectively. 5 geophones are installed in 100 m deep boreholes and build the inner circle of the network within a radius of approximately 1 km around the geothermal borehole. A second circle with a radius of 4 km is equipped with 1 Hz seismometers. Two additional geophones are installed in boreholes of 180m depth.

Due to the position of the borehole in direct vicinity to the major city of Hannover and several highways nearby the noise conditions are relatively bad for the detection of small seismic events. The noise conditions as well as the position of Hannover in a more or less aseismic area allows us to detect only a few seismic events up to now. These are for example a controlled detonation of an aircraft bomb in a distance of about 3 km or mining induced events of magnitude 3.5 - 4.0 in the Polish mining area. The only event which is directly connected to the geothermal project and we have detected so far, is the recording of the perforation shoot which took place at a depth of 3706 m on the 20th June 2010.

In the poster we present the design of the seismic monitoring system, the data flow as well as an automatic detector which is tested on the data streams to detect small events in case of difficult signal-to-noise conditions. Furthermore, we show some data examples, an estimation of the sensitivity of the network and we compare the conditions of the GeneSys-borehole with those of other geothermal projects in Germany.

On the potentials and limitations of a seismic network's sensitivity when monitoring induced seismicity

K. Plenkers^{1,2}, D. Schorlemmer³, G. Kwiatek¹ and the JAGUARS group

¹ German Research Centre for Geosciences GFZ Potsdam

² now at: Karlsruhe Institute of Technology KIT

³ University of Southern California, Los Angeles

The recording of seismic events is crucially depending on the sensitivity of the recording network. This is especially true for induced seismicity as most induced events display magnitudes $M < 2$, which is near the lower limit of most recording networks.

To give some insights into the potentials and limitations of recording networks, we present a detailed study on the spatial-distribution of recording completeness of the JAGUARS (Japanese German Underground Acoustic Emission Research in South Africa)-network that is today one of the most sensitive seismic networks existing, monitoring induced seismicity in Mponeng Gold Mine, Carletonville, South Africa (*Nakatani et al. SRL 79,2, pp.311, 2008*). Seismic networks in mines have the advantage that the realization of short source-receive distances is possible, which can increase the network's sensitivity. Mine networks thus allow to study micro- ($M=0$ to 2), nano- ($M=-2$ to 0) and pico- ($M=-4$ to -2) seismicity that is missed in most surface networks monitoring induced seismicity.

The JAGUARS network monitors induced seismicity at very high-frequencies (frequency range 700 Hz to 180 kHz) at seismogenic depth (-3540m) inside Mponeng Gold Mine in Carletonville/Republic of South Africa (*Nakatani et al., SRL, pp.79311, 2008*). It incorporates a triaxial accelerometer as well as acoustic emission (AE) sensors. The magnitude range monitored is $-5 < M_w < -1$ (*Kwiatek et al., BSSA, 100, pp.1165-1173, 2010*). The observational volume monitored is approximately 300m x 300m x 300m in size. Seismicity is induced by ongoing mining activity that is located as close as approximately 100m from the network. During two years of passive monitoring several hundred thousand seismic events were detected (*Plenkers et al. SRL, 81, pp.467-479, 2010*).

We analyze the completeness of the JAGUARS network using the probability-based magnitude of completeness (PMC) method of *Schorlemmer and Woessner (BSSA, 98, pp.2103-2117, 2010)*. Unlike traditional completeness estimation methods, the PMC method is based on detection probabilities rather than on earthquake samples. Because it takes into account the location of stations and recorded events, it allows to resolve the spatial distribution of magnitude of completeness. In order to incorporate the complex heterogeneities in the observational space of the JAGUARS network, as e.g. geological boundaries and cavities, we develop the extended PMC method that allows to analyze the observational space in three dimensions by taking into account the direction of observation.

We estimate the magnitude of completeness of the JAGUARS network to vary in space between -4.8 and -3.0. We demonstrate that the completeness is not solely depending on the distance to the network but is affected crucially also by local heterogeneities. We estimate that areas introducing local damping to high frequencies,

as e.g. highly-fractured rock or dominant geological boundaries, reduce the recording completeness in that area noticeably. We compare the spatial-distribution of magnitude of completeness with the spatial distribution of high-frequency recording. We estimate that the complete recording of seismic events with magnitudes below -4.5 requires the recording of frequencies $f > 100\text{kHz}$ and the recording of events with magnitudes below -4 the recording of frequencies $f > 25\text{kHz}$. The recording of seismic waves with frequencies $f > 100\text{kHz}$ was realized for distances up to 30m; with frequencies $f > 25\text{kHz}$ up to 110m.

The results demonstrate that the complete recording of seismic events with magnitudes $M_w > -4.8$ in mines is possible in limited areas. The results demonstrate clearly that high frequency recording is necessary to record very small magnitudes. Local heterogeneities that increase the attenuation of high-frequency waves reduce the probability of recording significantly.

We demonstrate the effect of recording limitations owing to the sensitivity of the seismic network by comparing the JAGUARS network with the mine's seismic network. The mines network extends throughout the mine and incorporates mainly 4.5Hz three-component geophones. Frequencies below 15kHz are monitored, which results in the recording of magnitudes $M > -2$. On December 27th, 2007 a magnitude $M_w = 1.9$ event occurred about 30m from the JAGUARS network (*Yabe et al. Earth Planets Space, 10, e49-e52, 2009*). The mainshock and 25 aftershocks were recorded by the mine's seismic network. The JAGUARS network recorded 25,000 aftershocks, delineating clearly the rupture plane (*Naoi et al., GRL, submitted*). The results of the JAGUARS project suggest that a large portion of seismic activity is nowadays missed in the recording of induced seismicity, also it could give valuable information about the deformation process.

Relationship between Reduced Injection Rates and Reduced Induced Seismicity - 3 Years of Field Data from the Commercial Geothermal Power Plant Landau (Germany)

B. Schmidt¹, B. Rogulic² and J. Ritter³

¹ Geological Survey Rhineland-Palatinate

² geo x GmbH Landau

³ Karlsruhe Institute of Technology

Relatively short-term injections to induce hydrofractures for oil, gas or geothermal recovery pose little or often no induced-seismicity threat to the public. This behaviour was also observed during induced seismicity that occurred during stimulation tests in the area of Landau and Insheim (Southwest Germany) since November 2007. However, during geothermal power production a magnitude 2.7 (*ML*) seismic event on August 15, 2009 and a *ML* 2.4 seismic event occurred in summer 2009 underneath the center of Landau, close to the geothermal site. These events triggered a significant number of adverse comments to geothermal power production by the local and international press, concerning the unclear hazard due to induced seismicity. This reaction could adversely affect the development of the geothermal energy sector in Germany, especially in SW Germany. Even though, a correlation between the reinjection pressure at the geothermal site and the seismic events is not proved, authorities defined a strict, relatively low limit to the reinjection pressure in order to prevent future seismic events.

We present our research on potential relations between the geothermal activities and the seismicity rates before September 2009 (incl. the occurrence of events with increased magnitude) and after December 2009 with reduced injection pressure. Seismological data are compiled from industry (geo x), university (KIT) and earthquake services (LED, LER, BGR).

Towards quantifying the seismogenesis of fluid injections in rocks

S. A. Shapiro, C. Dinske, C. Langenbruch, F. Haney and J. Kummerow

Freie Universität Berlin, FR Geophysik, Malteserstr 74-100, 12249, Berlin, Germany

Recently we have found that under rather general conditions a number of fluid-injection induced earthquakes with a magnitude larger than a given one increases approximately proportionally to the injected fluid mass. This is the case in Enhanced Geothermic Systems as well as by hydraulic fracturing of hydrocarbon reservoirs. Here we show that using the seismicity rate of such events and the fluid injection rate a parameter (seismogenic index) can be derived, which quantifies the seismotectonic activity of the injection location. This index is independent of injection parameters. It is only a function of tectonic features of the injection site. The seismogenic index can be used to quantitatively compare different tectonic locations of a possible fluid injection (e.g., for a geothermic or a CO₂ injection) in terms of a potential risk to induce an event of a magnitude larger than a given one. Along with injection parameters, knowledge of the seismogenic index permits to estimate the occurrence probability of a given number of such events during a given time period. Moreover, the seimogenic index can be used for feasibility studies of microseismic monitoring.

As a particular case study we use an injection experiment at the German Continental Deep Borehole (KTB). We determine magnitudes of microseismic events measured at the single borehole seismometer during the injection phase 2004/2005. Standard magnitude determination could not be used because of the limitation that most events (95%) have only been recorded at one single borehole seismometer and only few at near surface seismometer. Furthermore, the borehole seismometer was installed at four different positions during the different time periods of the experiment. Its orientation and coupling was different and unknown. The magnitude estimation included three steps. First, local magnitudes of the larger events were estimated with a standard method based on amplitude measurements at near surface stations. Second, we investigated a series of parameters to characterize the size of these events using the seismograms of the borehole sensor, and we compared them statistically with the local magnitudes. Third, we extrapolated the regression curves for events that have been only measured at the borehole seismometer to obtain magnitudes of all recorded events. Using these data we also were able to estimate the seismogenic index at the KTB location.

A consideration of seven case studies shows that the largest seismogenic index characterises the Basel geothermic site. The smallest ones are observed at hydrocarbon reservoirs and at the KTB (after a fluid-extraction experiment). It has been already earlier found that injections at geothermic sites are characterized by lower b-values than injections at hydrocarbon reservoirs. From this study it becomes clear that geothermic locations are often characterized also by higher seismogenic index. These two factors explain the observation that geothermic injections have a tendency to induce significant events more frequently than hydrocarbon ones. On the other hand this observation implies that microseismic monitoring of hydrocarbon reservoirs usually requires a higher level of sensitivity than such a monitoring of geothermic systems.

Laboratory study of temporal-spatial peculiarities of microseismicity spreading due to pore pressure change

S. B. Turuntaev, E. I. Ereemeeva and E. V. Zenchenko

Institute of Geosphere Dynamics, Russian Academy of Sciences, Moscow, Russia.

A possibility to use data on microseismicity variations in space and time due to pore pressure change for estimation of the permeability is considered.

The analysis is based on laboratory experiments made for study of relation between acoustic emission (AE, which corresponds to microseismic events in real scale) activity and pore pressure change due to water injection/release into/from a porous sample under load.

The study showed a possibility to resolve an inverse problem of defining local permeability by registering microseismic activity variation in particular volume of the porous medium.

Experiments were made with the help of laboratory setup (Fig.1), which consists of long rod (1060 mm in length) with rectangular cross-section (117×82.5 mm). A channel with rectangular cross-section was milled in the rod. The channel was filled by a mixture of pebbles and crushed pine rosin in proportion 1 to 3; then the sample was vertically loaded. A number of pressure and acoustic emission sensors were placed at both lateral and bottom sides of the rod. Assembled setup was vacuumized and filled by distilled water. Valves at both tips of the box were used for fluid injection (through inlet) and pore pressure release (through outlet).

In one set of the experiments, pumping unit injected water into the cell with constant flow rate $0.35 \text{ cm}^3/\text{s}$. Vertical load was maintained constant. The water injection leads to the pore pressure increase along the cell. In another set of the experiments, the pore pressure was increased by water injection into undrained cell up to 10-11 MPa, then, after 3 hours from the pore pressure increase, the pressure was released through the outlet. Typical duration of the AE pulses record was 100 seconds in both sets.

The experimental study showed close relation between change of pore pressure with time and variation of mean acoustic event activity. A model is suggested which describes a relation between acoustic events and pore pressure change in time. The model is based on an assumption that the events occurred when pore pressure reaches a critical value, which is distributed under some probability function. As the probability functions, Weibull distribution, Gaussian error function and Log-normal distribution were considered. The comparison of AE mean activity change in time with calculation based on considered models showed that Weibull distribution is preferable (Fig.2). In case of pore pressure increase, the value of pore pressure defines the number of AE events; in case of pore pressure decrease, a difference between external load and pore pressure can be considered as a critical value for AE events triggering.

The study showed significant change of permeability on non-stationary stage of fluid flow during both pore pressure increase and decrease. Permeability variations were calculated based on data of pore pressure change in time at several points along the

sample and with the help of microseismic activity variation data. Results of permeability evaluations based on two above methods are compared with each other (Fig.3). It was found that permeability variation as well as resulting permeability on stationary stage can be estimated by means of microseismic activity registration.

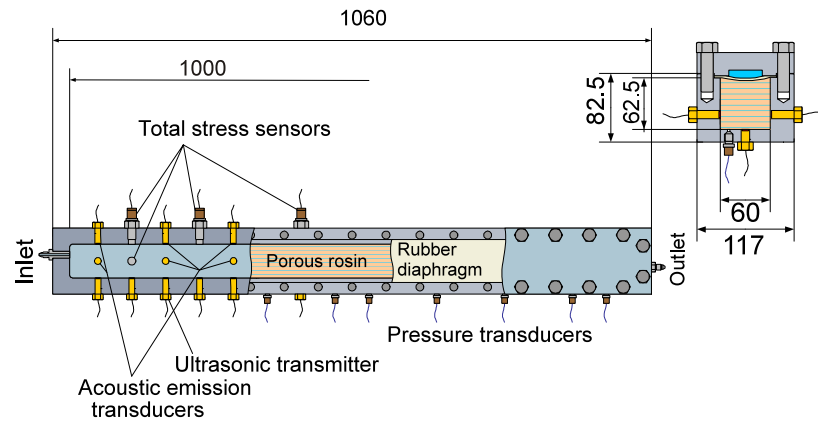


Figure 1. Layout of the laboratory setup.

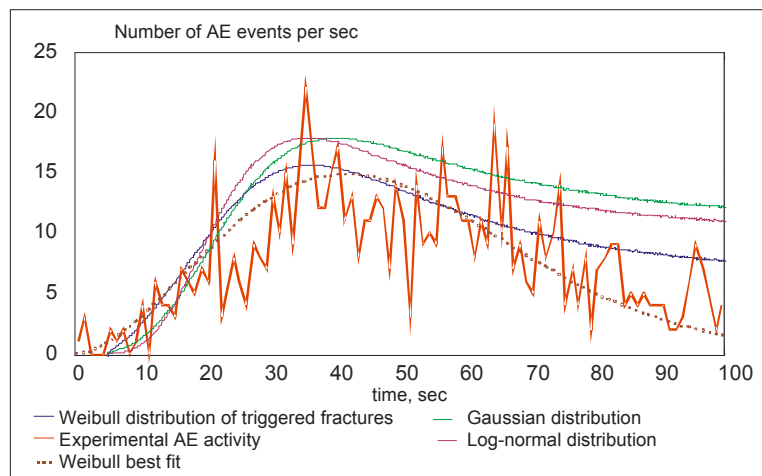


Figure 2. Comparison of experimental data on AE activity change in time during water injection with mean AE activity calculated in accordance with several critical pressure

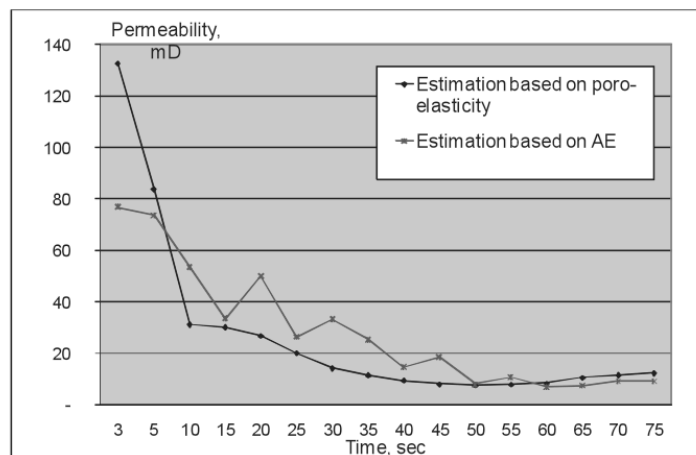


Figure 3. Comparison of permeability changes in time, estimated by different methods based on AE activity.

Non-linear analysis of seismic regime response to electromagnetic powerful source actions

S.B. Turuntaev and O.Yu. Melchaeva

Institute of Geosphere Dynamics, Russian Academy of Sciences, Moscow, Russia.

A study of strong EM pulse actions on seismic regime in the region of Bishkek test site (Kyrgyzstan) is made with the help of non-linear dynamics methods. It is supposed that, if any change in seismic regime regularities occurs due to EM actions, it will be reflected in corresponding dynamic system parameters at least. The obtained results show an increase of seismic regime regularity after beginning of EM pulses action. The model of possible reaction of the geomechanical system governed by rate-and-state friction law on perturbations due to EM actions is considered numerically. It was found, that small change of fault and fracture strengths under EM action leads to diminishing of attractor and embedded space dimensions.

Introduction

A possibility to change seismic regime characteristics by strong electromagnetic field excitation in rocks was studied experimentally in several research works at Garm test site, Tadzhikistan, and Bishkek test site, Kyrgyzstan. A short-time increase in the daily number of minor earthquakes, a concentration of the earthquake epicenters near the electromagnetic field source and some others aftereffects of the EM-field excitation were reported (Tarasov and Tarasova, 2004, Velikhov et al., 2006). Meanwhile both physical mechanism of EM action on seismic processes and confident detection of EM seismic effects are not resolved yet definitely. A complexity of the full geomechanical model of geophysical medium, which should include an interaction between mechanical processes and fluid flows, makes it worth to look for generalized approaches to the description of the complex systems, developed at present in nonlinear dynamics. One of the attractive and, perhaps, most frequently used methods is the procedure of determination of a dimension of an attractor, corresponding to a stable state of analyzed system, and the determination of the minimum dimension of the space, containing this attractor – embedded space (Grassberger and Procaccia, 1983). The last one can be interpreted as the number of the independent variables necessary for description of the considered system behavior in the stable state (Malinetsky and Potapov, 2002).

In the presented paper, a study of strong EM pulse actions on seismic regime in the region of Bishkek test site is made with the help of non-linear dynamics methods. It is supposed, that if any change in seismic regime regularities occurs due to EM actions, it will be reflected in corresponding dynamic system parameters at least.

The study of the seismic activity variations is made by means of the phase portrait reconstructions and calculations of the portrait parameters (an embedding space dimensionality and correlation dimension of an attractor, if that one exists). It is shown that the influence on the geophysical medium leads to increase of regularity of the seismic regime. The model of possible reaction of the geomechanical system governed by rate-and-state friction law on perturbations due to EM actions is considered numerically. It is shown, that small change of fault and fracture strengths under EM action leads to diminishing of attractor and embedded space dimensions.

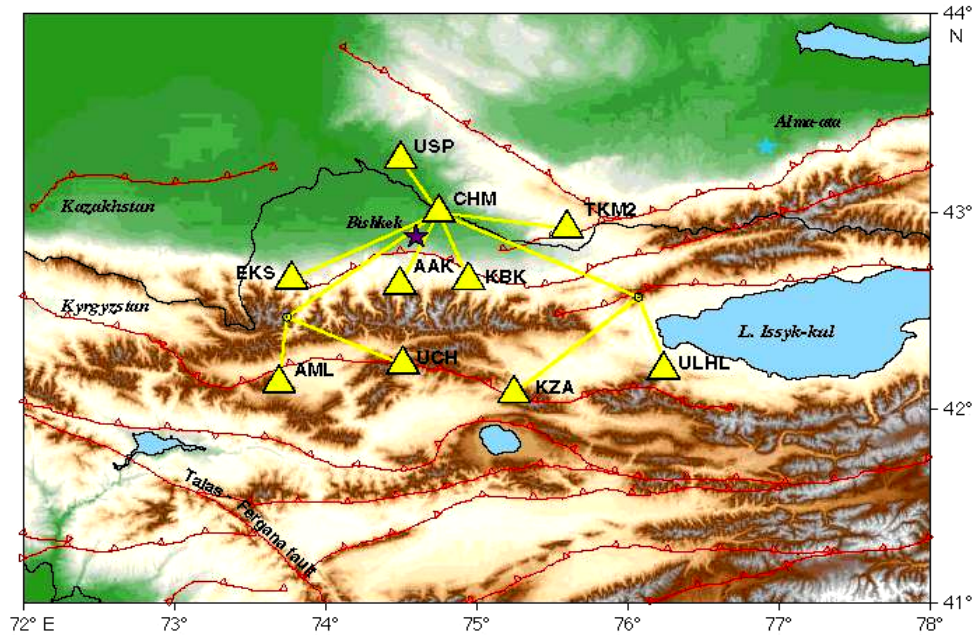


Figure 1: Map of the studied region and KNET seismic station locations. Yellow lines show telemetry links.

Data characteristics

As a source of EM actions, a powerful electro prospecting installation ERGU-600-2 was used. Probing pulse of ERGU-600-2 represents a series of periodic sign-changing square pulses of a current with amplitudes 600-800A and the period 10 sec. Duration of one session was about 20 minutes. The total duration of the experiment was 6 years (since 2000 till 2005). The details of the experiment were published by Velikhov et al., 2006. The analysis of seismic activity was made on the basis of local seismic network data (KNET, Fig. 1). The catalog contains 6623 earthquakes with magnitudes $M=1-6$, registered from 6.01.1994 till 12.30.2008 in the area with coordinates $\varphi=37.35-45.77$ N; $\lambda=68.67-82.24$ E.

The considered area of possible EM excitation influence was 200x200 km in size with the center coincident with EM source position.

Analysis method

The earthquake catalog was divided into two parts of the same durations: before EM excitations and during the excitations. Seismic activity was calculated as a sum of cubic roots from energies of seismic events occurred during a week (3 days overlap of the time intervals was used). The obtained time series were analyzed with the help of Grassberger-Procaccia method of correlation integral calculation for different embedding space dimensions. The integral was calculated as follows:

$$C(\varepsilon) = \frac{1}{N^2} \sum_{\substack{i,j=1 \\ i \neq j}}^N \theta(\varepsilon - \|z_i - z_j\|)$$

where \bar{z}_i is the vector describing position of a point in phase space at the moment of time $t_i = t_0 + i\tau, i = 1 \dots N$, τ is the time delay (lag), N is the sample volume, $\theta(x)$ is

the Heaviside's function: $\theta(x) = \begin{cases} 1, x \geq 0; \\ 0, x < 0. \end{cases}$, m -dimensional vectors \vec{z}_i are obtained by shifting of the original time series x_i by a fixed lag τ .

The value $C(\varepsilon)$ defines relative number of pair points, the distance between which is no greater than ε . At small ε the correlation integral $C(\varepsilon) \propto \varepsilon^d$ therefore the attractor dimension d can be estimated on an inclination of linear dependence of $\ln C$ on $\ln \varepsilon$: $\ln C(\varepsilon) \cong d \ln \varepsilon + c$. Parameters of the time delay were chosen based on autocorrelation functions.

Results

The variations of the seismic activity in time are shown in Fig. 2 for the time periods before EM action start and during actions of EM source.

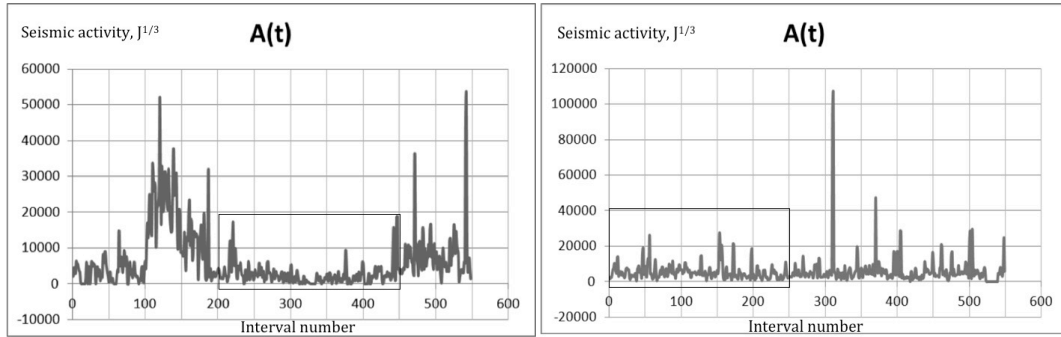


Figure 2: Change of the seismic activity in time before (left graph) and after (right graph) EM action start. On the X-axis the numbers of consecutive intervals for which the seismic activity was calculated are postponed.

The correlation integral was calculated for several dimensions of embedded space, which were varied from 1 to 20. Obtained relations between the fractal correlation dimensionality and the dimensions of the embedded phase space are shown in Fig. 4. Dimensionless time delay values (or lags - the value of shifting the time interval used for seismic activity calculation) were chosen based on autocorrelation function local minimums (Fig. 3); their meanings are shown in Fig. 4. It can be concluded that during EM actions the correlation dimensionality diminishes from 7.4-7.8 to 4.7-5.2, the embedded space dimensionality decreases from 14 to 6.

One can suppose that some natural perturbations of seismic regime could influence the above results. To avoid it, the calculations were made for the periods of observations, which have no significant peculiarities. The periods are shown in Fig. 2 by rectangles. Dependences of the correlation dimensionality on the embedded space dimensions are shown in Fig. 5. It can be seen, that before the EM action start, the seismic process didn't show any stable state indications, while during EM action the seismic process gains an attractor of dimensionality 5.6-6.0.

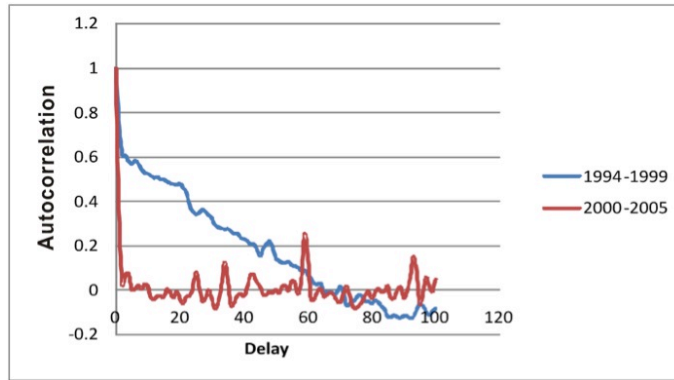


Figure 3: Autocorrelation function before (1994-1999) and during (2000-2005) EM actions. Time delay is dimensionless unit.

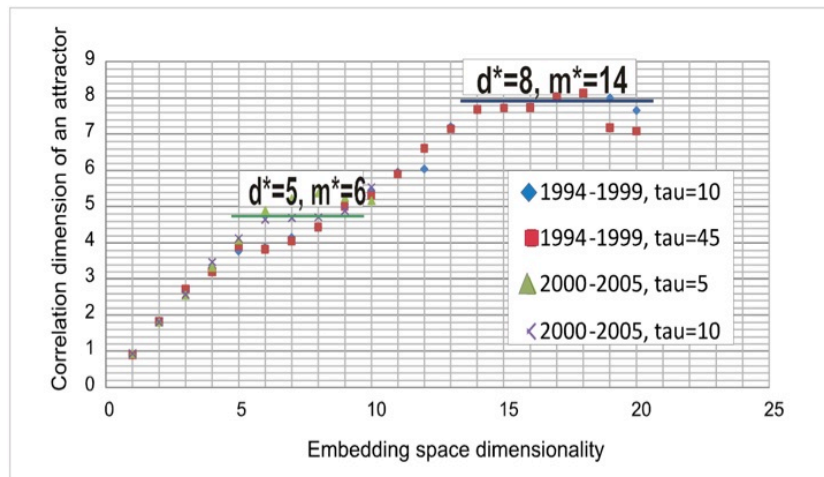


Figure 4: Fractal correlation dimension vs. embedding space dimensionality of the seismic activity before and during EM actions.

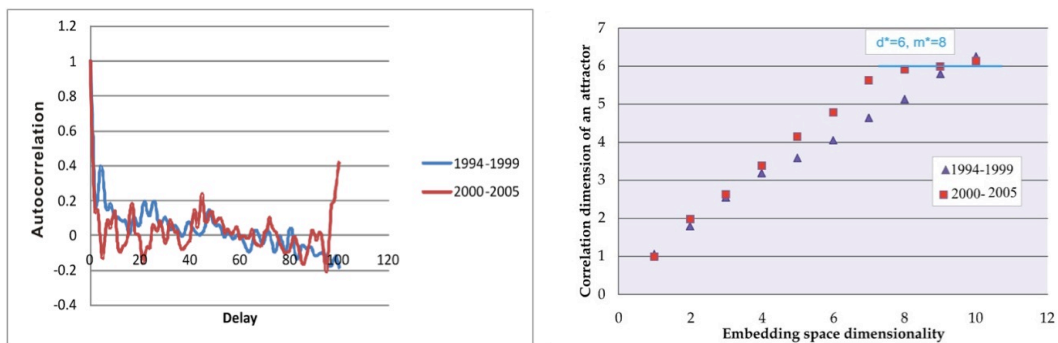


Figure 5: Autocorrelation functions (left graph) and fractal correlation dimension vs. embedding space dimensionality of the seismic activity before and during EM actions for time periods without peculiarities.

Model

To analyze the obtained results, we consider the widely used “stick-slip” model of seismic regime with “rate-and-state’ friction law for description of the movements along tectonic faults. The main distinctions of used approach from the common one (see, for example, Hobbs, 1990; Erickson et al., 2008) are the followings: we consider two-parameters type of the friction law and we vary the value of critical shear stress. The motion equation can be written as

$$m\ddot{u} = k(vt - u) - \tau s,$$

where k is stiffness, v is velocity at infinity, τ is frictional shear stress, which can be written as

$$\tau = \tau^* + A \ln(v / v^*) + \theta_1 + \theta_2.$$

Here τ^* is critical shear stress, which can be changed by EM actions,

$$\tau^* = C + \mu(\sigma - p),$$

C – cohesion, μ – friction coefficient, p – pore pressure, σ - normal stress, θ_i - state variables which characterize sliding surface state:

$$\dot{\theta}_i = -\frac{v}{L_i} [\theta_i + B_i \ln(v / v^*)],$$

where L_i are characteristic dimensions of the fault roughness. Values of parameters in the above equations were taken from experiments (Gu et al., 1984), and are shown in Table 1.

Table 1: Parameters of the “rate-and-state” equation.

A	B1	B2	L1	L2	v^*
$5 \cdot 10^4 \text{Pa}$	$1 \cdot 10^5 \text{Pa}$	$1 \cdot 10^4 \text{Pa}$	$1 \cdot 10^{-2} \text{m}$	$1 \cdot 10^{-3} \text{m}$	10^{-1}ms^{-1}

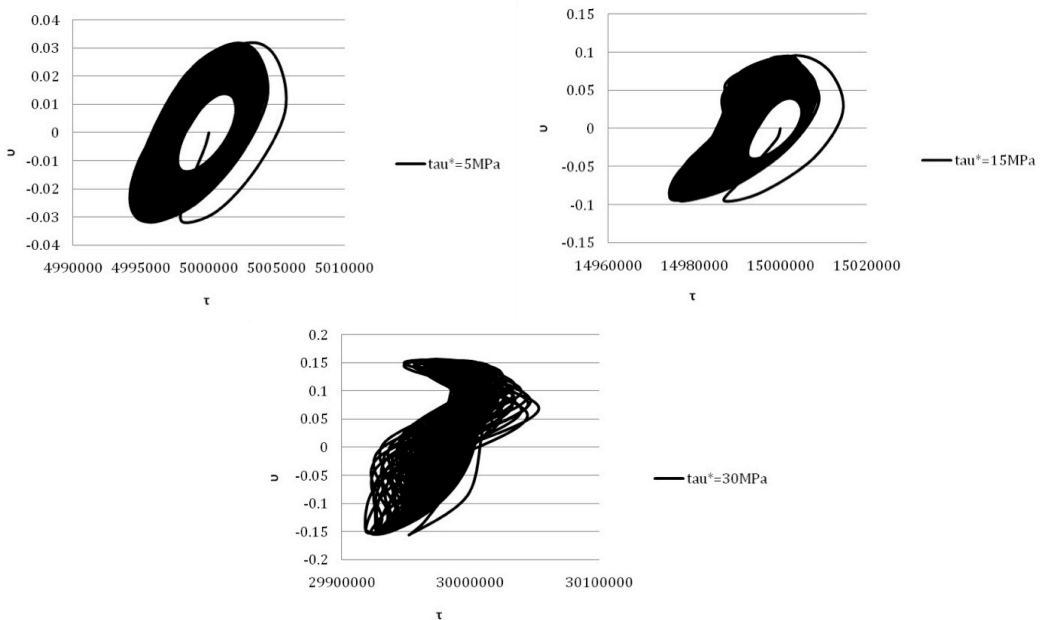


Figure 6: Projections of phase trajectories of a fault sliding on τ - v plane for several values of critical shear stresses. τ is in Pascals, v is in m/s.

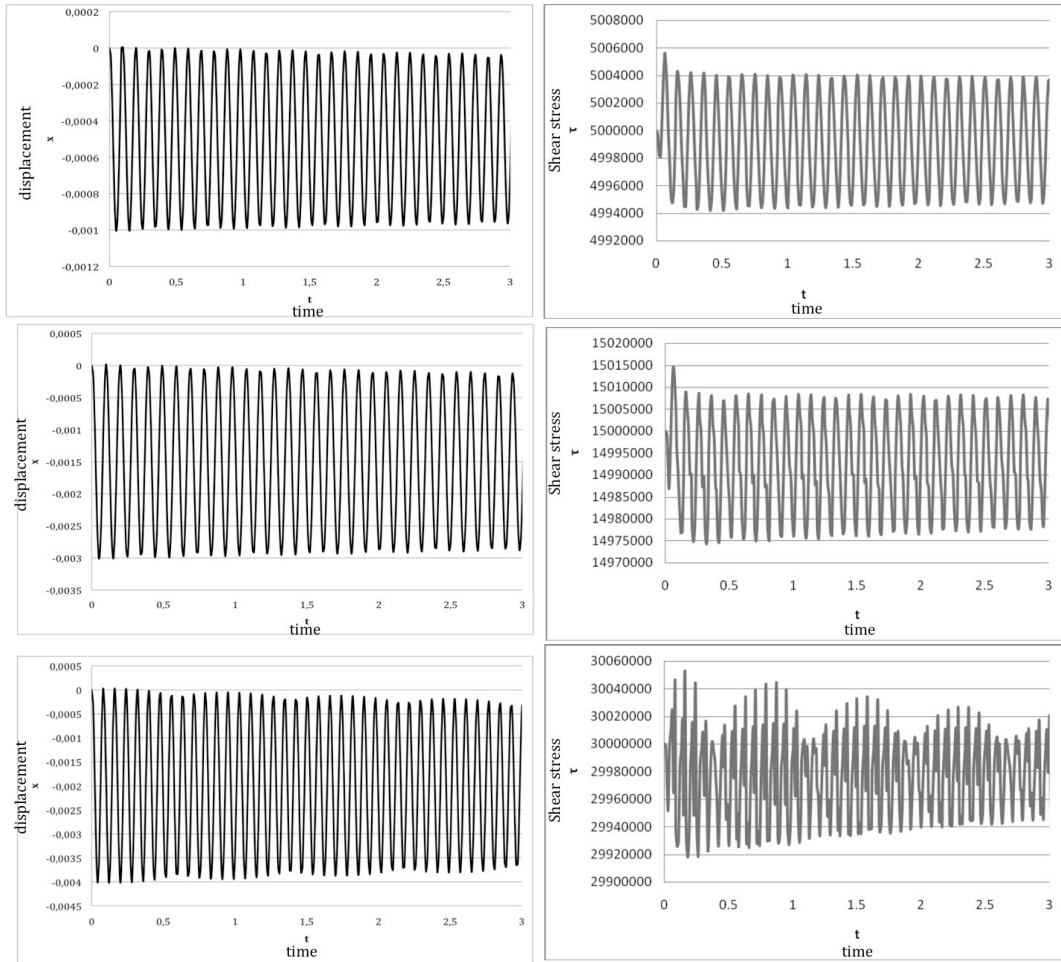


Figure 7: Dependencies of shear stresses τ (Pa) on time and displacement x (m) on time for several values of critical shear stresses (from left-up to right-down): $\tau^*=5\text{MPa}$; $\tau^*=15\text{MPa}$; $\tau^*=45\text{MPa}$.

Results of numerical calculations for several values of critical stresses are shown in Fig. 6 as projections of the phase trajectories on t - v plane. Dependencies of shear stresses on time and displacement on time are shown in Fig. 7. The time is in arbitrary units.

It was found that if the critical stresses increase, the system behavior changes significantly. Oscillations of the fault sliding become nonharmonic, and when the critical stresses reach 45 MPa, the oscillations become quasi-chaotic (Fig. 7). An estimation of the obtained attractor dimensions by Grassberger-Procaccia method showed that an increase of the critical stresses results in an increase of the attractor correlation dimensionality: $\tau^*=5\text{MPa} - 1.4$; $\tau^*=15\text{MPa} - 1.8$; $\tau^*=45\text{MPa} - >3$.

A difference between dimensionalities obtained for seismicity data and correlation dimensions calculated for the considered model data can be diminished by taking into account the presence of the seismic events, which are not related with EM influence and which can be considered as stochastic background. An addition of random component with signal/noise ratio 2 to the model data resulted in increase of the model correlation dimensionality to 4-5, which is in good correspondence with studied seismic activity data during EM source actions.

Conclusions

The obtained results show an increase of seismic regime regularity after beginning of powerful EM pulses action: before EM excitation, the correlation dimensionality of the possible attractor was not less than 8 with corresponding embedded space dimension 14. After start of EM excitations, the attractor correlation dimensionality diminished to 4.6, embedded space dimension to 6.

The model of possible reaction of the geomechanical system governed by rate-and-state friction law on perturbations due to EM actions is considered numerically. It was found that a change of fault and fracture strengths under EM action leads to a diminution of attractor and embedded space dimensions.

References

- Erickson B., Birnir B., Lavallée D. (2008) A model for aperiodicity in earthquakes. *Nonlinear Processes in Geophysics*. 15, 1-12.
- Grassberger, P., Procaccia, I. (1983). Measuring the strangeness of strange attractors. *Physica*, 9D, 189-208.
- Gu, J-C., Rice, J. R., Ruina, A. L., and Tse, S. T.: Slip motion and instability of a single degree of freedom elastic system with rate and state dependent friction, *J. Mech. Phys. Solids*, 32, 167–196, 1984.
- Hobbs, B.E. (1990). Chaotic behaviour of frictional shear instabilities. *Rockbursts and Seismicity in Mines*. (Fairhurst, ed.). Balkema, Rotterdam. 87-91.
- Malinetsky, G.G., Potapov, A.B. (2002). *Modern problems of non-linear mechanics*. Editorial URSS, Moscow.
- Tarasov N.T., Tarasova N.V. (2004). Spatial-temporal structure of seismicity of the North Tien Shan and its change under effect of high energy electromagnetic pulses. *Annals of Geophysics*. 47, 1, 199-212.
- Velikhov E.P., Zeigarnik V.A., Novikov V.A., Avagimov A.A., Sobolev G.A., Ponomarev A.V., Nikolaev A.V., Tarasov N.T., Tarasova N.V., Bogomolov L.M. (2006). High- Power Electromagnetic Impact on the Earth Crust for Prevention of Catastrophic Earthquakes, AGU-2006 Fall Meeting, NG42A-03.

Project MAGS – Microseismic Activity of Geothermal Reservoirs

Ulrich Wegler and Christian Bönemann

Bundesanstalt für Geowissenschaften und Rohstoffe (BGR), Hannover, Germany

The MAGS research project aims at developing concepts to limit the microseismic activity of deep geothermal reservoirs. The joint research project started in May 2010 and is funded for three years by the German Federal Ministry for the Environment, Nature Conservation and Nuclear Safety. The goals of the project are to measure and characterize the seismicity near sites of deep geothermal reservoirs in Germany. Moreover, methods to compute the seismic hazard caused by deep geothermal wells will be developed. Strategies to avoid perceptible earthquakes during hydraulic fracturing as well as during operation of the geothermal power plants will be worked out. Finally, the project aims at contributing to a better understanding of fluid induced seismicity. Besides Bundesanstalt für Geowissenschaften und Rohstoffe (the project coordinator), Karlsruhe Institute of Technology, Ludwig-Maximilians-Universität München, Freie Universität Berlin, and Clausthal University of Technology are contributing to the project.

Occurrence probability and earthquake size of post shut-in events in geothermal projects

Friedemann Wenzel¹, Andreas Barth¹, Cornelius Langenbruch² and Serge S. Shapiro²

¹ Karlsruhe Institute of Technology, University of Karlsruhe, Geophysical Institute, Hertzstr. 16, 76187 Karlsruhe, Germany

² Freie Universität Berlin, Fachrichtung Geophysik, Malteserstr. 74-100, 12249 Berlin, Germany

It is known that fluid injections at geothermal sites, which are performed to develop the reservoirs, can induce low magnitude earthquakes in critically stressed zones of the surrounding rock. Even after shut-in of fluid injections, that is, after the pressurized fluid injection into the borehole is stopped, a significant number of seismic events can occur. The understanding, characterization, and forecasting of post shut-in events is in particular important, because during recent geothermal projects such as Soultz-sous-Forêts, Basel, and Landau it has been observed that the largest earthquakes tend to occur after shut-in. This makes it still more difficult to control such events.

We demonstrate in this paper (a) that the largest earthquakes should occur after the shut-in of injection in the context of the “Seismicity Based Reservoir Characterization Theory (SBRC)”; (b) that even larger earthquakes have to be expected, if injection would be continued; (c) that the largest expected magnitude can be estimated. All three statements apply in a probabilistic sense only.

There are two fundamental laws in statistical seismology, namely the Omori Law, which describes the decay rate of aftershock activity after tectonically driven earthquakes and the Gutenberg-Richter relation describing the frequency magnitude distribution of earthquakes. It was observed and verified in recent works that both fundamental laws are also valid in the context of injection induced seismicity (Shapiro et al., 2007; Langenbruch & Shapiro, 2010).

We describe the fluid injection source by a point source in a permeable fluid-saturated medium with pre-existing fractures and assume that the fluid is liberated from this source with constant strength until the shut-in time t_s . In general, the behavior of seismicity triggering in space and time is controlled by the relaxation process of stress and pore pressure perturbation that was initially created at the injection source. This relaxation process can be approximated by linear pressure diffusion in the pore fluid of rocks. Following the Mohr-Coulomb failure criterion the resulting increase in pore pressure can lead to rock failure along pre-existing, sub-critically stressed cracks. If critical pore pressures leading to reactivation of individual pre-existing fractures are equally distributed between a lower bound $C_{min}=0$ Pa and a maximum value C_{max} larger than the overpressure between source and reservoir, Omori's law can be utilized to describe the decay rate of seismic activity after shut-in of injection in the following modified form:

$$v_1(t) = \bar{v}_1 \cdot \left(\frac{t_s}{t} \right)^q, \quad (1)$$

with the constant seismicity rate \bar{v}_1 during injection, time $t \geq 0$ from injection start, the shut-in time t_s , and the exponent q between 1 and 2. The upper bound of q is the

better value to describe the decay rate close after termination of injection while the lower bound applies for much larger times.

We assume that the occurrence of induced earthquakes represent a Poisson process in time. By combining eq. 1 and the Gutenberg-Richter relation we show that the probability P_0 of not exceeding a given magnitude M is still decreasing after shut-in according to:

$$P_0(M, t \leq t_s) = \exp(-\bar{v}_M t) \quad (2)$$

and

$$P_0(M, t \rightarrow \infty) = \exp\left(-\bar{v}_M t_s \cdot \left(1 + \frac{1}{q-1}\right)\right), \quad (3)$$

where \bar{v}_M is the constant seismicity rate of events with magnitudes larger than M during injection.

Let us give an example: If the probability to exceed magnitude M at the time of the shut-in is given by $1 - P_0 = 10\%$, this probability increases to $1 - P_0 = 19\%$ considering all events occurring after the shut-in ($t \rightarrow \infty$) and an exponent of $q=2$.

Another implication is the probabilistic determination of the change in magnitude M of an earthquake given a constant probability level of occurrence: Assuming a 50% chance that no earthquake larger than M occurs, we can ask by what amount ΔM would the maximum magnitude increase, if we keep the occurrence probability fixed and continue injection. For $t = 2t_s$ and $b = 1.5$ we get:

$$\Delta M = \frac{1}{b} \log\left(\frac{t}{t_s}\right) \approx 0.2. \quad (4)$$

Accordingly, we can stop injection and wait until $t = 2t_s$. That results in:

$$\Delta M = \frac{1}{b} \log\left[1 + \frac{1}{q-1} - \frac{1}{(q-1) \cdot (t/t_s)^{q-1}}\right] \approx 0.12, \quad (5)$$

showing that the maximum magnitude occurring with a 50% probability of occurrence is 0.12 magnitudes higher after shut-in, whereas a continuation of injection results in a still higher increase of 0.2 magnitudes.

References

- Langenbruch, C. & Shapiro, S. A. (2010). Decay Rate of Fluid Induced Seismicity after Termination of Reservoir Stimulations. *Geophysics*, Geo-2009-0404 (accepted).
- Shapiro, S. A., Dinske, C. and Kummerow, J. (2007). Probability of a given-magnitude earthquake induced by a fluid injection. *Geophys. Res. Lett.*, 34. doi:10.1029/2007GL031615.

Recent earthquake activity at Haradh region, western Saudi Arabia

Zahran, H. M., Sy. El Hadidy, Kh. Yosef

Saudi Geological Survey, Jeddah, P.O.B. 54141, 21514

Since July 2005 there have been more than 200 earthquakes close to Ghawar oil field in the Haradh region, western Saudi Arabia which have been recorded by permanent seismograph stations of the network operated by the Saudi Geological Survey, National Center for Earthquakes and Volcanoes. The level of seismic activity in the Haradh area is surprisingly high for a supposedly inactive region.

On the middle of August 2010, an earthquake swarm have been occurred with the maximum (4.4 on local Richter scale), this earthquake was widely felt by many due to its shallower depth, its depth is 6.7 km. The locations, magnitudes and focal depths are shown plotted on Landsat images and also on a topographic base map. The earthquakes are very shallow, with a maximum depth of 7.0 km and a mean depth of only 3.0 km.

From the waveform analysis, it can be seen that there are different groups having different waveform and different spectral content. From the magnitude-frequency histogram, it appears that most events greater than magnitude 1 have been located. The times of the events are shown in a histogram, in which there are no really obvious peaks such as those observed when regular quarry blasting is being carried out. It appears that most events are therefore random in time.

However, given the potential for future events which may be damaging, it is certainly worthwhile to monitor the area more intensively. Additional more detailed data on the earthquake activity would help to locate the events more accurately and possibly enable them to be correlated with known geological structure. A more quantitative estimate of earthquake risk or hazard should also be of considerable importance in any engineering activities in the region. At present our data is limited, it is important to locate as many small earthquakes as possible, since although they may not cause any damage themselves, they do contribute to the statistics of activity in the region, from which the frequency of occurrence of larger and more damaging events can be calculated.

The data indicate the need for more detailed geological investigations and a more careful analysis of earthquake risk along Haradh region. While the maximum magnitude (4.4 on the Richter scale) is not particularly large by global standards, the occurrence of these events in an otherwise fairly quiescent area should be of some concern given the development of the area for oil production. It cannot at this stage be determined whether the activity is related to oil extraction, or whether it is due solely to natural variability in normal tectonic seismicity.

It is proposed that an additional dense network of seismographs should be established in order to obtain improved coverage with better determination of earthquake source parameters and statistics.

SECTION II

ARTICLES

The difficulty to distinguish natural and human related seismicity in a complex tectonically active area

Thomas Braun¹, Jens Heinicke², and Torsten Dahm³

¹ Istituto Nazionale di Geofisica e Vulcanologia, Seismological Observatory, Arezzo, Italy

² Sächsische Akademie der Wissenschaften zu Leipzig, Office TU Bergakademie Freiberg, Germany

³ Institut für Geophysik, Universität Hamburg, Germany

Abstract

Human operations, such as mining, fluid production and the construction of a barrier lake in a tectonically active area can play an important role of triggering seismic events. An interesting area to study those phenomena is the northern part of the Upper Tiber Valley, which is characterized by the presence of a Low Angle Normal Fault, the so called Alto Tiberina Fault (ATF). The recent seismic activity of this fault line reflects the geodynamic behaviour in the regional stress field. Close to this fault zone, a 4.8 km deep borehole PSS1 is located which will be reopened at the end of 2010 to extract CO₂. This will possibly lead to a change in the hydraulic equilibrium in this region with potential consequences for the overall local geodynamics. Crustal deformation and micro-seismicity could be induced by the extraction. Fluid pressure changes and their influence to the hydraulic conduits up to the natural fluid emissions sites (mofettes) will be investigated as part of an actively controlled forcing experiment on this fault. Further human activities like mining industry and the filling of water reservoirs influence the local stress field. The derivation of natural and human induced seismicity can be improved by a comprehensive analysis.

Introduction

The Upper Tiber Valley is situated in the northern part of the Central Apennines and is setting of a number of geological phenomena typical for volcanic areas, like CO₂ degassing, moderate earthquakes ($M \leq 6$) and a strong microseismicity. The major part of the recorded seismicity can be associated to a Low Angle Normal Fault (LANF) – the so called Alto Tiberina Fault (ATF, see Figs. 1 and 2), but some of the recorded seismograms show signals similar to those recorded on active volcanoes. In the vicinity of the ATF human activity provides a number of candidates, capable to influence the seismic release in the area:

- a huge barrier lake with a dam height of 52 m and a water holding capacity more than 150 million m³ is directly situated on the ATF and is characterized by seasonal water level oscillation of up to 12 m.

- a cement plant, quarries and decommissioned mines present in the area are in the direct vicinity of epicentres of tornillo-like seismograms and episodes of non-volcanic tremor.
- CO₂ extraction – also this candidate influences the local stress regime: with the original scope to find methane, between 1982 and 1984 a perforation well has been sunk to a depth of 4800 m at a distance of about 5 km from the Montedoglio-Lake, the so called PSS well. Instead of finding methane, carbon dioxide has been encountered, with the consequence, that the borehole was closed and sealed. In 2004 the well has been reopened and prepared for a future commercial use of carbon dioxide by a company that will start with continuous extraction from December 2010 on.

Since 2003 many field experiments as e.g. gas flux measurements and the installation of a webcam (Heinicke et al., 2006), different seismic network and array configurations (Braun et al., 2004; Piccinini et al., 2009) have been carried out to monitor the different geophysical phenomena. Interesting in the near future will be the controlled extraction of CO₂ by a private company. In order to study its influence on the seismicity at July 2010 a small aperture array (CAMI in Fig. 2) was installed in the vicinity of the well. In 2011 the set up of a seismic network (S1-S8 in Fig. 2) will complete the seismic monitoring capabilities in the area.

Tectonic setting of the study area

The Upper Tiber Valley is a Pliocene–Quaternary basin, bounded westwards by a Low Angle Normal Fault, the Alto Tiberina Fault, whose northern end has not been well determined. Barchi *et al.* (1998) analysed data from the seismic profile CROP03 and found the northernmost known part of the ATF in the area between *Monterchi—Sansepolcro—Bocca Trabaria* (see dashed line in Fig. 1 and green line in Fig. 2).

The ATF strikes SSE–NNW from Perugia in the South to the inadequately detected northern end at Sansepolcro (see Fig. 2). The ATF was recognized by Boncio *et al.* (2000) as being part of the Etrurian Fault System. The same authors proposed a possible explanation for the prolongation of the fault: the northernmost edge of the ATF could be transected by a left lateral segment as a transition zone of the Casentino basin (NW). Fault scarps near Caprese Michelangelo (red lines in Fig. 2), striking elements along the distribution of the fluid emission sites, and visible striking elements in the rock basement in a NW–SE direction, support this fault architecture. The ENE dipping of this low-angle fault (<30°) was also detected in the CROP03 deep seismic reflection profile (Fig. 1 and Barchi *et al.* 1998). As confirmed by passive seismic observations (Piccinini et al., 2003), the easternmost of these LANFs, shows a strong microseismic activity with more than 3200 seismic events ($M_L \leq 3.2$) in 8 months (red circles in Figure 1).

The topography of the ATF is well imaged up to the town of Sansepolcro (CROP03) by active and passive seismic observations. High-angle antithetic normal faults east of the ATF were also recognized in the CROP03. They are still active tectonic elements characterized by recent seismicity (Piccinini et al., 2009). Another hypothesis presumes that the northern part of the ATF continues to strike in a NNW direction. This opinion is based on stratigraphical data obtained from the deep borehole PSS (see Fig. 2).

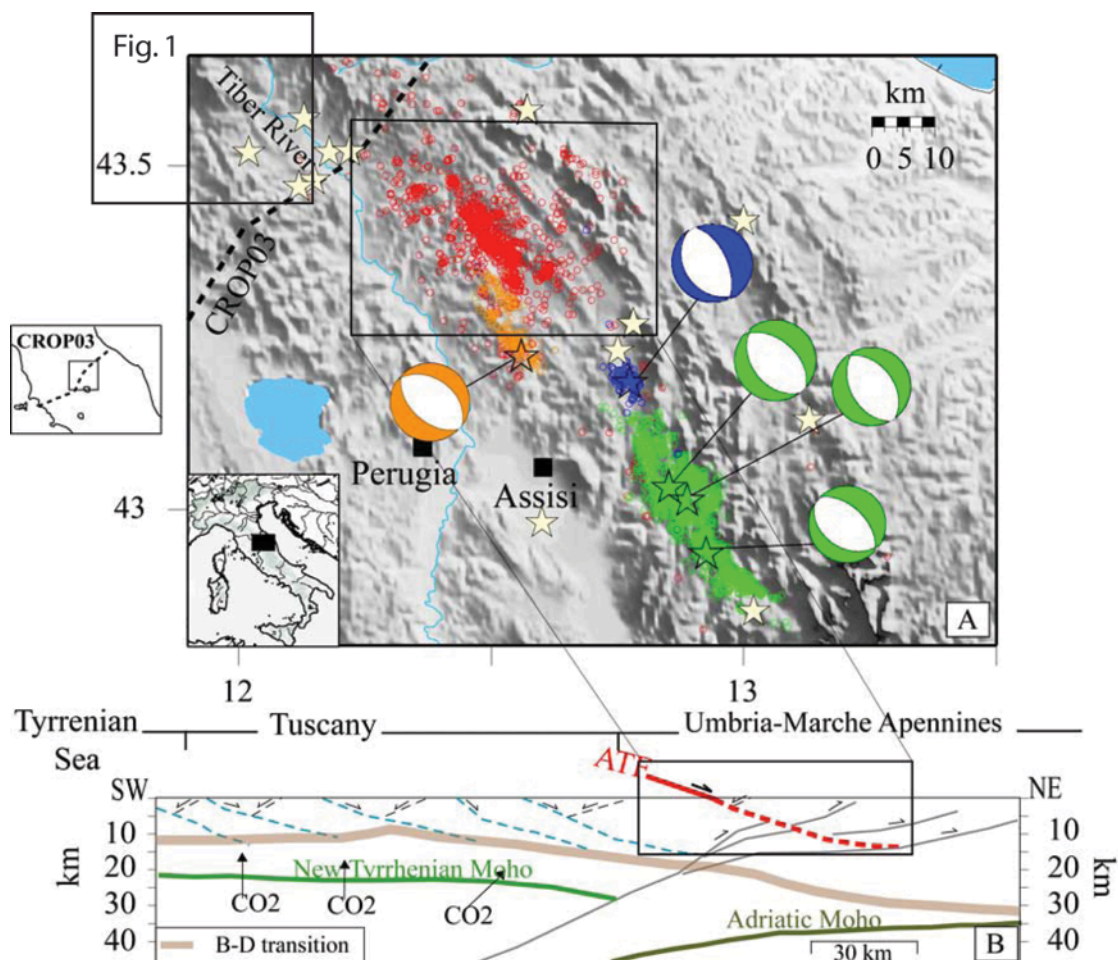


Figure 1: The microseismicity located on the Alto Tiberina Fault (Chiaraluce et al. 2007). White stars indicate the strongest historical earthquakes. Red symbols show the hypocenters of the earthquakes recorded during the 2000–2001 seismic survey. Orange, blue and green symbols indicate the aftershocks of the 1984 Gubbio (M_w 5.1), the 1998 Gualdo Tadino (M_w 5.1) and the 1997 Colfiorito sequence, respectively. Focal mechanisms of the three largest shocks: M_w 6.0, M_w 5.7, and M_w 5.6 from NW to SE, respectively) are plotted. Crustal-scale cross section interpretation of the CROP03 seismic profile running from the Tyrrhenian to the Adriatic coasts [Barchi et al., 1998; Collettini and Barchi, 2004]. The ATF is drawn in red, while other low-angle normal faults in the Tyrrhenian and Tuscany sectors are shown in blue. The rectangle in the upper left corner of the figure indicates the study area.

Variations in the fluid emission

Cold CO_2 gas emission sites in rainwater-filled pools, so called mofettes, are widely distributed all over Italy. Their gas reservoir is of magmatic and/or metamorphic origin. The CO_2 gas reservoir in the Upper Tiber Valley (Fig. 2) is dominated by a metamorphic origin (Heinicke et al., 2006). Results from the PSS well investigation show that the main component of the supercritical fluid is carbon dioxide under a static pressure of 700 bars and a temperature of 120°C at depth. The chemical

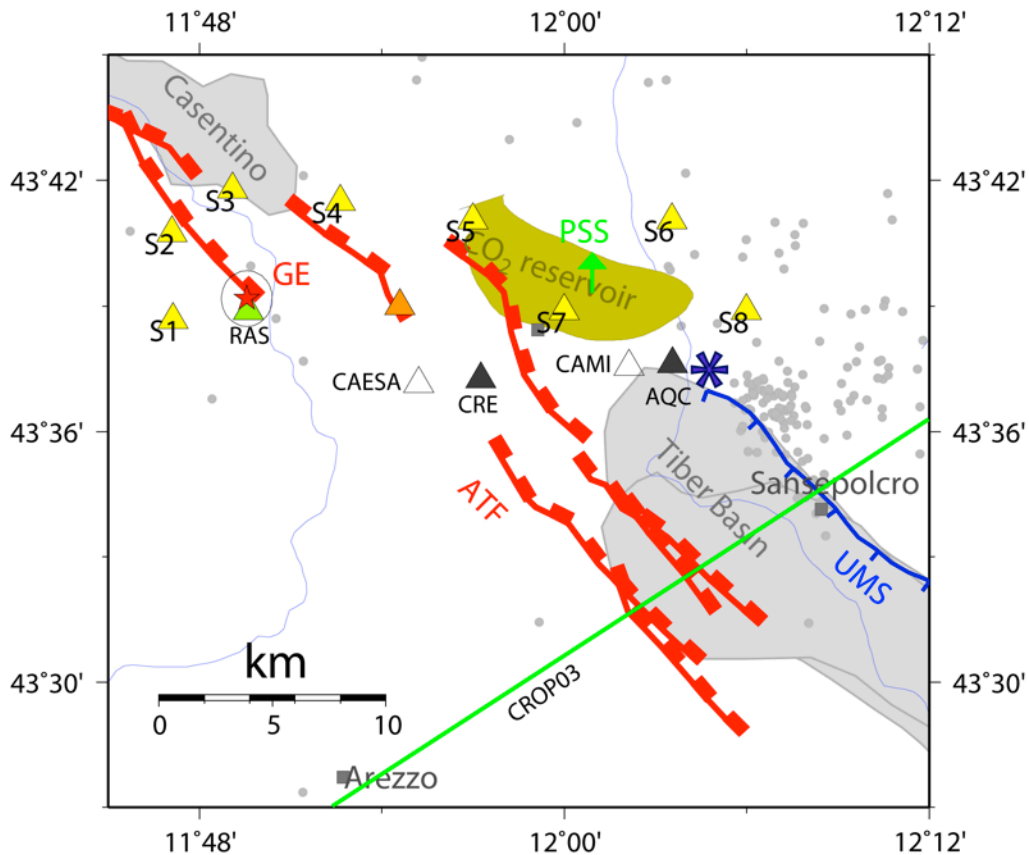


Figure 2: Overview to the study area. The PSS borehole is indicated by a green arrow, the CO₂ reservoir at ≈ 4 km depth by the golden-filled polygon. The ATF (red faults) dip in NE, and its antithetic normal faults (blue faults, e.g. UMS) in SW. Instrumental micro-earthquakes are declared by small grey-filled circles. GE indicate the location Tornillo-like events. Coloured triangles give the location of permanent seismic stations. Unfilled triangles indicate temporary array installations: CAESA (2005) and CAMI (2010). Other planned seismic stations are indicated by yellow triangles (S1-S8). Grey dots indicate the background seismicity. The blue asterisk indicates the Mw 4.6 main shock of the 2001 seismic sequence.

composition of the fluid is CO₂ = 92.2 %, N₂ = 7.6 %, CH₄ = 0.03 %t, O₂ = 0.01 %, H₂S = < 0.02 %. Water exists in that fluid only as a minor component with a content of less than 0.5 per cent. The well-known mofettes in that area near Caprese Michelangelo (CAMI) show the same chemistry and the same isotope signature as the crustal fluids. That means a transport path exist between reservoir and mofettes along a seismically active fault zone.

Therefore, anomalous fluid emissions have been observed as long-term variations in the long-distance fluid transport process from the reservoir induced by the local tectonic settings. In the northern part of the Alto Tiberina Fault, a fault intersection was reactivated by a seismic sequence which started on 2001 November 26, and continued for approximately four months. The magnitude of the main shock was M_w 4.6. The fluid transport was activated by this seismic crisis as a consequence of the improved transport conditions by increased fracture apertures as a result of the rupture process. A migration of the hypocentres towards the surface provides hints of a

possible pore pressure diffusion process. The consequence is an increased fluid transport to the mofettes. The first indications of anomalous fluid expulsions at the mofettes of Caprese Michelangelo were detected 18 months after the seismic events. The delay in the increased fluid release gives the opportunity to approximate the physical transport parameters like hydraulic diffusivity with $0.25 \text{ m}^2/\text{sec}$ as a typical value for fracture zones. These results confirm also the critical stage of the local stress regime which could be influenced by pore pressure variations (Heinicke et al., 2006).

Multiparameter studies of the influence of human activity to the geodynamic processes on site

Human related influences, as realized by the activities of cement plants, quarries or superficial mines may produce seismic signals, but will not directly have an impact on the mechanical behaviour of an active fault system at crustal depth. However, water level changes in a huge barrier lake, as the Montedoglio-Lake, or long term CO_2 -extraction from the upper crust have the capability to directly influence the stress field at depth. A large scale field experiment gives us the opportunity to study the overall influence of human activity at this LANF.

Beginning from December 2010, the user of the CO_2 reservoir will re-open the PSS borehole and plans to produce 5 tons per hour of reservoir gases for commercial usage and trading. This production will lead to a pore pressure change and slow depletion of the reservoir formation, similar to many other gas fields under production. Since production volumes and pore pressure changes are relatively well known, we will consider the local depletion-induced stress changes on the ATF and in the surrounding rock as driving forces to the system. We consider the geodynamic response of the ATF as result of a pore pressure perturbation by crustal fluids which influence the static stress regime in the reservoir. The installation of monitoring stations and seismic arrays even before the beginning of the CO_2 -extraction is essential for estimating the background rate of the gas flux and seismicity. Seismic monitoring in the region is performed by INGV Arezzo since 2003. The monitoring of the gas-flux measurements and continuous visual observation of the CO_2 -mofettes has started during the last year, and will be improved within 2011. Water level changes in the nearby reservoir are measured since the beginning of filling in 2007. The purpose of the study is to compile and measure a reference dataset for the discrimination problem of natural and human related seismicity in a complex tectonic region, and to investigate possibly fluid migration in response to crustal stress changes.

References

- Barchi, M., R. Minelli and G. Pialli (1998): The CROP03 profile: a synthesis of results on deep structures of the Northern Apennines. *Mem. Soc. Geol. Ital.*, 52, 383 – 400.
- Boncio, P., F. Brozzetti and G. Lavacchia, 2000. Architecture and seismotectonics of a regional lowangle normal fault zone in central Italy. *Tectonics* 19, 1038-1055.

Articles

- Braun T., J. Schweitzer, R. M. Azzara, D. Piccinini, M. Cocco and E. Boschi (2004): Results from the temporary installation of a small aperture seismic array in the Central Apennines and its merits for the local event detection and location capabilities. *Ann. Geophys.* 47/5, 1557-1568.
- Chiaraluce L., C. Chiarabba, C. Collettini, D. Piccinini and M. Cocco (2007): Architecture and mechanics of an active low-angle normal fault: Alto Tiberina Fault, northern Apennines, Italy. *J. Geophys. Res.*, 112, doi: 10.1029/2007JB005015
- Heinicke, J., T. Braun, P. Burgassi, F. Italiano and G. Martinelli, 2006. Gas flow anomalies in seismogenic zones in the Upper Tiber Valley, Central Italy. *Geophys. J. Int.* 167, 794–806, doi: 10.1111/j.1365-246X.2006.03134.x.
- Piccinini D. et al. (2003) : Microseismic study in a low seismicity area of Italy : The Città di Castello 2000 – 2001 experiment. *Ann. Geofisica*, 46(6) 1315-1324.
- Piccinini D., N. Piana Agostinetti, P. Roselli, M. Ibs-von Seht and T. Braun, 2009. Analysis of small magnitude seismic sequences along the Northern Apennines (Italy). *Tectonophysics*, 476, 136-144.

How to discriminate induced, triggered and natural seismicity

T. Dahm¹, S. Hainzl², D. Becker¹, and the FKPE* group DINSeis³

¹ Institute of Geophysics, University Hamburg, Germany

² GFZ, Potsdam, Germany

³ M. Bischoff, S. Cesca, B. Dost, R. Fritschen, D. Kühn, S. Lasocki, C. D. Klose, Th. Meier, M. Ohrnberger, E. Rivalta, S. Shapiro, U. Wegler

Abstract

Human operations, such as mining, hydrocarbon production, fluid withdrawal or injection, drilling, hydro-fracturing and reservoir impoundments, can positively and negatively impact tectonic stresses, pore pressure, fluid migration and strain in the sub-surface. Earthquakes occurring in spatial and temporal proximity to such operations are immediately under suspicion to be triggered or induced. The **discrimination between natural, triggered, and induced earthquakes** is a difficult task, and clear rules and scientific methods are not well established or commonly accepted. The current practice to distinguish possible causes of earthquakes is not quantitative and individual cases are treated unequally, which often leads to questions on general liability. This situation has a negative drawback for private and public claimants and for companies performing the operations. Moreover, estimations of earthquake-related risk is still difficult.

Introduction and status quo

Figure 1 shows a number of significant earthquakes ($M > 3$) in Germany and adjacent areas that are associated with geo-engineering operations. The events are related to different types of human operations, ranging from salt mining, coal mining, gas extraction to fluid injection associated with deep geothermal power generations. Some of the plotted events caused cessation of the mining or hydrothermal operations (Saarbruecken, Basel). Other operations as waste fluid injection, CO₂ sequestration or gas storage facilities may also induce or trigger seismicity. However, in the same way geo-engineering activities can bring fault zones close to failure, they can also bring them away from failure (for instance refilling of a gas reservoir or the decline of a water table in a mine). This means that the seismic risk in the vicinity of the operation point is reduced (Klose, 2010). Figure 1 indicates that operations affecting a larger area in the subsurface, such as salt mining, gas withdrawal or coal mining induced/triggered the strongest events with magnitudes up to $M_I = 5.5$. However, the problem of the possible magnitude of a triggered earthquake is complex and additionally depends on the regional stress and pre-existing faults. Additionally, triggered/induced earthquakes typically occur within the uppermost 6 km of the crust and are often superficial. Therefore, even weak events with $M < 3$ can be felt by the population and may pose a seismic hazard at the epicenter and are thus important for

* Forschungskollegium Physik des Erdkörpers

the subject (e.g. Soultz-Sous-Forêt, MI 2.9, 10 June 2003; Landau, MI 2.7, 15 August 1009; Unterhaching; MI 2.5, 3 July 2010). They have been discarded in Fig. 1 for the purpose of a complete catalogue.

The FKPE working group proposed three major tasks to assess the triggered seismicity problem: (1) monitoring, (2) discrimination of natural and human-related seismicity, and (3) legal aspects. The discrimination between natural and human-related earthquakes is difficult to assess. Basic structural, geophysical/geological data and detailed information about man-made operations are often missing. Additionally, our scientific understanding of the earthquake triggering process is incomplete. The aim of the working group is to develop recommendations how to assess the discrimination problem, and how the probability of occurrence of a triggered or induced earthquake can be estimated.

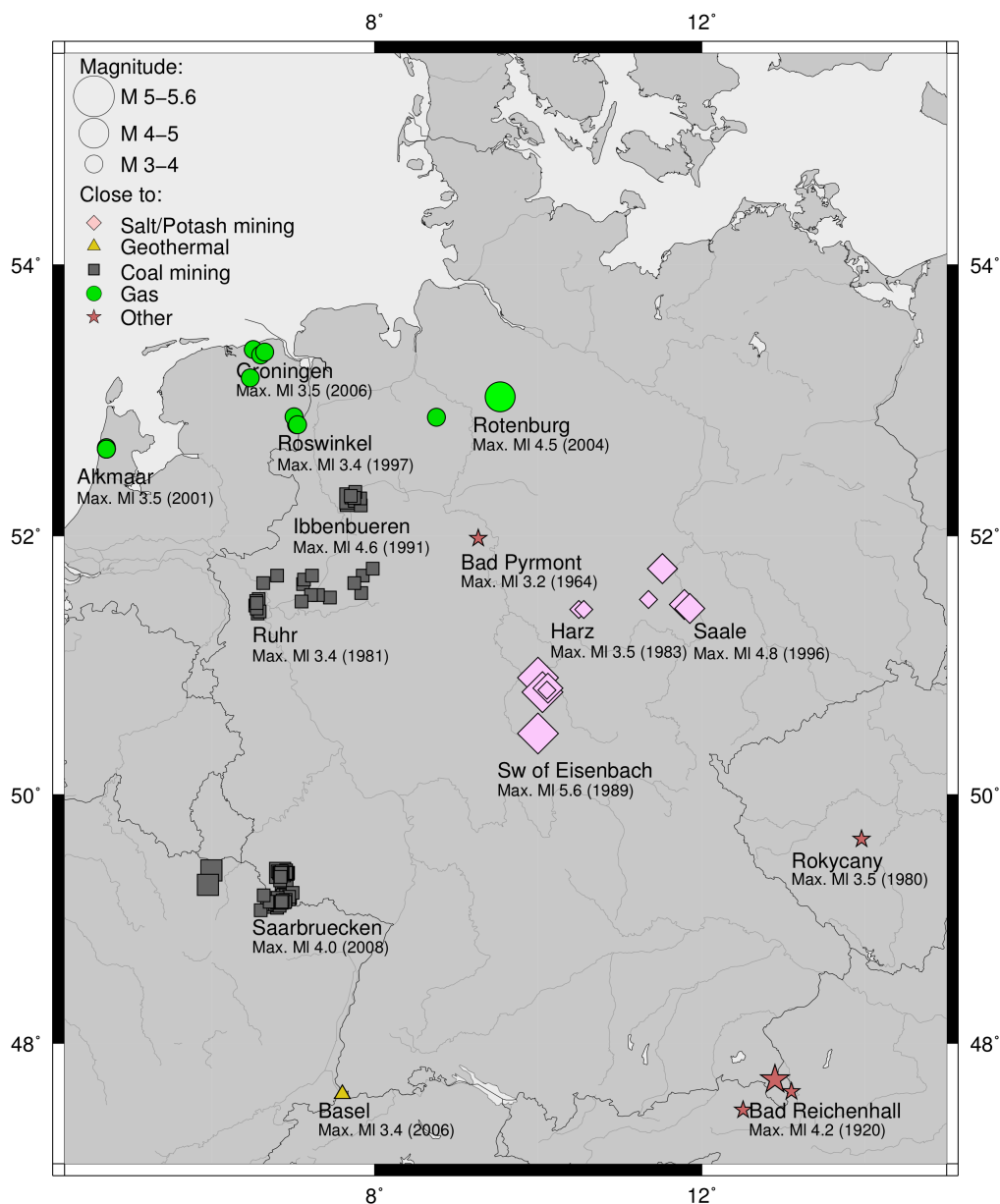


Figure 1: Earthquakes with $M_I > 3$ from 1899 until 2010 in Germany and adjacent areas with suspicion to be triggered or induced.

A common approach to assess the probability if an earthquake has been triggered/induced is given by answering some plausible questions (modified from Davis et al. 1995). The more of these questions are answered by yes, the higher is the probability that the event was triggered or induced.

1. Is it the first known event of this character in the region?
2. Did the events begin only after the human operation had commenced?
3. Is there a clear correlation between operation and seismicity?
4. Are the epicenters within a specified distance from the affected area (e.g. from wells)?
5. Do some earthquakes occur at or near the depth of operation?
6. Do epicenters appear spatially related to the region affected by the operation?
7. Did the operation cause a significant change in stress and/or fluid pressure?
8. Did the seismicity begin only after the significant stress or pressure change?
9. Is the seismicity explainable in terms of current models relating the operations and the induced mechanical/hydrological processes to fault activity?

The approach is only qualitative and cannot be used for planning purposes before operations start. It does not motivate to improve the monitoring or pre-operation survey. As it stands, it cannot be used to delineate areas of potentially expected earthquakes (seismic hazards mapping).

Basic assumptions and definitions

A standard assumption is that the stress in the Earth's crust at depth of already a few km is controlled by the strength of the crust. Pre-existing zones of weakness and fault zones experience continuous tectonic loading and maintain a stress state close to failure. In this situation already a small positive Coulomb stress or overpressure increase may **trigger the nucleation** at the hypocenter. Under steady state tectonic loading, a steady state rate of background seismicity is observed which is incorporated in seismicity models as the background rate against which possible rate changes are measured (e.g. Dieterich, 1994; Ogata and Zhuang, 2006). The frequency-size distribution usually follows the Gutenberg Richter relation with a constant b-value, if there are steady state conditions and the region considered is sufficiently large. However, there are also exceptions (e.g. Wiemer and Wyss, 2002). If induced weak earthquakes and aftershocks are considered, a typical assumption is that pre-existing planes of weakness in arbitrary orientation may be triggered. The planes of maximal Coulomb failure stress increase (ΔCFS) are considered to assess the triggering problem.

The **subsequent rupture** of stronger earthquakes may affect faults of several hundred meters or kilometers length. Rupture is driven by stress drops in the order of few MPa. Such large Coulomb stresses are assumed to be available on pre-existing faults at larger depths if they are favorably orientated, but it is typically not observed at very shallow depth and within soft sediments (see e.g. Zoback, 2007, for stress-depth profiles at shallow levels and in sedimentary basins). However, magnitude 3 and 4 tectonic earthquakes have also been observed at very shallow depth (1-3 km) within sediments close to the city of Fribourg, Switzerland (e.g. Kastrup et al., 2007).

Human operations comprise different actions affecting stress, pore pressure, strain, fluid saturation, fluid flow and rock strength in the subsurface. Induced stresses can range from a few tens of KPa, to several MPa. We assume that operations are

monitored and pressure, stress, injection volume or other parameters of relevance are available or can at least be estimated in order to assess the discrimination question¹.

The **earthquake case** may consist of a single or of a sequence of earthquakes in the neighborhood of the site. The epicenter, depth, occurrence time and strength must be provided. Uncertainties shall be provided as probability density function (PDF, see e.g. Lomax et al., 2000). In some cases, the source mechanism and the size and parameters of the rupture may additionally be known. The questioned earthquake(s) may be (see also McGarr and Simpson, 1997; McGarr, Simpson and Seeber, 2002):

- **natural/human-made:** Triggering and driving of the rupture is controlled by natural or by human-made stress or pressure perturbations. For steady state loading the background rate of natural earthquakes is often constant and the frequency-size distribution obeys a power law (parameterized in log-log formulation by a- and b-values). Human-made loading is typically not steady state and modifies the seismicity rate and b-values (e.g. Harsh, 1972; Gibowitz, 2001). However, also some natural processes like static and dynamic triggering from other natural earthquakes and natural pore pressure changes have the potential to modify the seismicity rate.

- **triggered/induced:** Triggering concerns the nucleation. The occurrence of a triggered event is advanced in comparison to the background rate, but the size of the event is controlled by the existing natural stress field and fault structure. The induced event is evaluated on terms of its size. For instance, the rupture is driven by the human-related (induced) stress or pressure perturbation, or by a strong stress perturbation induced by a natural transient process (dissolution, magma-diking, earthquake). The size of the rupture plane of the induced event is equal or smaller than the spatial extension of the induced stress or pressure perturbation. The earthquake would not occur without the human operation.

Distinguishing triggered and induced earthquakes may become important if the seismic hazard and earthquake size is questioned.

Modules in probabilistic influence diagrams

In order to obtain a measure of the probability that an event is either natural or human-related, and whether it is triggered or induced, qualitative criteria like those of Davis et al. (1995) have to be transformed into a quantitative formulation that can be integrated into the decision process. Such a scheme may consist of different modules, each of which may define a probability of a triggered event or sequence. Similar to developments in volcanology and seismic hazard analysis, the probabilistic outputs of the different modules may be combined into **probabilistic influence diagrams** (Bayesian belief network, Fig. 2).

In the following we present some examples of possible modules that may be implemented in a future decision scheme. This list is neither complete nor can it be expected that all modules are applicable for every study which is especially true in the

¹ Completeness of monitoring and earthquake location accuracy is crucial for assessing the discrimination problem. Recommendations regarding the monitoring concept are developed within the monitoring group and not considered here. Furthermore, a close cooperation with the operating company is necessary to obtain information about underground activities and to get access to a list of explosion times in case such operations are performed.

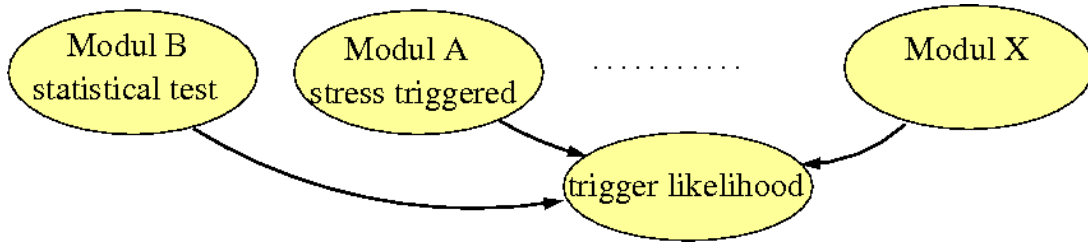


Figure 2: Schematic sketch of a probabilistic influence diagram to assess the event character.

case of only very few observed events in a historically aseismic region which makes a statistic evaluation almost impossible. However, the modularity of the approach allows to choose the appropriate modules and makes it easy to include new or modified components into the decision process. Thus, further input and the development of additional modules from the seismological and engineering community is welcome and highly encouraged. Each proposed modul shall be discussed with a field case with a summary of main characteristics and related papers, in order to develop catalogs of useful human-related and natural triggered events.

Sample Modul A- stress based seismicity model (Pst):

The seismicity model of Dieterich (1994) (rate and state dependent friction) is used to estimate the probability of an event to be triggered as a function of space and time. Input values are background seismicity rate $r(x,y,z)$ and $\Delta CFF(x,y,z;t)$. Parameters of the model are an aftershock decay constant and the sensitivity of the rock to stress loading. The loading history of the rock volume has to be estimated from the specific operation using for instance numerical models of stress transfer, pore pressure or pore fluid diffusion. The output of the rate and state dependent model is a theoretical seismicity rate $R(x,y,z;t)$. The probability that the earthquake case of given size was natural is r/R , and the theoretical probability to be triggered is $P_{sm}(x,y,z;t) = 1 - r/R$. The Pdf of the earthquake is multiplied by the normalized probability of triggering to calculate the probability that the specific event was triggered (Fig 3).

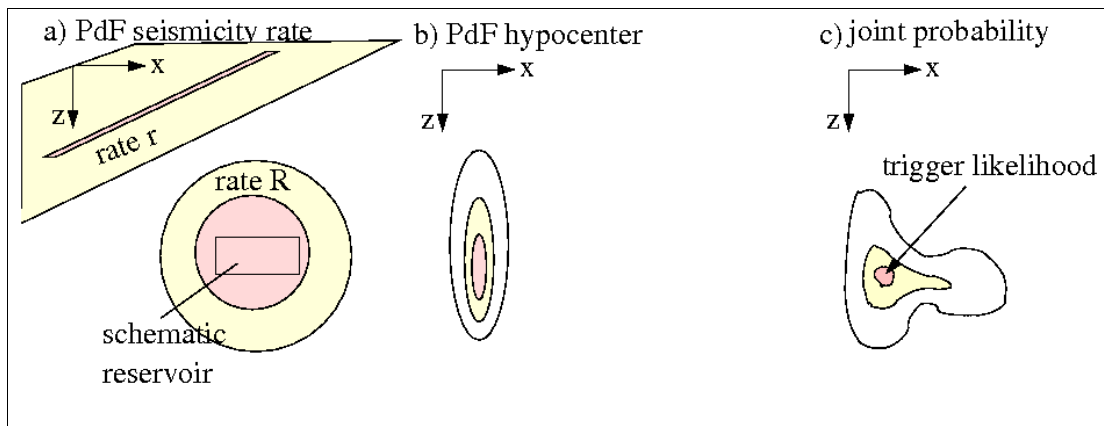


Figure 3: Schematic sketch in 2D showing the Pdf of the natural and induced seismicity rate (a), the Pdf of the event hypocenter (b) and the joint Pdf of the likelihood of a triggered case (c).

Sample Module B – Probabilistic seismicity model (Ppr):

The short term characteristics of natural seismicity can be usually well described by a combination of constant background activity and triggered aftershock sequences. In particular, the epidemic type aftershock sequence (ETAS) model (Ogata, 1988; Ogata and Zhuang, 2006) has been shown to reproduce the spatiotemporal characteristics of earthquake clustering very well (Woessner et al., 2010). The application of this model to a specific region can directly yield the probability that the earthquake under consideration is a natural event, i.e. that it can be related to background activity or ongoing aftershock sequences.

Sample Module C – Past induced earthquake model (Ppi)

If induced earthquakes are common in some region and tectonic events are unlikely in the same region, then new earthquakes are classified as “induced” without further detailed analysis. Such simple discrimination is common practice during routine analysis in earthquake centers to classify the large amount of small induced earthquakes in certain areas. The Ppi-module takes up this common practice in a systematic way: If the human activity is more or less stationary or changes occur only on a long time scale, the rate of induced earthquakes can be approximated to be more or less stationary in many cases. E.g. Shapiro et al. (2007) give several examples for a stationary induced earthquake rate caused by a stationary fluid injection rate. If the assumptions apply, the probability of a new event to be induced is “number of past induced events” divided by “number of all past events”.

Sample Module D – Consistency of the earthquake slip to background stress (Psl)

This refers to question 1 of the Davis scheme. Slip of a natural event is typically in the direction of the maximal shear stress resolved on the fault. Slip of a purely induced event is controlled by the induced stress perturbation. For instance, an earthquake induced in the central section of the over- and under-burden of a mining gallery or an oil field formation favors reverse sense of slip. The Pdf of the expected and observed slip direction may be obtained by bootstrap analysis. Multiplying both Pdf's gives Psl.

Sample Module E – Non-double couple source mechanisms (Pnd)

In mining seismicity the percentage of non-double-couple components is often quite high. High percentage of non-double couple component indicates high probability of induced events in mines.

Sample Module F – Fluid-Induced Events (Pfi)

Different sites of borehole fluid injections are characterized by different levels of seismotectonic activity. The "Seismogenic Index" (SI) is introduced as natural constant quantifying the seismotectonic activity of the injection site. The SI along with the injection rate controls the magnitude distribution of induced events (Shapiro et al., 2010). Shapiro et al. (2010) suggest that if the seismogenic index and the b-value can be estimated from the observed induced seismicity, the occurrence probability of induced events in the future can be calculated. For an event or a series of events of interest one can try to estimate if their occurrence does fall outside of the probability expected (thus, a higher likelihood of tectonic triggering in such a case).

Other criteria and models may be proposed and developed, which is a major aim of the group. For instance, waveform similarity may be used, the temporal evolution of earthquake strength in relation to injection pressure (injection case), or the

multimodality of the Gutenberg Richter relation (mining). Additionally, the role of tectonics/geology and engineering plans need to be considered in the different modules.

It is expected that the different operations may use different criteria, and that often only a subset of criteria can be estimated. Therefore, probabilistic influence diagrams shall be developed in future in order to help decision makers, claimants and companies to assess the question. Essential for this development is the availability of calibration data. Better data and open data policy will play a crucial role to calibrate modules.

Acknowledgements

We thank an anonymous reviewer for constructive comments and suggestions to improve the clarity of the text.

References

- Davis, S., P. Nyffenegger, C. Frohlich (1995). The 9 April 1993 earthquake in south-central Texas: was it induced by fluid withdrawal? *Bull. Seism. Soc. Am.*, 85, 1888-1896.
- Dieterich, (1994). A constitutive law for rate of earthquake production and its application to earthquake clustering. *J. geophys. Res.* 99, 2601-2618.
- Gibowicz, S.J. & Lasocki, S. (2001). Seismicity induced by mining: Ten years later. *Advances in Geophysics*, 44, 39-181
- Harsh K. Gupta, B. K. Rastogi, and Hari Narain (1972). Common features of the reservoir-associated seismic activities *Bulletin of the Seismological Society of America*, 62(2):481-492
- Kastrup, U., N. Deichmann, A. Fröhlich, D. Giardini, (2007). Evidence for an active fault below the northwestern Alpine foreland of Switzerland. *Geophys. J. Int.* 169, 1273-1288.
- Klose, C.D. (2010). Human-triggered Earthquakes and Their Impacts on Human Security, Achieving Environmental Security: Ecosystem Services and Human Welfare, In: P.H. Liotta et al. (eds.), *NATO Science for Peace and Security Series - E: Human and Societal Dynamics*, vol. 69., 13-19.
- Klose, C.D. and L. Seeber, (2007) Shallow Seismicity in Stable Continental Regions *Seismological Research Letters* 76(5), 554-562.
- Lomax, A., J. Virieux, P. Volant and C. Berge, 2000. Probabilistic earthquake location in 3D and layered models: Introduction of a Metropolis-Gibbs method and comparison with linear locations, in *Advances in Seismic Event Location* Thurber, C.H., and N. Rabinowitz (eds.), Kluwer, Amsterdam, 101-134.

- McGarr and Simpson (1997). A broad look at induced and triggered seismicity. In: *Rockbursts and Seismicity in Mines*, Eds. Gibowicz, S.J. and Lasocki, S. A.A. Balkema, Rotterdam, pp. 385-396.
- McGarr, Simpson, Seeber and Balkemaar (2002). Case histories of induced and triggered seismicity. In: *International Handbook of Earthquake and Engineering Seismology*, Eds. Lee, W.H.K. and Kanamori, H, Jennings, P.C. and Kisslinger, C., Academic Press, London, pp. 647-661.
- Ogata, Y.(1988). Statistical models of point occurrences and residual analysis for point processes, *J. Am. Stat. Assoc.*, 83, 9-27.
- Ogata, Y. and Zhuang, J. (2006). Space-time ETAS models and an improved extension. *Tectonophysics* Vol 413, 13-23, 10.1016/j.tecto.2005.10.016.
- Shapiro, S, C. Dinske and J. Kummerow (2007). Probability of a given-magnitude earthquake induced by a fluid injection, *Geophys. Res. Lett.*, vol. 34, L22314, doi: 10.1029/2007GL0316115.
- Shapiro, S, C. Dinske and C. Langenbruch and F. Wenzel (2010). Seismogenic index and magnitude probability of earthquakes induced during reservoir fluid stimulations. *The Leading Edge*, v. 29, pp 304-309, 10.1190/1.3353727.
- Wiemer and Wyss (2002), Mapping spatial variability of the frequency-magnitude distribution of earthquakes, *Advances in Geophysics*, 45, 259-302.
- Woessner, J, S. Hainzl, W. Marzocchi, M. Werber, A.-M. Lombardi, F. Catalli, B. Enescu, M. Cocco, M. Gerstenberger and S. Wiemer (2010). A retrospective comparative forecast test on the 1992 Lander sequence. *JGR*, submitted.
- Zoback (2007), *Reservoir Geomechanics*, Cambridge University Press, 504 pages.

Tensile earthquakes: view of seismology and geomechanics

Tomáš Fischer^{1,2} and Alice Guest³

¹ Charles University in Prague, Faculty of Science, Czech Republic, fischer@natur.cuni.cz

² Institute of Geophysics, Academy of Sciences, Czech Republic

³ ESG Solutions, Calgary, Canada

Abstract

The occurrence of crack opening became recently a focus of many seismological studies that search for the non-double-couple components of the seismic moment tensors. However, the results are ambiguous – the studies of fluid related earthquakes like earthquake swarms and industrial injection-induced seismicity shows source moment tensors of both pure double-couple of the dipole and crack type. We find that the observed moment tensors can be successfully modelled by a tensile earthquake with slip vector that deviates from the fault plane. The percentage of volumetric component is controlled by the relative magnitude of Lamé coefficients. We further combine the concepts from seismology and rock mechanics in order to explore the stress conditions under which non-shear earthquakes occur. We find that presence of non-double-couple components depends on the differential stress and the fracture orientation with respect to the stress field direction – tensile events can occur for fractures oriented close to σ_1 if the differential stress is small enough. This can occur either at small depths or in overpressurized formations at greater depths. We argue that in the presence of natural fractures of various orientations different fractures can break at different stress levels; the optimally oriented as shear and the others in tensile mode.

Introduction

Fluid injection into the rock formation is often accompanied by induced seismicity. This is routinely utilized in the exploitation of hydrocarbons and geothermal energy. The induced seismic events make injection audible, which makes it possible to use methods of seismology to localize the fluid flow and to determine parameters of the stimulated or newly created fractures. However, in some cases, namely in the geothermal projects, the seismic activity exceeds acceptable level and may invoke concern of the population. A better design of fracturing operations and their more effective realization requires a deeper understanding of the physical processes accompanying the hydraulic fracture stimulations and also the more effective utilization of the information provided by seismic monitoring.

It has been assumed for many years that pure shear events accompany the fracturing operations. The microseismic data were routinely inverted for the double-couple (DC)

component of the focal mechanism and the non-double-couple (non-DC) components were usually neglected, because the data were not of sufficient quality required for a reliable determination of full moment tensors (Nolen-Hoeksema and Ruff, 2001; Rutledge et al., 2004; Vavryčuk, 2007). However, few recent studies using high-quality data (e.g. Šílený et al. 2009; Baig and Urbancic 2010; Julian et al., 2010) indicate that the non-DC moment tensors become a more frequent case. The non-DC moment tensors can be, for example, interpreted by a combination of pure shear and tensile faulting of cracks with different orientation (Julian et al. 1998). Another approach uses the concept of a tensile earthquake (Vavryčuk, 2001) with a slip vector deviated from the fault surface (Fig. 1), which results in observing a full moment tensor comprising the DC as well as the non-DC components. In this paper we explore the synthetic moment tensor of tensile earthquake and test the stress state leading to a combined shear and tensile faulting.

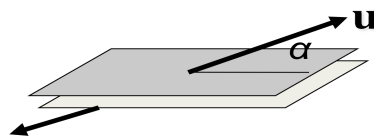


Figure 1. The schematic model of tensile earthquake; the slip vector is deviated from fault plane by α .

Moment tensor of tensile earthquake

The detection of fault opening or closure during earthquakes is now of concern to seismologists. The related change in volume of the source area is a proxy to the possible role of high-pressure fluids in the seismogenic process. Volume increase indicates an elevated fluid pressure preceding the earthquake, which leads to the coseismic opening of a newly formed or pre-existing fracture. In contrast, a volume decrease indicates that releasing the fault planes during seismic slip allowed the confining stress to close some of the open space in the fault zone. The information about the portion of the shear and volumetric components of the seismic slip is carried by the radiated seismic waves and can be inverted to get the seismic moment tensor. The moment tensor contains the information about the orientation of the fault plane, and also about the double-couple and non-double-couple components of the seismic source, which are thought to be signs of fluid presence. The studies of moment-tensor of fluid-related earthquakes show ambiguous results. Some give significant non-DC components of swarms, like microearthquakes induced by hydraulic injection in gas formations and geothermal fields (Horálek et al, 2002; Šílený et al., 2009; Baig and Urbancic, 2010; Julian et al., 2010). Others conclude that some earthquake swarms and seismicity accompanying injections into a granitic geothermal reservoir are almost pure-DC (Horálek et al, 2010a; Horálek et al., 2010b).

Interestingly, the moment tensors of many non-DC earthquakes plot along the dipole coordinate of the source-type plot of Hudson (1989), see Fig. 2, which corresponds to the moment tensor with principal axes $[0, 0, 1]$. Similar moment tensors of dipole type were obtained also by Baig and Urbancic (2010), Julian et al. (2010) and Horálek et al. (2010). To explain the moment tensors of dipole character, concept of a combined source composed of pure tensile and pure shear failures was proposed by

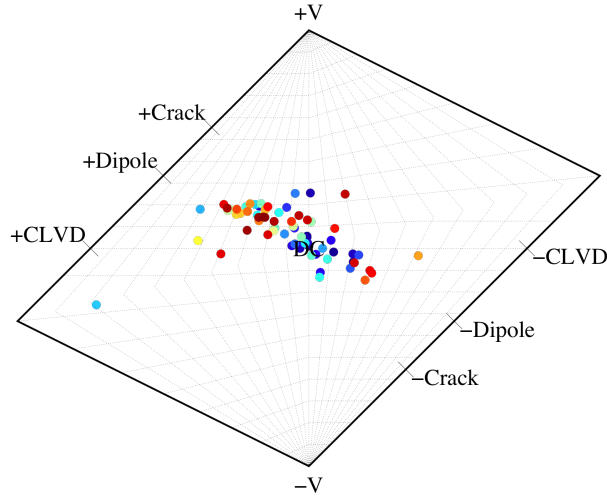


Figure 2. Moment tensors for 70 earthquakes (M_L in the range from 0.3 to 2.9) of the 1997 earthquake swarm in West Bohemia (Horálek et al., 2002) in the source type plot of Hudson (1989). The color is proportional to the sequential event number so that the earliest events are blue and the latest events are red. The axes labels indicate elementary moments; $+V$ and $-V$ standing for pure explosion and implosion.

Julian et al. (1998). In the next we show that also the tensile earthquake with slip vector deviated from the fault plane (Vavryčuk, 2001) can explain the observed moment tensors. To this purpose we calculated the unit moment tensor of point-source tensile earthquake as

$$\mathbf{M} = \begin{bmatrix} \lambda \sin \alpha & 0 & \mu \cos \alpha \\ 0 & \lambda \sin \alpha & 0 \\ \mu \cos \alpha & 0 & (\lambda + 2\mu) \sin \alpha \end{bmatrix} \quad (1)$$

(Vavryčuk, 2001), where λ and μ are the Lamé coefficients of the fault and α is the deviation of the slip vector from the fault (see Fig. 1). Fig. 3 shows the source-type plot of the tensile earthquake for different ratios $\kappa = \lambda/\mu$. It appears that $\kappa=1$ (Poissonian solid) corresponds to a fault of crack character showing moment tensor with principal axes $[1, 1, 3]$. The dipole type of moment tensor requires $\kappa \rightarrow 0$, which implies the ratio $v_p/v_s = 1.41$ and Poisson ratio $\nu=0$, i.e. a fully compressible solid. On the other hand, the pure isotropic source $[1, 1, 1]$ would occur for $\kappa \rightarrow \infty$, which corresponds to $\mu \rightarrow 0$, $v_s \rightarrow 0$ and $\nu=0.5$, i.e. an incompressible matter. Note also that the tensile earthquake of compensated linear vector dipole (CLVD) type requires negative λ , which would imply a structural instability of the rock. Luckily, most of the published moment tensors lie above (for $\text{CLVD} > 0$) or below (for $\text{CLVD} < 0$) the dipole axis, thus the rather unphysical situation of $\lambda < 0$ is not required to explain the observed moment tensors by the tensile earthquake model.

Stress conditions for tensile earthquakes

A common clue to the elevated fluid pressure is the presence of opening of the fault, which results from the tensional effective normal stress acting on the fault plane. The

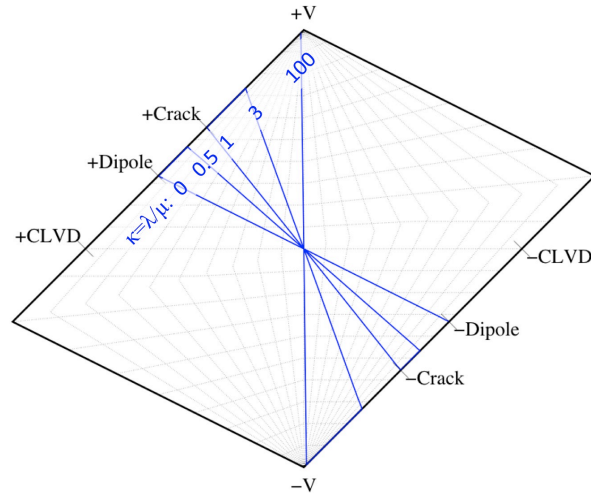


Figure 3. Source types of the tensile earthquake for different ratio of Lamé constants $\kappa = \lambda/\mu$. The indicated values of κ (0, 0.5, 1, 3, and 100) correspond to the v_p/v_s ratios of 1.41, 1.58, 1.73, 2.24 and 10.

traction on a fault plane is controlled by the relative orientation of the stress tensor and the fault plane. This is analyzed graphically by the Mohr-Coulomb diagrams, which describe the relation between the shear traction τ on the normal traction σ_n resolved on a plane (Fig. 4a). In a 2D case the state of stress in the rock is fully described by the Mohr circle of the diameter $\sigma_1 - \sigma_3$ with the center at $(\sigma_1 + \sigma_3)/2$; σ_1 and σ_3 being the maximum and minimum effective stress, respectively. The i -th component of effective stress σ_i is defined as

$$\sigma_i = \sigma_i^{abs} - P, \quad (2)$$

where σ_i^{abs} is the absolute stress and P is the pore fluid pressure. The shear and normal tractions on the fracture oriented at the angle θ to the σ_1 direction are determined by the intersection of the radius at angle 2θ with the Mohr circle. The pressure of the injected fluid acts against the absolute stress decreasing the effective stresses, which results in shifting the Mohr circle to the left. When the strength of the rock is reached, either by increasing the fluid pressure or the differential stress, the rock breaks by creating a fresh fracture oriented according to the internal rock friction. All stress states described by Mohr circles that do not touch the strength envelopes are stable. The resulting non-linear strength envelope is often replaced by a linearized Mohr-Coulomb failure criterion (Fig. 4a)

$$\tau_f = S_0 + \mu_i \sigma_n, \quad (3)$$

which proves valid for most rocks (e.g. Zoback, 2007); here S_0 is the rock cohesion. For non-linear failure envelopes, eq. 2 describes the failure envelope tangent.

The polarity of the normal traction affects the possible coseismic opening or closure of the fault plane and associated volume changes and defines the extensive and compressive failure domains (Fig. 4b). In the extensive domain when the tensile

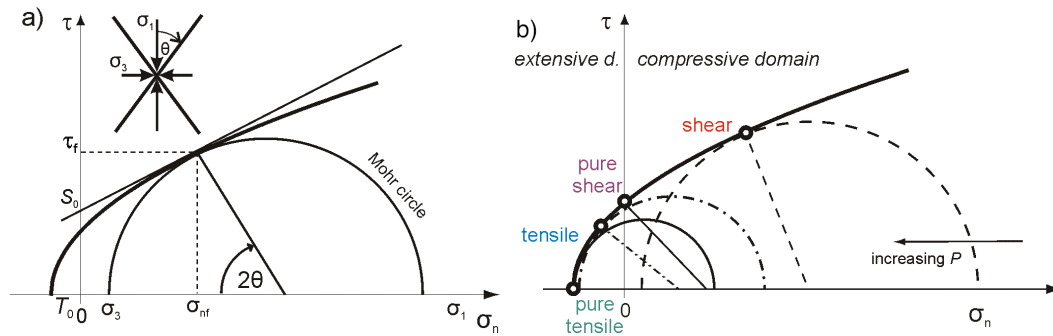


Figure 4. Stress and rock failure, σ_1 and σ_3 are the maximum and minimum effective principal stresses, $\sigma_i = S_i - P$. a) The Mohr's circle shows the locus of shear traction τ and normal traction σ_n upon a plane deviated from σ_1 by θ . Failure occurs when Mohr circle intersects the failure envelope. The tangent corresponds to the linearized failure criterion. b) The failure envelope may be determined empirically by increasing the differential stress ($\sigma_1 - \sigma_3$) or pore pressure P . According to the relations between τ and σ_n , the pure tensile, tensile, pure shear and shear failure modes are defined.

strength of the rock is exceeded by the effective normal stress fracture opening occurs in all cases. In contrast, the compression of any magnitude does not always suffice for a fracture closure. This could happen either if the fault is propped by a roughness of the fault surface or by over pressurized fluids. In the former case the seismic slip may allow for fault closure as a result of fitting in the fault surface irregularities. Such situation is quite seldom in natural earthquakes: despite all of them occur in compressive domain, the negative volumetric components of moment tensors are not observed. In the latter case the fault closure would result from pressure decrease in the post-injection period of hydraulic treatments as observed e.g. by Baig and Urbancic (2010) or Julian et al. (2010). As fracture opening and closure is of a direct interest of hydraulic fracturing, we explore under which conditions such an earthquake can occur.

Failure of intact rock. In order to understand shear deformation of rocks, which occurs for the positive confining pressure, i.e. if $\sigma_n > 0$, the failure criterion can be approximated by the linear strength envelope. However, in order to learn about the behavior of rocks in the tensile regime, one must focus on the relatively small region of the strength envelope where the effective normal stress is negative and the strength envelope is strongly non-linear. In terms of possible coseismic volume changes the intersection of Mohr circle with the strength envelope enables definition of stress intervals of pure tensile ($\sigma_n < 0$, $\tau_f = 0$; crack opening with no shear component), tensile ($\sigma_n < 0$, $|\tau_f| > 0$; shear accompanied by crack opening), pure shear ($\sigma_n = 0$, $|\tau_f| > 0$; no volume change) and shear ($\sigma_n > 0$, $|\tau_f| > 0$; shear accompanied by possible closure) fractures (Fig. 4b). The tensile fractures, which represent a continuous transition from pure tensile to shear fractures are also known in the literature as combined fractures, hybrid shear fractures, mixed-mode fractures or transitional-tensile fractures. As discussed by Engelder (1999), their existence has been doubted based both on observations in the field and linear fracture-mechanics models. However, a strong support for their occurrence was brought by the laboratory experiments of Ramsey and Chester (2004). As illustrated in Fig. 4b, the stress window of this regime is much wider than for the pure tensile opening, which makes the occurrence of combined failure more likely. It is further in accordance with the model of tensile earthquake by

Dufumier and Rivera (1997) and Vavryčuk (2001), see Fig. 1. Provided the slip takes place along the traction, the pure tensile, tensile, pure shear and shear fracture correspond to the slip vector oriented perpendicular, inclined inward, parallel and inclined outward to the fault plane, respectively.

The probability of the non-shear component depends on the differential stress represented by the diameter of the Mohr circle so that the Mohr circle intersects the strength envelope at the point where effective normal stress is negative and shear stress is smaller than cohesion. The condition for a tensile component thus depends on the failure envelope and fracture orientation θ . The intervals of fracture orientation and differential stress that are plausible for tensile failure are obtained by determining the coordinates of the intersection between the failure envelope and Mohr circle. Fischer and Guest (2010) used the Griffith failure criterion $\tau_f^2 = S_0(2\sigma_n + S_0)$ and found that the maximum angle $\theta_{MAX} = 22.5^\circ$ and the maximum differential stress $(\sigma_1 - \sigma_3)_{MAX} = 2\sqrt{2}S_0$. Thus, for the Griffith's failure criterion the tensile opening will occur on all fractures trending within 22.5° of $SHmax$ if the differential stress is smaller than $\sim 2.8 S_0$. If one these two conditions is not met, the rock will fail in shear mode. For the typical rock cohesion $S_0 = 20$ MPa the maximum differential stress for the occurrence of tensile faulting thus reaches 56 MPa. Under real conditions this value is probably much smaller due to preexisting fractures with significantly smaller cohesion as discussed below.

The differential stress depends on the regional stress, where the more tectonically active region has higher differential stress. Along with the vertical stress also the differential stress increases with depth (Zoback, 2007), which could result in a decreasing occurrence of crack opening with depth. However, the differential stress is affected by the pore pressure. In overpressured formations where pore pressure approaches the vertical stress the least principal stress must always exceed the pore pressure (Zoback, 2007) in order to avoid natural hydrofracturing. Thus all three principal stresses must be close to the vertical stress, which puts significant constraints to the differential stress. It is worth to note that the mechanism leading to this equilibrium is the same as illustrated in Fig. 4b. The gradually increasing pore pressure, which took place during the overpressure buildup in the geological past, lead to shifting the Mohr circle to the left and a stepwise release of differential stress on well-oriented faults (Zoback, 2007). As a result, the high pore pressure in large depths leads to smaller differential stress (smaller diameter of the Mohr circle) and higher probability of crack opening.

Failure of preexisting fractures. So far we focused to the situation when a new fracture is created in a homogeneous rock whose strength is characterized by the failure envelope and coefficient of internal friction (Fig. 4a). However, plenty of natural fractures and joints exist in real rocks. Two features characterize each of them: (i) the orientation, which, along with the stress state constrain the shear and normal tractions, and (ii) the failure envelope whose strength is smaller than the strength of intact rock (Fig. 5a). If pore pressure increases, the radii representing the stress on the fractures shift to the left until they touch the corresponding failure envelopes (Fig.

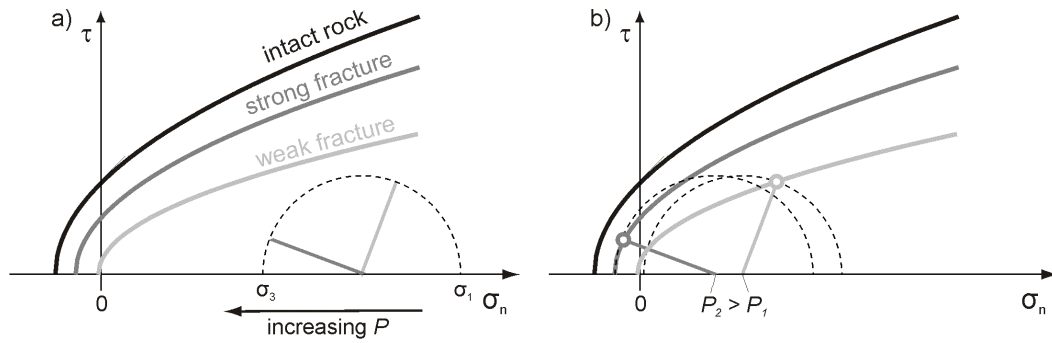


Fig. 5. Influence of preexisting fractures to the occurrence of tensile component. The fractures A have smaller cohesion and are optimally oriented for shear compared to more cohesive fractures B that strike subparallel to σ_1 (a). With increasing pore pressure first the A fractures break as shears ($\sigma_n > 0$) and are followed by fractures B that break as tensile events ($\sigma_n < 0$, $\tau > 0$) (b).

5b). Thus the individual fractures break, each at different normal and shear stress. With increasing pore pressure, the less cohesive fractures A would break first in the compressive domain and would be followed by a tensile failure of the more cohesive fractures B striking at smaller angle to σ_1 . A similar behavior was observed during the 1997 swarm in West Bohemia (Horálek et al., 2002) when two different focal mechanisms occurred. The oblique-normal events in the first swarm period showed shear with small compressive component (blue symbols in Fig. 2 - crack closure), while in the second swarm period events with large tensile component prevailed (red symbols in Fig. 2 - crack opening).

Discussion and conclusions

The rare occurrence of tensile events in seismological studies raised the question of whether these events are so small that they are not detectable or if they even exist. To explore the conditions for their occurrence we combined the approaches of seismology and rock mechanics. We find that the observed moment tensors of dipole and crack types can be successfully modeled by a tensile earthquake with slip vector, which deviates from the fault plane. The percentage of volumetric component is controlled by the relative magnitude of Lamé coefficients.

Our analysis of seismic failure and corresponding crack opening or closure is based on the Griffith failure criterion. Its simple analytic form enabled determine favorable conditions for occurrence of tensile earthquakes. Because real rock behavior does not fully follow the Griffith failure predictions, real stress and angle limits for tensile fracture occurrence will partially differ from those given above. However, the shape of the particular failure envelope does not affect the facts that tensile events would be limited to fractures trending close to the SH_{max} direction and areas with small differential stress. These involve either shallow depths at hydrostatic stress conditions or overpressurized reservoirs at greater depths.

We explored the static problem in terms of the stress preceding the earthquake rupture nucleation. We are aware that the dynamic effects accompanying crack growth and

rupture propagation could change the ratio between the tensile and shear components. However, the fact that observations show significant non-DC components in some fluid-induced microearthquakes implies that fault opening should be taken in account in exploring the role of extensional stress at earthquake sources.

Acknowledgments

The discussions with Václav Vavryčuk, Josef Horálek and Jan Boháč are highly appreciated. The work of the first author was supported by the Czech research project MSM0021620855 and Norway Grants project A/CZ0046/2/0015.

References

- Baig A. and Urbancic T. (2010). Microseismic moment tensors: A path to understanding frac growth. *The Leading Edge*, March 2010, 320-324.
- Dufumier, H., and L. Rivera (1997). On the resolution of the isotropic component in moment tensor, *Geophys. J. Int.*, 131, 595-606.
- Engelder, T. (1999). Transitional-tensile fracture propagation: a status report: *Journal of Structural Geology*, 21, 1049-1055.
- Fischer T. and Guest A. (2010). Shear and tensile earthquakes caused by fluid injection, *Geoph. Res. Lett.* submitted.
- Horálek, J., Šílený, J. and Fischer, T. (2002). Moment tensors of the January 1997 earthquake swarm in West Bohemia (Czech Republic): double-couple vs. non-double-couple events. *Tectonophysics*, 356, 65-85.
- Horálek J., Jechumtálová Z., Dorbath L., Šílený J. (2010). Source mechanisms of micro-earthquakes induced in a fluid injection experiment at the HDR site Soultz-sous-Forêts (Alsace) in 2003 and their temporal and spatial variations. 181, 1547–1565.
- Hudson, J. A., R. G. Pearce, and R. M. Rogers (1989). Source type plot for inversion of the moment tensor, *J. Geophys. Res.*, 94, 765–774.
- Julian, B. R., A. D. Miller, and G. R. Foulger (1998), Non-double-couple earthquakes 1. theory, *Rev. Geophys.*, 36, 525 – 549.
- Julian, B. R., G. R. Foulger, F. C. Monastero, and S. Bjornstad (2010), Imaging hydraulic fractures in a geothermal reservoir, *Geophys. Res. Lett.*, 37, L07305.
- Nolen-Hoeksma, R. C. and Ruff J.R. (2001). Moment tensor inversion of microseisms from the B-sand propped hydrofracture, M-site, Colorado. *Tectonophysics*, 336, 163-181.
- Ramsey, J. M., and Chester, F. M. (2004). Hybrid fracture and transition from extension fracture to shear fracture: *Nature*, 428, 63-66.

- Rutledge, J.T., Phillips, W.S., and Mayerhofer, M.J. (2004). Faulting induced by forced fluid injection and fluid flow forced by faulting: An interpretation of hydraulic-fracture microseismicity, Carthage Cotton Valley gas field, Texas, *Bulletin of the Seismological Society of America*, 94, 1817–1830.
- Šílený, J., D.P. Hill, L. Eisner, and F.H. Cornet (2009). Non-double-couple mechanisms of microearthquakes induced by hydraulic fracturing: *Journal of Geophysical Research*, 114, B08307.
- Vavryčuk, V. (2001). Inversion for parameters of tensile earthquakes, *Journal of Geophysical Research*, 106, 16339-16335.
- Vavryčuk, V. (2007). On the retrieval of moment tensors from borehole data, *Geophysical Prospecting*, 55, 381-391.
- Zoback, M. D. (2007). *Reservoir geomechanics*: Cambridge University Press, Cambridge, UK 1–499.

Seismic noise: A challenge and opportunity for seismological monitoring in densely populated areas

Jörn Groos and Joachim Ritter

Geophysical Institute, Karlsruhe Institute of Technology, Hertzstr. 16, 76187 Karlsruhe, Germany, joern.groos@kit.edu, joachim.ritter@kit.edu

Abstract

We discuss the ambient seismic noise in densely populated areas which significantly complicates the seismological monitoring of induced seismicity due to geothermal power plants or CO₂ sequestration. We use a statistical time series classification scheme in combination with a spectral time-frequency analysis to demonstrate the most important properties of the urban seismic noise. The analysis focuses on the frequency range above 1 Hz which is important for the seismological monitoring of micro-earthquakes ($M_L < 3$). We select amongst others representative measurements in the vicinity of geothermal power plants in the densely populated south-western part of Germany. Finally we review the promising opportunities to turn seismic noise into a signal for seismological monitoring.

Introduction

Several of the new techniques using the deep underground, such as geothermal power exploitation or CO₂ sequestration, have to be installed in densely populated areas to be economically successful. Geothermal power plants need access to the district heating network to efficiently use the low-temperature heat remaining after electric power production. Therefore, even weak and non-destructive induced micro earthquakes became a serious problem for operators of geothermal power plants as such events are felt by many residents (Giardini, 2009). This induced seismicity causes a loss of acceptance for new technologies in the local population. The potential application of CO₂ sequestration struggles with similar problems as large coal power plants are also installed in densely populated areas. A transparent and comprehensive (seismological) monitoring of new interventions in the underground is crucial to achieve and keep the public acceptance.

Seismological monitoring in cities and densely-populated areas is a challenging task due to the complexity of the man-made seismic noise. Especially the important identification of micro-earthquakes, which are unnoticeable for humans, is made difficult by numerous man-made sources of seismic energy such as traffic and industry. Man-made seismic signals are the dominant source of seismic energy in the frequency range of interest above 1 Hz. A good knowledge and understanding of the seismic noise in densely populated areas is important for the successful planning and operation of seismological monitoring networks. Especially the identification of

suitable measuring sites at the surface is important as the installation of entire networks in boreholes is hardly possible for economic and/or practical reasons. Furthermore, the reliable identification of micro-earthquakes requires a good knowledge of the local seismic noise besides other parameters (e.g. seismic velocity structure, etc.).

Data set and analysis

In the following the properties of seismic noise in densely populated urban areas are demonstrated with the help of seismological measurements in the Upper Rhine Graben (URG) in Southwest Germany. From December 2004 until May 2006 the TIMO network (Ritter et al., 2008) was operated and since July 2009 the second phase TIMO2 is under way (Figure 1). The URG is interesting for the installation of geothermal power plants due to heat flow anomalies (Hurtig et al., 1991). The first geothermal power plants are already in operation, some 20 plants are in the planning phase. Since historical times, the URG is densely populated and of high economical importance due to the mild weather conditions, the good farmland (sediments) and the vicinity of the river Rhine.

Seismic noise is high in the URG due to major traffic lines (railway, highways), industry and unconsolidated sediments. Numerous of the important urban areas worldwide have developed in such sedimentary settings near rivers comparable to the URG. The map in Figure 1 displays the station locations. TIMO2 stations TMO26, TMO54 and TMO70 are located on cemeteries at the outskirts of small towns. TMO52 is inside a former mill which now is used as a residential building outside a village. TMO57 is situated on a farm. For comparison also seismological measurements outside the URG are included in the following. We demonstrate the significant influence of the dense population and the sedimentary setting on seismic noise by a comparison with seismological measurements at the Black Forest Observatory (BFO). The BFO is located in a remote old mine in a hard-rock setting. The BFO is known for high-quality measurements with low noise conditions even on a global scale.

The properties of the urban seismic noise are discussed with the help of a statistical time series classification and a spectral time-frequency analysis. The time series classification (Groos & Ritter, 2009) uses ratios of amplitude intervals (I) and percentiles (P) to identify and quantify the deviations of the time series histogram from the Gaussian distribution. In the case of a zero mean Gaussian distribution, 68% of the measurements lie within an interval of one standard deviation away from zero (I68). 95.45% of the measurements are within two times the standard deviation (I95) and 99.73% of the measurements are within three times the standard deviation (I99). This is also known as the 2- σ and 3- σ , or the ‘empirical’, rule.

We introduce the ratio between I99 and I95 as the new quantity peakfactor (pf) to determine the “peakedness” of the histogram. The peakfactor of a Gaussian distributed time series equals 1.5. Furthermore, the ratios of the lower and upper boundaries of the intervals (e.g. the 16-percentile (P16) and the 84-percentile (P84) for I68) can reveal a possible asymmetry of the histogram. The peakedness and the asymmetry of a time series histogram, especially in comparison to the Gaussian

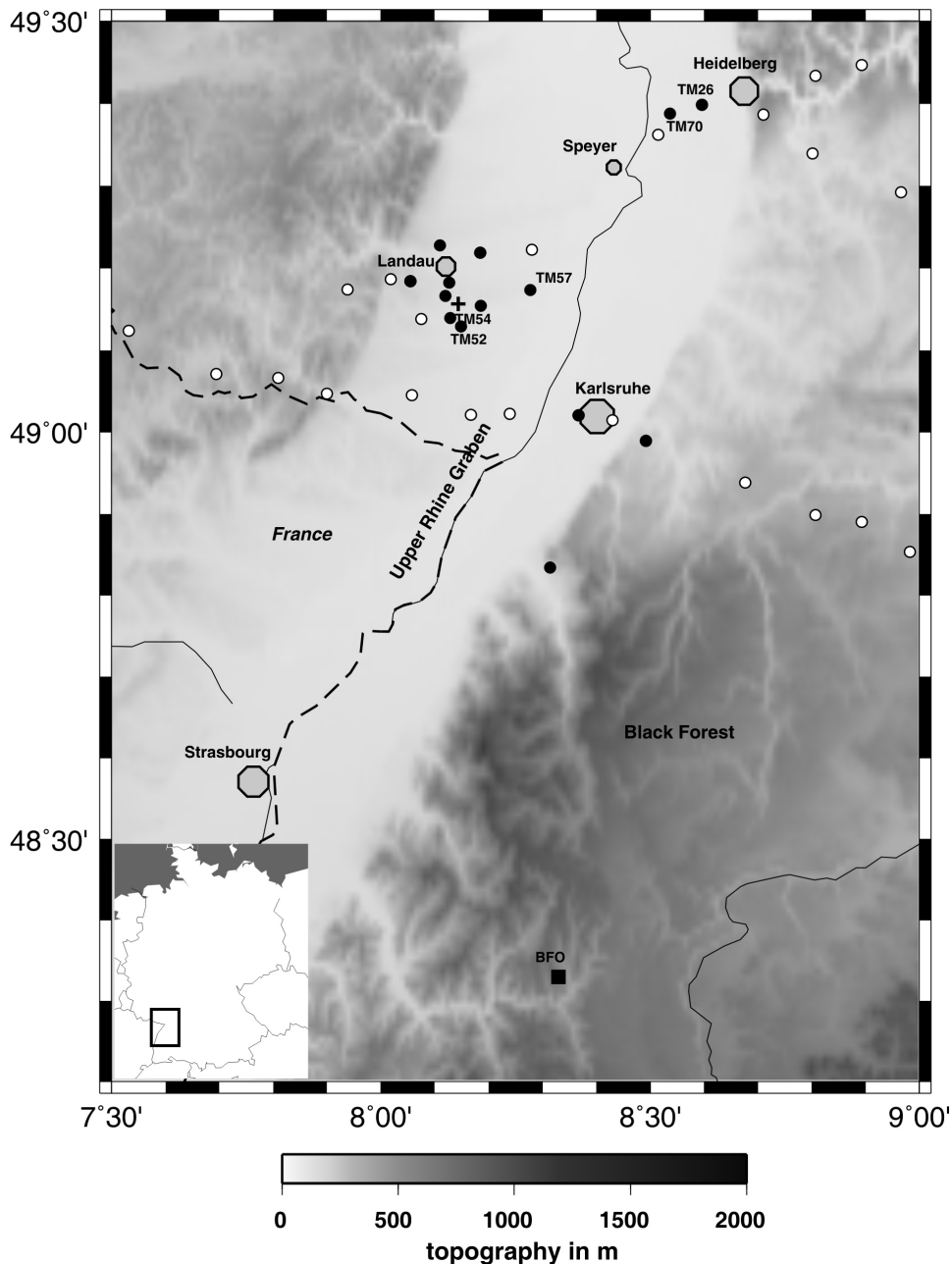


Figure 1: Recent seismological broadband experiments in the region of the Upper Rhine Graben: TIMO experiment (white circles) and TIMO2 experiment (black circles). The approximate epicentre area of 2 events on 9. Apr. 2010 is given by the cross.

distribution, are commonly described by the statistical measures kurtosis and skewness of a time series. Unfortunately, the common statistical estimators for the kurtosis and skewness are not suitable for broadband seismic noise time series with more than 1 million samples (Groos & Ritter, 2009). Therefore, the ratios between the amplitude intervals (e.g. the peakfactor) and the amplitude percentiles (e.g. P84/P16) of the time series are used to classify the seismic noise time series (see Table 1 and below). The ranges of the amplitude intervals are used for quantification.

Noise class	I95/ I68	I99/ I68	Peakfactor			P84/ P16	P97.5/ P2.5
1	2±0.05	3±0.15				1±0.015	1±0.015
2			1.4≤	pf	≤1.6	1±0.030	1±0.047
3			1.6<	pf	≤2	1±0.030	1±0.047
4			2.0<	pf		1±0.030	1±0.047
5				pf	<1.4	1±0.030	1±0.047

Table 1: Criteria for the interval and percentile ratios to classify symmetric time series as noise classes NC1-NC5.

We introduce six noise classes to classify the typically observed deviations of seismic noise time series from the Gaussian distribution (Groos & Ritter, 2009). Time series are assumed to be Gaussian distributed if the interval ratios exhibit only very small deviations from the empirical rule and the histograms are symmetric (Table 1). Gaussian distributed time series are classified as noise class 1 (NC1). Non-Gaussian but symmetric time series are classified as NC2-NC5 depending on the observed deviation properties (Table 1). Time series which exhibit determinable but rather small and unspecific deviations from the Gaussian distribution ($pf \approx 1.5 \pm 0.1$) are classified as noise class 2 (NC2). Time series with a gentle peaked histogram in comparison to the Gaussian distribution ($1.6 < pf \leq 2$) due to few transient signals are classified as noise class 3 (NC3). A more pronounced peakedness of the histogram ($pf > 2$) results in a classification of the time series as noise class 4 (NC4). Symmetric time series with a flattened histogram in comparison to the Gaussian distribution ($pf < 1.4$) are classified as noise class 5 (NC5). All time series which are not identified as symmetric time series (see criteria for the ratios $P84/|P16|$ and $P97.5/|P2.5|$ in Table 1) are classified as noise class 6.

Only the four noise classes NC1 to NC4 are relevant for the following discussion of the seismic noise in the URG. Time series of seismic noise classified as NC5 or NC6 are in general seldom observed (Groos & Ritter, 2009). Naturally, the detection of seismic waves excited by micro-earthquakes is less complicated, if the seismic noise itself exhibits only few transient signals. Therefore, the noise classification is a valuable tool for the selection of measuring sites. Next to the seismic noise amplitudes (e.g. the I68 and I95 amplitudes) also the frequency of occurrence of transient signals can be considered for site selection. Assuming the same noise amplitudes, a station site with a lower noise class should be preferred.

The urban seismic noise

A comprehensive and complete literature review of the current knowledge about the seismic noise wave field in general is given by Bonnefoy-Claudet et al. (2006). A detailed discussion of the Urban Seismic Noise (USN) in the frequency range from 8 mHz to 45 Hz is given by Groos & Ritter (2009). In the following, we discuss briefly the USN above 1 Hz which is dominated by man-made signals.

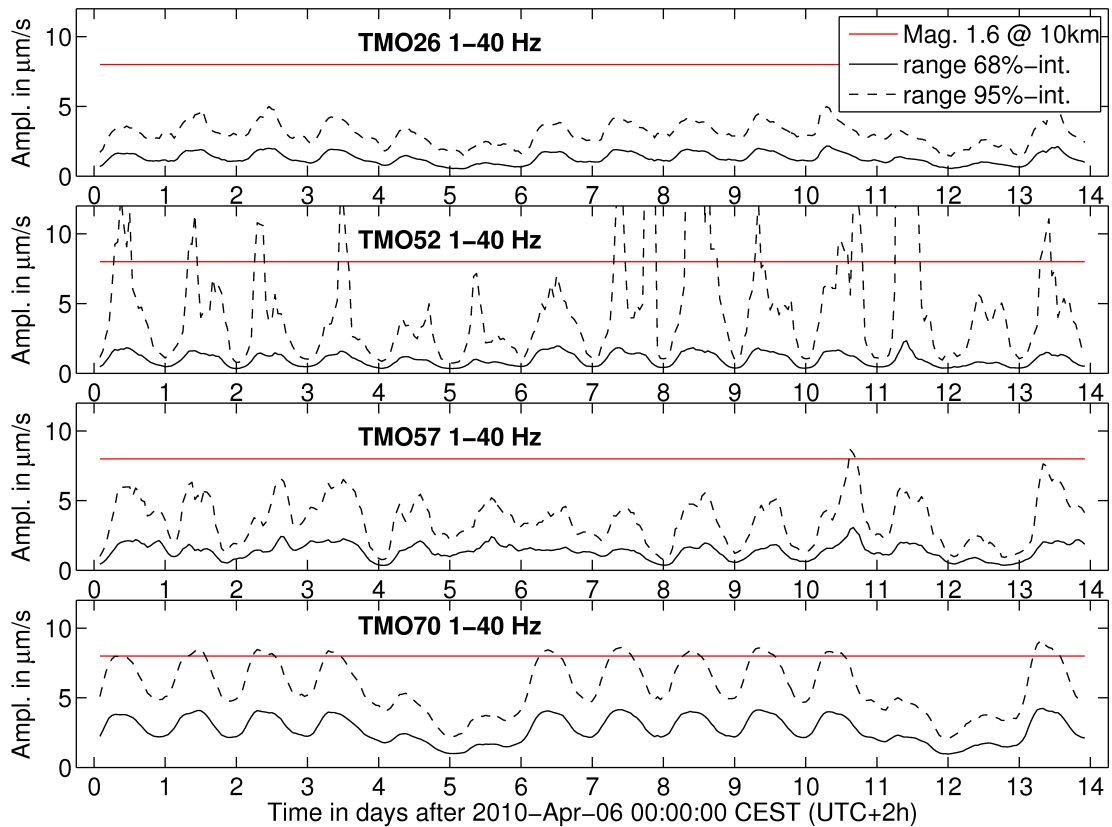


Figure 2: The seismic noise amplitudes (ranges of amplitude intervals I68 and I95) determined in a sliding 4 hour time window (step length 1 hour) in the frequency range 1-40 Hz at TMO stations 26, 52, 57 and 70. All sites are located in the URG. The red lines indicate exemplary the direct P-wave double amplitude of a M_L 1.6 earthquake near Landau (2010-04-07 09:04:04) observed in the URG at a distance of 10 km to the epicentre. The first day (2010-04-06) was a Tuesday.

The typical temporal variations of the vertical component USN (1-40 Hz) are demonstrated with the help of the noise amplitudes (ranges of the amplitude intervals I68 and I95) determined with a sliding 4 hour time window (step length 1 hour). The noise amplitudes (ground motion velocity) over 14 days in April 2010 are plotted in Figure 2 for several sites located in the URG. A distinct daily pattern at all sites demonstrates the dominant influence of human activity on the USN in the frequency range 1-40 Hz. The nightly amplitude lows of ~5 hours are much shorter than the daily highs of ~19 hours. Besides this daily pattern, the USN also contains a distinct weekly pattern at most sites (see the weekends at days 5 and 6 as well as 12 and 13).

The red lines in Figure 2 indicate exemplary the p-onset double amplitude measured at a distance of 10 km to the epicentre of a M_L 1.6 earthquake which occurred in the URG near the city of Landau. It is a rule of thumb that a transient signal should be larger as two to three times the 95% interval of the time series to emerge clearly from the background signals. The examples in Figure 2 illustrate that a P-wave with a double amplitude of ~8 $\mu\text{m/s}$ emerges not clearly from the seismic noise at several typical surface sites in the URG. For example, such a p-onset is only one transient signal amongst many others at sites such as TMO52 or TMO70 because the P-wave double amplitude is even smaller than the 95% amplitude interval at daytimes.

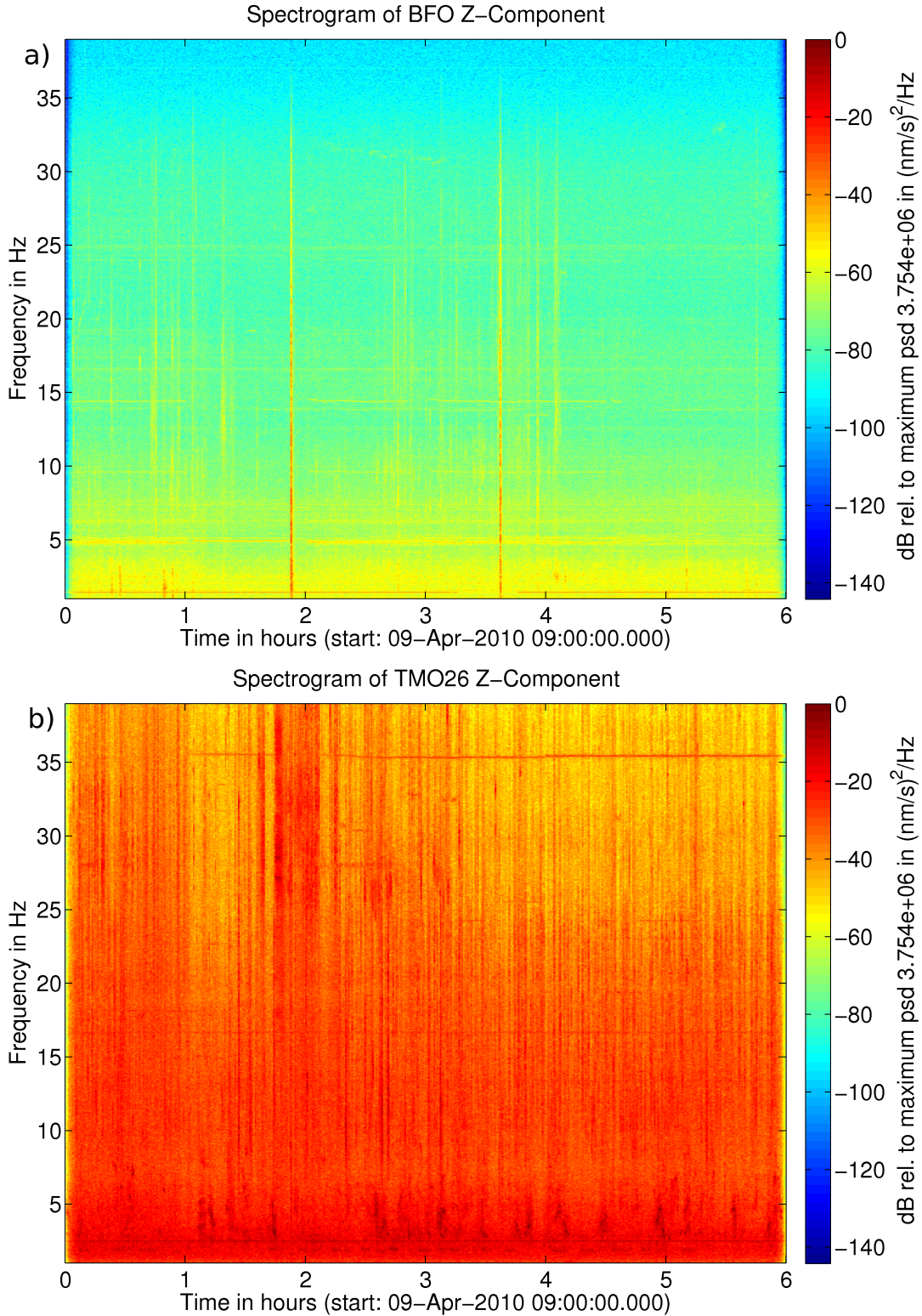


Figure 3: Spectral time-frequency analysis (power spectral density in dB by colour) of the vertical component seismic noise between 1 Hz and 40 Hz at station (a) BFO and (b) TMO26. The colour bars are normalised identically to the largest power spectral density observed at site TMO26 for comparison.

Therefore, a dense and sensitive seismological network is necessary in such a setting to ensure the observation and identification of micro-earthquakes at several stations for localisation. The examples illustrate furthermore, that the seismic noise amplitudes

exhibit a significant spatial variation (compare for example TMO26 with TMO52) which are further discussed in the next section about station site characterisation. A spectral time-frequency analysis as shown in Figure 3 gives a more detailed insight into the character of the urban seismic noise.

In Figure 3 the spectrograms of 6 hours duration of the vertical component seismic noise (1-40 Hz) are plotted for the stations BFO (Figure 3a) in a mine (solid rock) and TMO26 (Figure 3b) at the outskirts of a small town (sediments). In this time window two earthquakes of M_L 2.4 (2010-04-09 10:52 UTC) and M_L 2.2 (2010-04-09 12:36 UTC) occurred in the URG at the same epicentre near the village of Insheim. Both earthquakes are clearly visible in the recordings at site BFO at a distance of ~90 km to the epicentre due to the very low noise conditions at BFO. The broadband transient signals of the earthquakes are visible in the spectrogram (Figure 3a) as vertical lines of increased power spectral density (red colours). Due to the high noise conditions in the URG the signals of both earthquakes are not identifiable at site TMO26 located at a distance of only 38 km to the epicentre (Figure 3b). The colour scales of both spectrograms are normalised identically to the largest power spectral density (psd) observed at site TMO26 to visualise the tremendous difference of the noise amplitudes between BFO and TMO26.

The most important sources of the observed man-made seismic signals are traffic and industry. In the frequency range above 1 Hz traffic-induced seismic waves are excited by road traffic and trains or can be generated by traffic induced bridge oscillations. These contribute significantly to USN in a broad frequency range from ~1 Hz to more than 45 Hz with maximum amplitudes at 1-10 Hz. Long lasting and very narrow-band signals above 1 Hz, recognised as horizontal lines of increased psd in the spectrograms (e.g. ~2 Hz and ~5 Hz in Figure 3a as well as 16.7 Hz and ~35 Hz in Figure 3b) are sinusoidal-type seismic waves most probably excited by rotating machinery at sharp frequencies. Examples are electrical motors and gear boxes of industrial machinery, power generators and building services machinery. Due to gear boxes and frequency converters such sinusoidal signals can be observed in the whole frequency range from 1 Hz up to the electrical power frequency (50 Hz) but predominantly at frequencies around 2.08 Hz (48 poles; generators and engines), 12.5 Hz (8 poles; engines), 16.7 Hz (6 poles; engines), 25 Hz (4 poles; engines) and 50 Hz (2 poles; engines). A significant drop of psd by up to 20 dB can be observed above 25 Hz towards higher frequencies at most sites in urban areas (Figure 3b).

Site characterisation

The ranges of the amplitude intervals I68, I95 and I99 in combination with the derived noise classification provide a useful tool for site characterization and therefore site selection. It is illustrated by the examples in Figure 2 that not only the noise amplitudes quantified by the amplitude intervals but also the ratios between the amplitude intervals exhibit distinct spatial variations. The ratio between I95 and I68 is increasing with increasing deviations from the Gaussian distribution due to transient signals. As an example, significantly more transient signals are observed at station site TMO52 than at site TMO26 (Figure 2) resulting in an increased ratio I95/I68 at site TMO52. The capability to identify seismic waves excited by a micro-earthquake is therefore significantly limited at site TMO52 in comparison to site TMO26.

The classification results of the 14 days of USN with the sliding 4 hour time window are shown for several TMO sites and site BFO in Figure 4. For this analysis the frequency range 1-10 Hz is selected which is predominantly affected by transient traffic induced signals. For most 4 hour time windows of seismic noise recorded at TMO stations in the URG are classified as NC3 and NC4. They are therefore identified to exhibit a significant number of transient signals complicating the detection of earthquake waves. In contrast, up to 40 % of the 4 hour time windows of the seismic noise recorded at the BFO are Gaussian (NC1) or nearly Gaussian (NC2) distributed. The detection of micro-earthquakes at BFO is enhanced not only by the significantly lower noise amplitudes but also by the more suitable statistical characteristics of the seismic noise in terms of less transient signals.

The seismic noise in the URG above 1 Hz is dominated in general by transient signals but differences between the sites are revealed by the noise classification. The seismic noise at site TMO52 exhibits numerous transient signals which is illustrated not only by the high I95 amplitudes (Figure 2) but also by the classification of nearly 80 % of the 4 hour time windows as NC4 (Figure 4, upper right corner). As indicated by the I95/I68 ratio, the recording conditions are better at site TMO26 with less time windows classified as NC4 (Figure 4, upper left corner). From the statistical point of view, the seismic noise at site TMO70, a cemetery at the outskirts of a town, is most suitable to detect transient signals excited by micro-earthquakes as apparently less man-made transient signals exist. This is indicated by the lower amount of time windows classified as NC4 (below 20 %) and the observation of some nearly Gaussian distributed noise time windows (NC2). Nevertheless, the seismic noise amplitudes at site TMO70 are higher than at the other sites. Especially the comparably high I68 amplitudes even at nighttimes inhibit the detection of small transient signals at this site. Based on the combined analysis of the noise amplitudes and the noise classification sites such as TMO26 and TMO57 should be preferred in comparison to sites such as TMO52 or TMO70.

Concluding, a careful site selection including a statistical noise analysis is capable and necessary to improve seismological monitoring in densely populated areas.

Identification of earthquake signals

As demonstrated above, the discrimination of earthquake signals from other disturbing transient signals present in the ambient seismic noise is the major challenge for seismological monitoring above 1 Hz in densely populated areas such as the URG. Traditional tools such as trigger algorithms for the detection of transient signals alone are not suitable for this task as far most of the numerous transient signals are not related to seismic events. A successful automatic detection system for earthquake waves has to include further characteristics of the signals such as frequency content, waveform or duration. Furthermore it has to be capable to recognise similar and/or reoccurring signals and to provide some kind of signal classification to support and simplify a following manual analysis. A promising aspect is the application of machine learning and pattern recognition techniques to this seismological problem.

One suitable unsupervised pattern recognition technique is the Self-Organising Map (SOM) technique which was already applied successfully to seismological signal

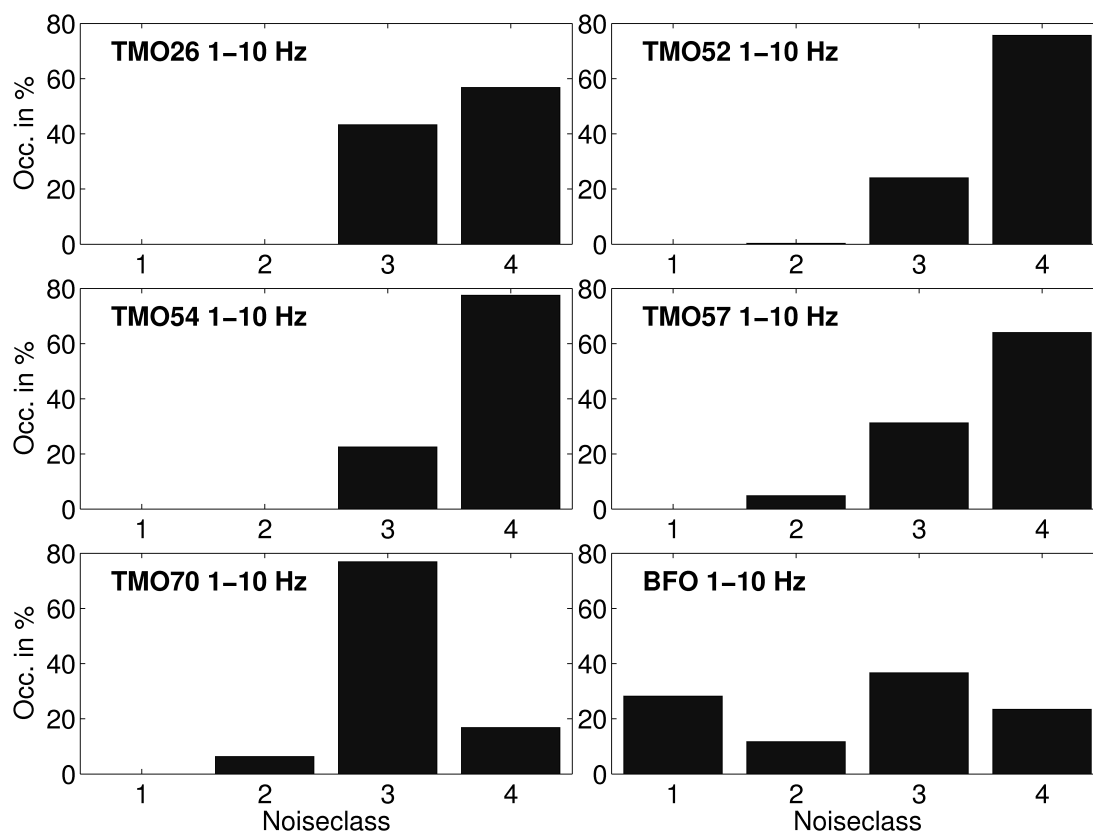


Figure 4: Histograms of the noise classification of 14 days of seismic noise in the frequency range 1-10 Hz with a sliding 4 hour time window (time step one hour) for the station sites TMO 26, 52, 54, 57 and 70 in the Upper Rhine Graben as well as site BFO in a remote mine in the Black Forest.

detection problems (Köhler et al., 2010). This technique is also used for an ongoing analysis of an urban seismic noise data set recorded in the URG in the town of Staufen im Breisgau about 20 km south of Freiburg (Baumann et al., 2010). The inner city area of Staufen ($\sim 200 \times 200 \text{ m}^2$) started to lift up after the drilling of boreholes (140 m) for shallow geothermal heat pumps next to the old town hall in September 2007. The still ongoing uplift is taking place with local uplift rates up to 8 mm/month (www.staufen.de). Between May 2009 and August 2010, up to 9 Karlsruhe BroadBand Array (KABBA) stations were operated with the objective of finding possible seismic signals related to the uplift. Although no seismic signals related to the uplift could be identified up to now, the SOM approach proved to be successful to identify reoccurring transient signals caused by traffic and other sources in the town. The automated discrimination of different types of reoccurring transient signals by machine learning techniques is a promising approach to improve seismological monitoring in complicated settings.

Future opportunities and outlook

The continuously recorded seismic noise, precisely the ambient vibrations of the ground, provides also opportunities for seismological monitoring. Promising in this context is the application of seismic interferometry (Snieder & Wapenaar, 2010). Seismic interferometry denotes the approach to retrieve Green's functions of the

underground from cross-correlations of seismic signals. Green's functions retrieved from seismic noise cross-correlations are successfully used for seismic tomography. Furthermore, subtle changes of the retrieved Green's functions with time can be used to obtain changes of the propagation velocity of seismic waves in the underground of 0.1% or even less (e.g. Sens-Schönfelder & Wegler, 2006). Both approaches are promising applications for the characterisation and monitoring of all kind of underground reservoirs. First tests of this noise based monitoring of reservoirs are taking place for example at the CO₂-sequestration site near Ketzin, Germany (Mündel et al., 2009) and at hydrocarbon reservoirs (Bussat & Kugler, 2009). Concluding, seismic interferometry can be expected to improve and extend the capabilities of seismological monitoring tremendously in the near future.

Acknowledgments

This study is funded by the Federal Ministry for the Environment, Nature Conservation and Nuclear Safety of the Federal Republic of Germany due to an enactment of the German Federal Parliament (Bundestag).

References

- Baumann, T., Ritter, J. & Köhler, A. (2010). Seismological signal classification in an urban environment using self-organizing maps. Abstracts of the European Seismological Commission, 32nd General Assembly, September 2010, Montpellier, France, 262.
- Bonnefoy-Claudet, S., Cotton, F. & Bard, P.-Y. (2006). The nature of noise wavefield and its applications for site effects studies: A literature review. *Earth-Sci. Rev.*, 79, 205–227.
- Bussat, S. & Kugler, S. (2009). Recording noise – Estimating shear-wave velocities: Feasibility of offshore ambient-noise surface-wave tomography (answt) on a reservoir scale. *SEG Expanded Abstracts*, 28, 1627–1631.
- Giardini, D. (2009). Geothermal quake risks must be faced. *Nature*, 462, 848-849.
- Groos, J. C. & Ritter, J. R. R. (2009). Time domain classification and quantification of urban seismic noise. *Geophysical Journal International*, 179, 1213-1231.
- Hurtig, E., Čermák, V., Haenel, R. & Zui, V. (1991). *Geothermal Atlas of Europe*, H. Haack Verlagsgesellschaft, Gotha.
- Köhler, A., Ohrnberger, M. & Scherbaum, F. (2010). Unsupervised pattern recognition in continuous seismic wavefield records using Self-Organizing Maps. *Geophysical Journal International*, 182, 1619-1630.

- Mündel, R., Sens-Schönfelder, C. & Korn, M. (2009). Noise based seismic monitoring of the CO₂-Sequestration site Ketzin, Germany. In: Sens-Schönfelder, C., Ritter, J., Wegler, U. & Große, C. (eds.) (2009). Noise and diffuse wavefields, *Mitteilungen der Deutschen Geophysikalischen Gesellschaft, Sonderband II/2009*, 101-106.
- Ritter, J. R. R., Wagner, M., Wawerzinek, B. & Wenzel, F. (2008). Aims and first results of the TIMO project – Tiefenstruktur des mittleren Oberrheingrabens, *Geotect. Res.*, 95, 151-154.
- Snieder, R. & Wapenaar, K. (2010). Imaging with ambient noise. *Physics Today*, September 2010, 44-49.
- Sens-Schönfelder, C. & Wegler, U. (2006). Passive image interferometry and seasonal variations of seismic velocities at Merapi volcano, Indonesia. *Geophysical Research Letters*, 33, L21302.

ASPECTS CONCERNING SEISMICITY ANALYSES OF THE VIDRARU – ARGES (ROMANIA) DAM AREA

Traian Moldoveanu¹, Klaus-Peter Bonjer², Mircea Pecingine³

¹ S.C. Geotec Consulting SRL, Bucharest, Romania, geotec.trm@mailbox.ro

² formerly with the Geophysical Institute, Karlsruhe Institute of Technology, Germany, kp-bonjer@online.de

³ S.C. Hidroelectrica SA, Filiala S.H. Curtea de Arges, Romania, mircea.pecingine@hidroelectrica.ro

Abstract

The Vidraru–Arges dam is located in a seismically active region of the southern Romanian Carpathian Mountains. The seismic hazard is determined by the strong intermediate-depth earthquakes of the Vrancea zone and by the local seismicity. The strongest local event had a magnitude of $M_S=6.5$. The initial filling of the reservoir started in 1965. After a rapid and complete emptying of the lake in 1974, seismic stations were deployed in 1975 in order to survey the operation of the reservoir after the re-filling. First data showed that the change of the frequency of occurrence of events could be related to the fluctuations of the water level. The maximum height of the water level is 167m and a maximum volume of $465 \times 10^6 \text{ m}^3$ water can be stored. The reservoir is operated at water levels in the average between 150 and 100m. The long-time comparison of the temporal changes of the seismic activity and the variation of the water level revealed that the seismic activity increases after the water level decreases to about 120 to 110m and that the seismic activity ceases when the water level is approaching the height of about 150m.

Introduction

The seismic hazard of the reservoir site is determined by the strong intermediate-depth earthquakes of the Vrancea zone at epicenter distances of about 120-185km, and by the local seismic activity of the nearby Arges-Făgăraș and Câmpulung focal areas (Fig. 1) with hypocenter distances of about 10-40km (e.g. Moldovan et al., 2006).

One of the strongest and well studied local earthquakes occurred on January 26, 1916 near the village of Cumpăna, which is situated at the tail of the Vidraru reservoir at a distance of 15km North of the dam. The source parameters are: $T_0=07:37:55$ (UT), Lat.=45.5°N/Lon.=24.6°E, $M_S=6.5$, $I_0=VIII$ (MSK), focal depth $h=20$ km (Radu, 1990). On-scale records of this earthquake from the Goettingen Seismic Observatory (Germany) are presented in Figure 2.

The seismic history of the Arges-Făgăraș-Câmpulung area clearly reveals a well-marked periodicity of the strong local earthquakes: 84 to 86 years for $I_0 \geq VII$ and 170 to 175

years for $I_0 \geq VIII$ (Fig. 3). The expected event of 2000–2002 (Radu, 1990) did not happen, but one may regard the $M_w=5.2$ Câmpulung earthquake of April 12, 1969 with an epicentral intensity of $I_0 = VI$ as the expected one. However, in Radu's original version of Figure 3 this earthquake is missing.

The initial filling of the Vidraru–Arges reservoir started in 1965. The maximum height of the water level is 167m and a maximum volume of $465 \times 10^6 \text{ m}^3$ water can be stored. The reservoir is operated at water levels in the average between 150 and 100m. Due to increased energy requests the stored water was used even down to the level of 70m in the time period from 1984 to 1996 (see Fig. 6).

The analysis of the local seismicity

The seismic surveillance of the Vidraru-Arges dam and reservoir started in April 1975 and is continuing until today. On the average, 74 earthquakes with magnitudes between $0.5 < M < 3.7$ are observed per year with two to three events in the 2-3 magnitude range. Focal depths are mostly concentrated around 10 km (Moldoveanu et al., 1982). The comparison of the temporal changes of the seismic activity with the variation of the water level reveals that the seismic activity increases when the water level decreases to about 120 to 110m and that the seismic activity ceases when the reservoir level is approaching the maximum height of about 150m (Fig. 5 and 6).

In Figure 5 the water level changes and the occurrence of the earthquakes at the Vidraru-Arges reservoir are summarized, showing that in the average a water level of 117m is the crucial level where seismic activity is changing.

In Figure 6 the annual changes of the water level of the Vidraru-Arges reservoir and the number of events per month in the lake area are shown. The hypocenter distances are less than 40km (i.e. $t_s - t_p \leq 5s$) with respect to the dam site. However, the majority of the events has hypocenter distances between 10 and 25km ($1s \geq t_s - t_p \geq 3s$). The number of earthquakes per loading cycle changes strongly over the 35 years of surveillance. The main reason is the change in the network configuration. From 1975 until mid 1982 three single-component telemetry stations around the lake and one 3-component station at the dam site were in operation. Since then only the dam station was kept running.

The repeatedly observed changes in the seismic activity could be understood on the one hand as a stabilization of the seismic regime by an increase of the load through filling the reservoir and on the other hand by a destabilization, i.e. triggering the seismic activity by unloading the reservoir. This hypothesis would be supported, if the area is experiencing a thrust regime. However, there is neither geological nor seismological evidence for thrust faulting in the lake area. E.g. a composite fault-plane solution from 22 events of the time period from January to June 1977 shows nearly pure normal faulting (Nourescu et al., 1979). Furthermore, the April 12, 1969 Câmpulung $M_w=5.2$ earthquake (at a distance of about 40 km from the reservoir) showed a strike-slip mechanism with a small normal faulting component (Radu, 1974).

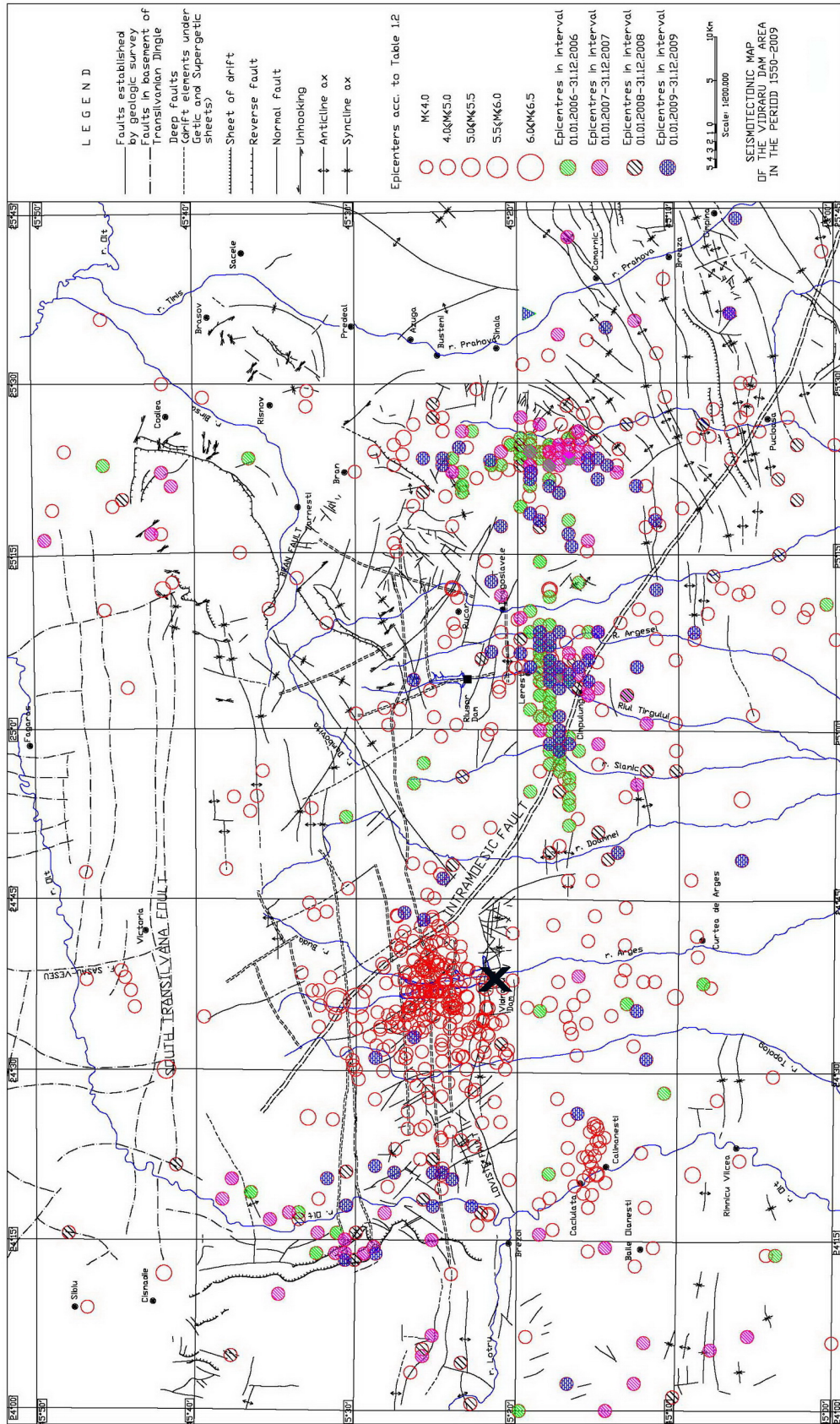


Figure 1: Epicenter map of the Argeș-Făgăraș-Câmpulung area. The bold black X marks the location of the Vidraru-Argeș dam. Seismic data are from Radu (1979), Oncescu et al. (1999), and Moldoveanu (1976-2010).

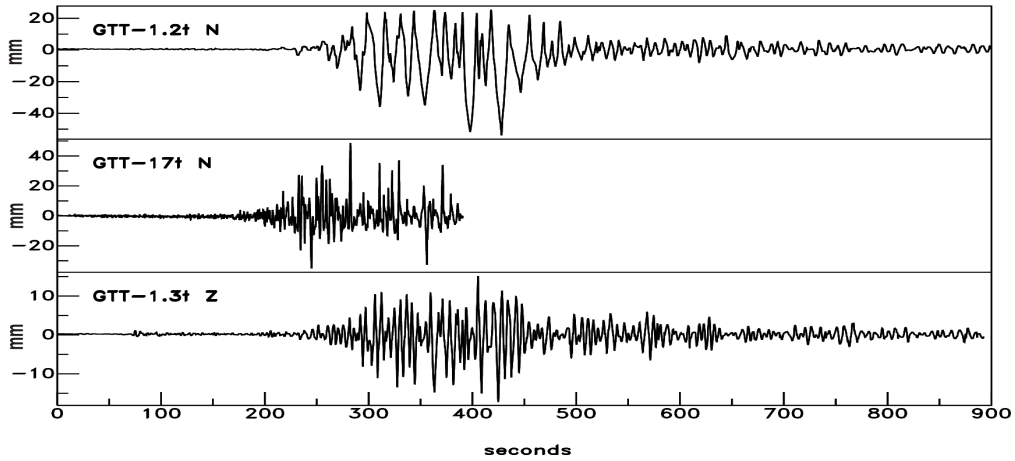


Fig. 2: Făgăraș Earthquake of January 26, 1916: Wiechert-recordings of Goettingen Observatory at an epicenter distance of 11.5 degrees.

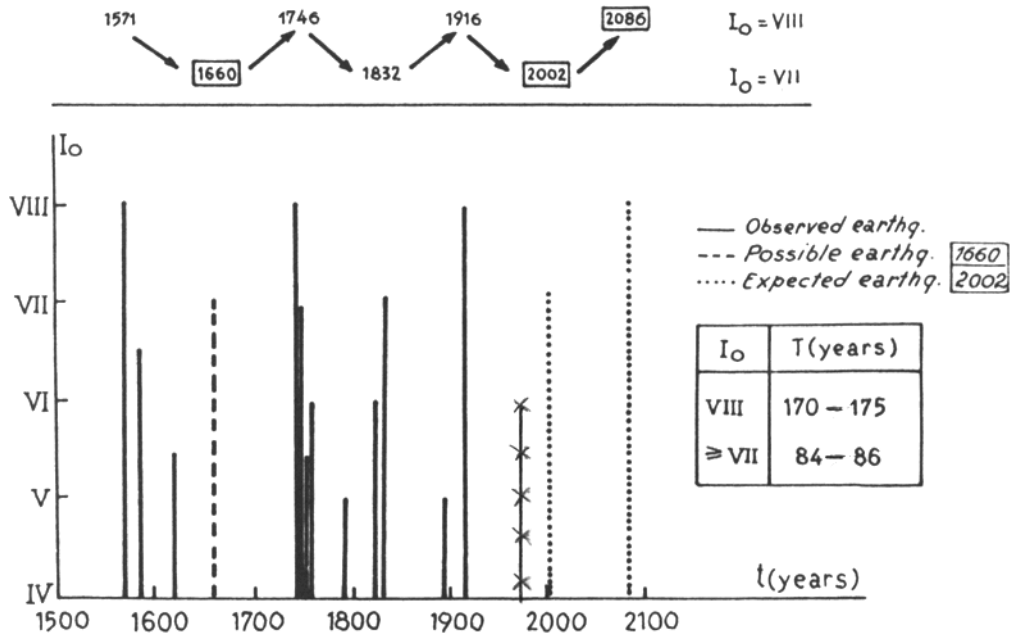


Figure 3: Seismic history of the Arges-Făgăraș-Câmpulung region (C. Radu, 1990). The earthquake of April 12, 1969 (line with crosses) might be regarded as the one expected to happen around 2002.

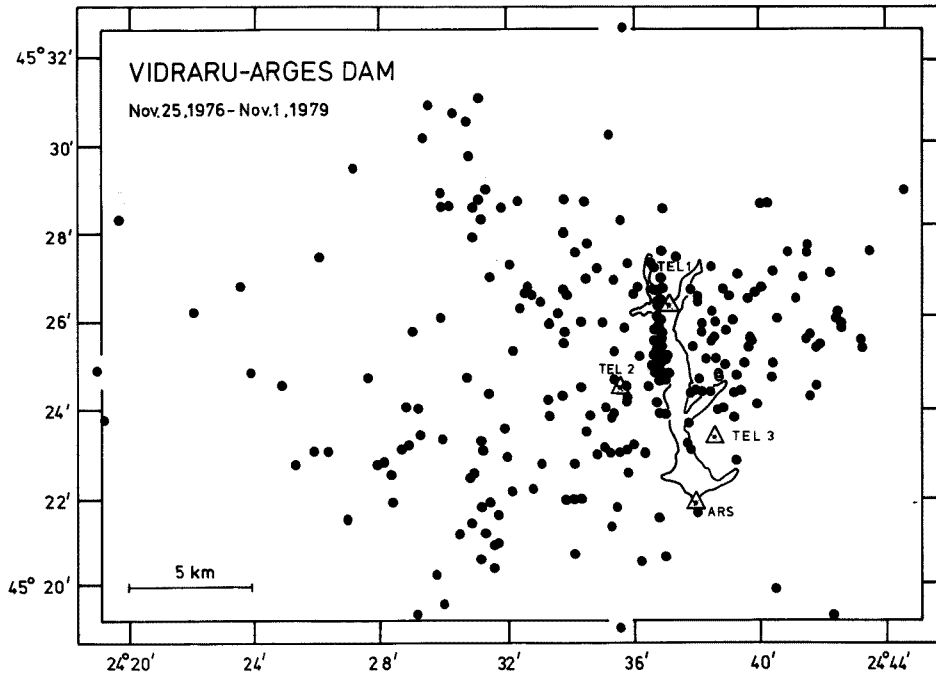


Figure 4: Epicenter distribution around the Vidraru-Arges reservoir for the period Nov. 25, 1976 - Nov. 1, 1979. Seismic stations are marked with triangles. Station ARS is located at the dam site.

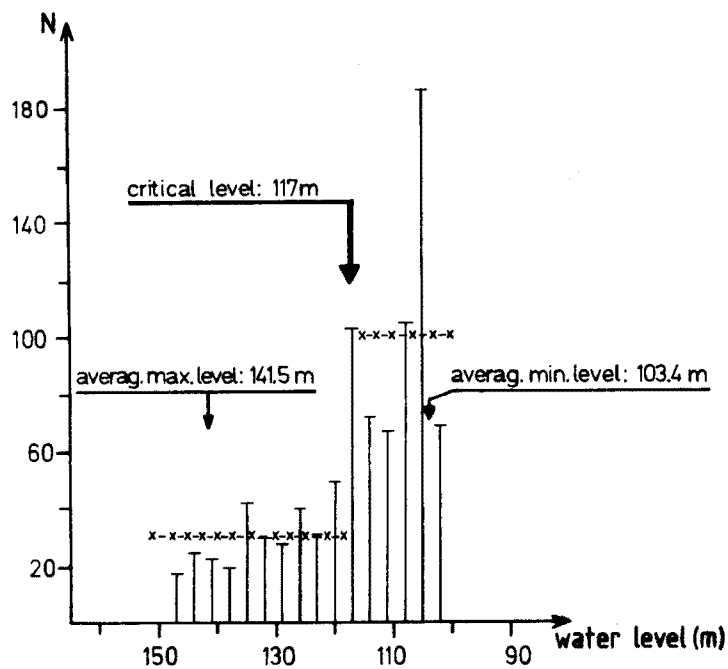


Figure 5: Average number of events as a function of water level for the time period: June 1975 to June 1982.

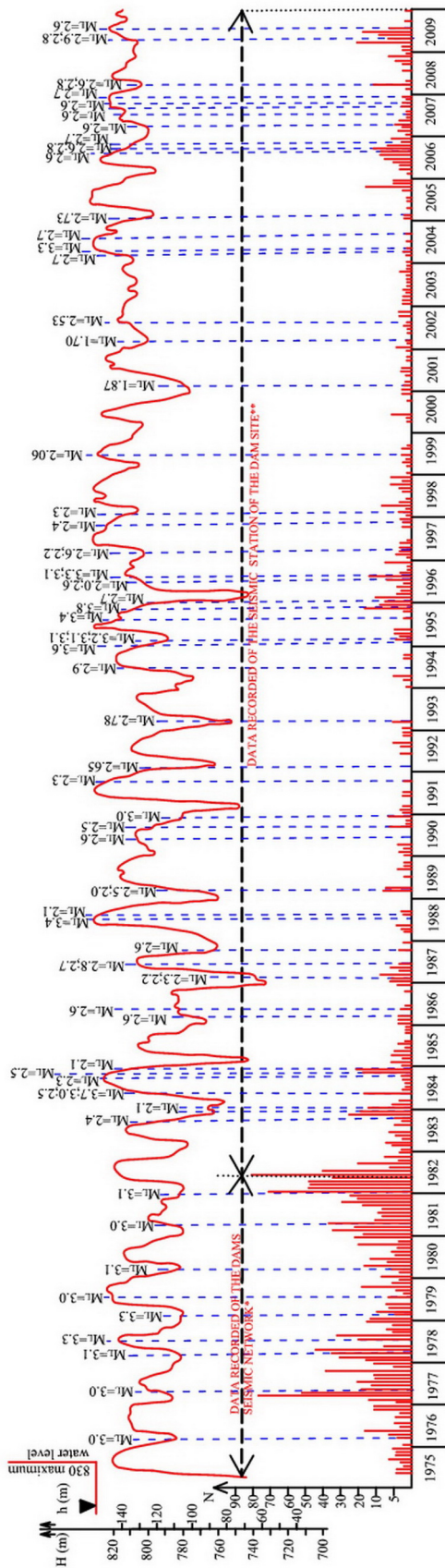


Figure 6: The annual changes of the water level of the Vidraru-Arges reservoir and the number of events per month in the lake area with hypocenter distances less than 40km with respect to the dam site are shown. The strongest earthquakes of each year are depicted additionally. Note the different resolution of the observations due to the change in the network configuration. From 1975 until mid 1982 three single-component telemetry stations around the lake and one 3-component station at the dam site were in operation. Since then only the dam station was kept running. This reduced the detection level significantly and did not allow proper localisation of the events.

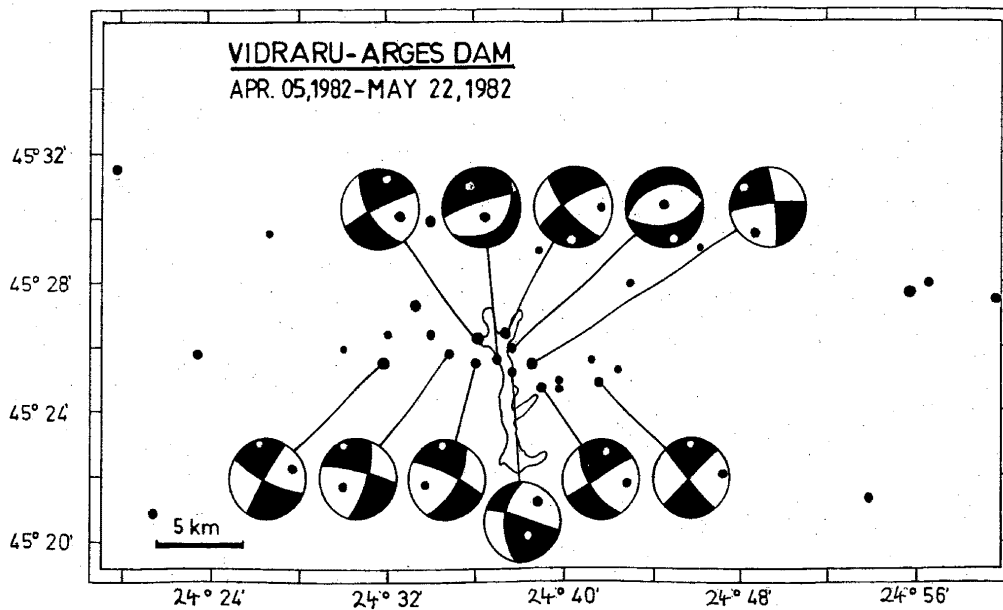


Figure 7: The 1982 Arges campaign (Moldoveanu et al., 1982): epicenter and fault-plane distribution. The solid line shows the contour of the filled reservoir. The dam is located at the southernmost part of the reservoir.

To increase the reliability of the determination of the focal parameters in the closer vicinity of the reservoir and to resolve the (apparent) discrepancy concerning the observation of normal faulting and a hypothetical thrust regime, a seismic survey with 10 mobile seismic stations was performed over a period of two months in April and May, 1982 (Moldoveanu et al., 1982). During this time about 30 locatable earthquakes were recorded.

Eleven events were well enough recorded (concerning the number of records and the azimuthal coverage) to allow the construction of fault plane solutions by the use of first motions (Fig. 7).

Most of the earthquakes occurred in the northern lake area. The epicenters show a pronounced E-W trend. The middle part of the reservoir and the dam area are free of events during this survey (Fig. 7). Further evidence for such lack of activity beneath the lake is provided by the epicenter distribution of the monitoring time period 1976-1979 (Moldoveanu et al., 1982), when a significantly greater number of earthquakes could be located (Fig. 4). However, the determinations of the focal parameters were less accurate. Compared to the Arges-82 survey with 14 stations, the permanent Arges network consisted only of 4 stations during 1976 to 1979 (Fig. 4), and the dam station ARS was very often disturbed by very local noise.

Concerning the focal mechanisms, no thrust mechanisms were found. Two events were nearly poor normal faulting mechanism but most of the earthquakes were of strike-slip type with small dip components. Both types of mechanisms are in agreement with the regional stress-field (e.g. Heidbach et al., 2007, Mueller et al., 2010).

The analyses of the Arges-82 campaign data as well as the data, which were recorded during 35 years of continuous seismic monitoring at Vidraru–Arges dam, reveal the following features:

- the existence of a correlation between the number of local shocks with $(t_s - t_p) < 5$ seconds, (i.e. at hypocenter distances ≤ 40 km) and the variation of the water level of the reservoir (Fig. 6);
- the number of the local shocks increased (1508 shocks) in the periods when the level of the lake decreased and decreased (1082 shocks) when the level of the lake increased (Moldoveanu, 1976-2010);
- the confirmation of a remarkable microseismic activity in the northern lake area as well as in the surroundings of the reservoir (up to about 8-25 km), and of an absence of events in the deeper parts of the reservoir (Figures 4 and 7);
- the greatest magnitude of the local events was 3.7, frequently magnitudes in the range from 2 to 3 are observed during the monitoring time period.

Conclusions

The discussed relation between the number of local shocks and the annual changes of the water level of the Vidraru-Arges reservoir has been observed over a time period of 35 years. It is not restricted to the initial phase of the filling of the reservoir (respectively the re-filling after the complete emptying). The annual amplitude of the water level changes with 30 to 80m is comparable or is at least a large fraction of the lowest water level of 120 to 70m (see Fig. 6). If large reservoirs are operated in such a way, the induced seismicity is governed by the frequency and the amplitude of the lake-level changes, as it is the case e.g. for the Lake Mead or the Koyna reservoir (Talwani, 1997). This seems to hold also for the Vidraru-Arges reservoir. The regional principal stresses are small and of similar magnitude, as advocated for by Heidbach et al. (2007) and Mueller et al. (2010). Therefore local stress sources, like the loading cycle, may play the predominant role. Figures 5 and 6 indicate this. A further factor in the earthquake generating process is the fluctuation of the pore pressure, which is well documented in numerous studies (e.g. Talwani, 1997). However, in the case of the Vidraru-Arges reservoir, information on the time-dependency of pore pressure changes at depth is not yet available.

The Vidraru-Arges area is an area of strong local seismic activity (e.g. Atanasiu, 1961, Radu, 1979) and, as we show in this paper, also an area of induced seismicity. The interpretation of the seismicity pattern, in particular the proper discrimination between natural and induced seismicity, will only be possible if the time dependent seismicity patterns can be resolved by long-term and high-quality monitoring.

Acknowledgments

The Federal Ministry for Research and Technology (BMFT), Germany, the Ministerul Energiei Electrice (MEE), Romania, and the S.C. Hidroelectrica SA, Curtea de Arges, Romania, provided financial, technical and operational support. The authors are grateful to Andreas Barth for digitizing the Goettingen Wiechert-recordings of the Făgăraș earthquake. We thank Andreas Barth also for a helpful review of the manuscript.

References

- Atanasiu, J. (1961). Cutremurele de pămînt din Romania, Editura Academiei, Bucuresti, pp 194.
- Heidbach, O., Ledermann, P., Kurfeß, D., Peters, G., Buchmann, T., Matenco, L., Negut, M., Sperner, B., Müller, B., Nuckelt, A., Schmitt, G (2007). Attached or not attached: slab dynamics beneath Vrancea, Romania, Proceedings. Int. Symp. on Strong Vrancea Earthquakes and Risk Mitigation, Bucharest, Matrix ROM, 3-20.
- Moldovan, I.-A., Moldoveanu, T., Popescu, E. (2006). Hazard Models in the central part of Romania for Dam's Rating in Risk Classes, Proc. First European Conference on Earthquake Engineering and Seismology, Geneva, Paper No. 829, 1-10.
- Moldoveanu, T., Apopei, I., Bonjer, K.-P. (1982). The Arges-82 Seismic Survey, Report of the Geophysical Institute, University of Karlsruhe, and the Institute of Hydroelectrical Studies and Design, Bucharest, pp 29.
- Moldoveanu, T. (2002). The contribution of geological methods for the investigation of the geological environment and the evaluation of the natural hazard (PhD Thesis), Bucharest University, pp 303.
- Moldoveanu, T. (1976-2010). The seismic annual-reports of Vidraru-Arges Dam.
- Mueller, B., Heidbach, O., Negut, M., Sperner, B., Buchmann, T. (2010). Attached or not attached: -evidence from crustal stress observations for a weak coupling of the Vrancea slab in Romania, Tectonophysics, 482, 139-149.
- Nourescu, A., Merkle, G. H., Moldoveanu, T., Tudorache, G., Fuchs, K., Bock, G., Bonjer, K.-P. (1979). Seismic Monitoring of some Dams in Romania, Treizième Congrès des Grands Barrages, New Delhi, 1013-1031.
- Oncescu, M. C., Mârza, V., Rizescu, M., and Popa, M. (1999). The Romanian earthquake catalogue between 984-1997, in F. Wenzel, D. Lungu and O. Novak (eds), Vrancea earthquakes: Tectonics, hazard and risk mitigation (Kluwer Academic Publishers, Dordrecht, The Netherlands , 43-49.
- Radu, C. (1974). Contribution à l'étude de la séismicité de la Roumanie et comparaison avec la séismicité du bassin méditerranéen en particulier avec la séismicité du Sud-Est de la France. Thèse Dr. Sci., Strasbourg, pp 453.
- Radu, C. (1979). Catalogul cutremurelor puternice produse pe teritoriul Romaniei. Partea I – înainte de 1901; Partea II – 1901-1979, In: Cercetari Seismologice asupra Cutremurului din 4 Martie 1977, eds. I. Cornea and C. Radu, Bucuresti, 723-752.

Articles

Radu, C. (1990). The Romanian Earthquake of January 26, 1916, Proceedings XXII General Assembly European Seismological Commission, Barcelona, 297-303.

Talwani, P. (1997). On the Nature of Reservoir-induced Seismicity, Pure Appl. Geophys., 150, 473-492.

Microseismic monitoring of fluid injection at the Longyearbyen CO₂-Lab, Svalbard

Volker Oye¹, Hom Nath Gharti¹, Daniela Kühn¹, and Alvar Braathen²

¹ NORSAR, Gunnar Randers vei 15, 2007 Kjeller, Norway, volker.oye@norsar.no

² The University Centre in Svalbard, UNIS, Norway, Alvar.Braathen@unis.no

Abstract

The Longyearbyen CO₂ storage lab project addresses the problem to turn Svalbard into a CO₂ neutral community. The project has now confirmed that an injective reservoir (800-1000 m depth) and a sealing cap rock section exist around Longyearbyen, and will proceed towards demonstration and monitoring studies of sub surface CO₂ storage over time. In this paper we focus on the seismic network installation and seismic analysis of continuous recordings during a series of 4 fluid injection tests. The preliminary analysis did not identify significant activity of microearthquakes. However, at least one relatively strong microearthquake occurred approximately 17 hours after the last injection test, which pumped water for about 5 days. A precise location of the microearthquake is difficult due to uncertainties in the velocity model and the station configuration. To better understand a potential link between the fluid injection test and the occurrence of the microearthquake, we currently investigate the data for smaller microearthquakes in the same area using cross-correlation techniques. We will also investigate the stress field changes in the reservoir that were introduced by the fluid injection.

Introduction

The Longyearbyen CO₂ storage lab project addresses the problem to turn Svalbard into a CO₂ neutral community (Sand and Braathen 2006; Braathen et al. 2010). The project has now confirmed that an injective reservoir (800-1000 m depth) and a sealing cap rock section exist around Longyearbyen, and will proceed towards demonstration and monitoring studies of sub surface CO₂ storage over time. The progressive construction of the Longyearbyen CO₂ storage lab is currently addressing detailed properties and geometry of the reservoir. Liquids other than CO₂ have been used in this initial phase (water, brine, gel). The reservoir below Longyearbyen is considered physically open (no closure) and, therefore, will likely experience drift of the injected CO₂ plume towards the Northeast, through gradual mixing and expulsion of saline groundwater. This offers a unique opportunity for studying the behavior of CO₂ in subsurface saline aquifers. Four wells have been drilled so far and several new monitoring wells are planned for this purpose. Attention is paid to the distance of approx. 15 km from the injection site where the reservoir appears at the surface. This

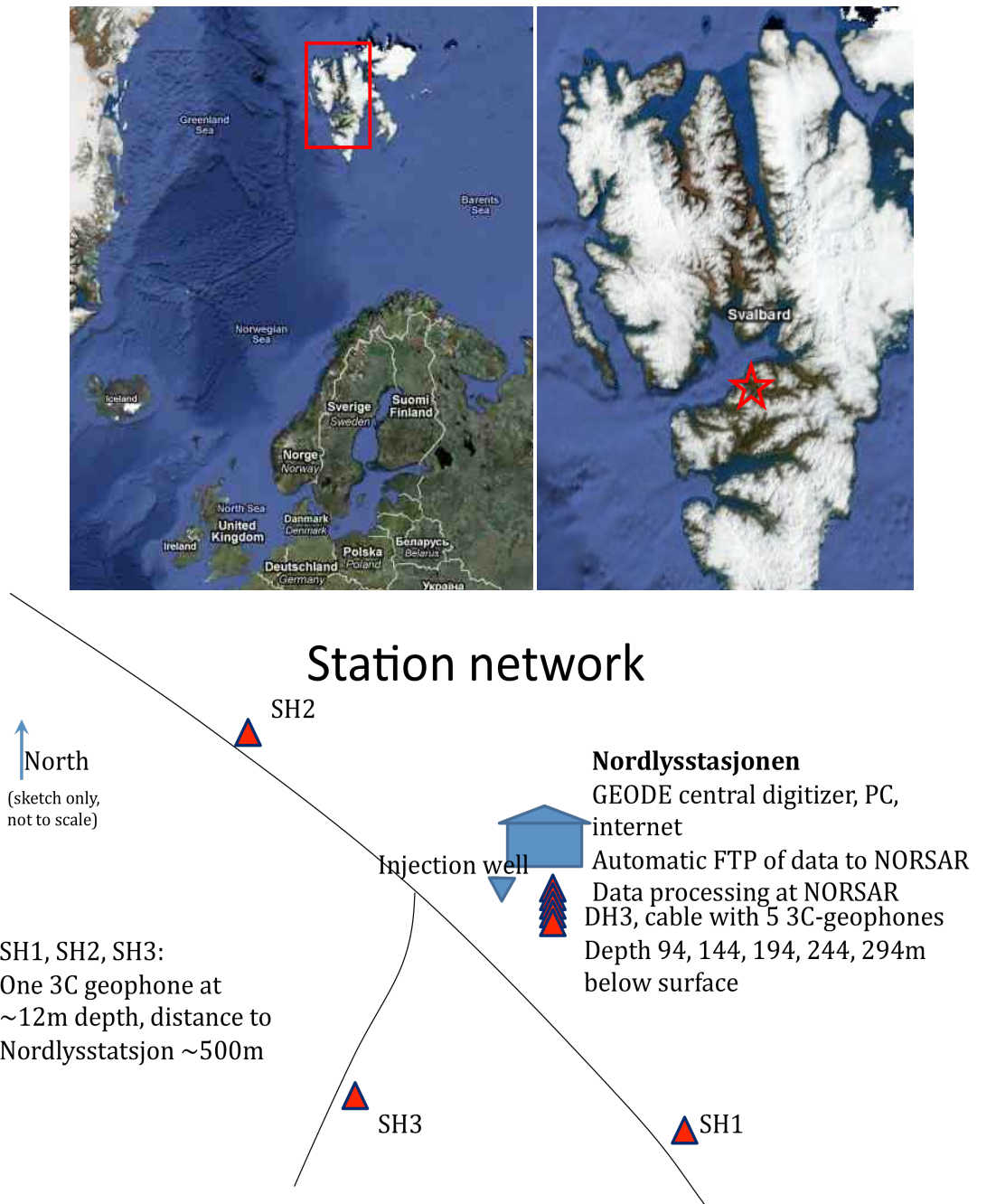


Figure 1: Upper panel – Map of Northern Europe (left) and Svalbard (right). The red star indicates the position of the field lab. Lower panel – Schematic view of the seismic field installation, the black lines are dirt roads, blue triangle is the position of the injection well, Dh4, red triangles denote seismic stations and the blue building is the Nordlysstation with high-speed internet connection.

fact and others will be considered in reservoir geo-models and subsequent flow simulations, which will predict flow in the reservoir and substantiate the odds for CO₂ leakage.

The seismic network

In August 2010 a fluid injection experiment was carried out at the CO₂ lab. In parallel, a microseismic monitoring network was deployed close to the injection well (see Figure 1 for schematic overview).



Figure 2: Left: Installation of the 5-level 3C-geophone string at the CO₂ lab. Right: deployment of borehole seismometers at 12 m depth, well within the permafrost.

The network consists of a 5-level string of 3-component geophones in a vertical observation well (DH3 in Fig. 3), with 50m distance between the instruments and a maximum depth of 294 meters. In addition, three shallow boreholes of 12 m depth have been drilled at about 500 m distance to the injection well, where the geophones have been lowered to the ground within a plastic tubing and the boreholes have been refilled with sand to ensure good coupling. Within a few days, also the permafrost will ensure good coupling to the ground. These additional surface stations are intended to provide more accurate locations for microearthquakes that are strong enough that their radiated seismic energy reaches to the surface. The deep borehole had an inner diameter of only 67 mm, therefore we decided to use small 15 Hz geophones for the deployment and sampled at 1000 Hz. All 24 channels of the geophones were connected to a GEODE digitizer and a PC. All channels have consistent timing information, which is provided by the internal PC-clock. The PC is connected to a fast internet connection and is updated every 2 hours with a world-time server. All data are sent in real-time to NORSAR where they are automatically processed.

The orientation of the horizontal components was unknown after the installation and we therefore used hammer blows and some very small explosions to orient the shallow borehole stations SH1, SH2 and SH3, assuming that the P-wave polarisation is identical to the direction of the P-wave propagation. The emitted energy of the hammer blows and the explosions was not strong enough to be registered at the downhole receivers, so we needed to use local or regional earthquakes to orient the downhole sensors. Some stronger explosions, however, would be very useful to orient the sensors more reliably and to get a better idea on the velocity structure. This will most likely be done during this winter.

Data processing

The data processing includes standard frequency and prediction filtering, detection and association of phases using STA/LTA and beamforming methods, respectively. P- and S-wave onsets are estimated by filtering with an autoregressive model and subsequent application of the AIC criterion (Akaike Information Criterion, a statistical approach to identify changes in time series (e.g. Oye and Roth, 2003)). The localization is generally conducted with the iterative master event method (Oye and Roth, 2003) and will be repeated once a more reliable velocity model is established for this site. Different location methods using envelop stacking (e.g. Gharti et al.

2010) will also be considered for selected periods where additional data from seismic lines are available (most likely during winter 2010 with snow-streamer acquisition). Following automatic processing, the detected seismic events need to be quality controlled manually. Noise along the road is a problem for single station detections and tube waves within the borehole may introduce false triggers on the downhole installation. In addition, regional earthquakes in the Storfjorden region and in the North Atlantic ridge are registered on all stations almost simultaneously. These events need to be extracted from the processing, but are useful to establish and quality control the orientation of the downhole sensors.

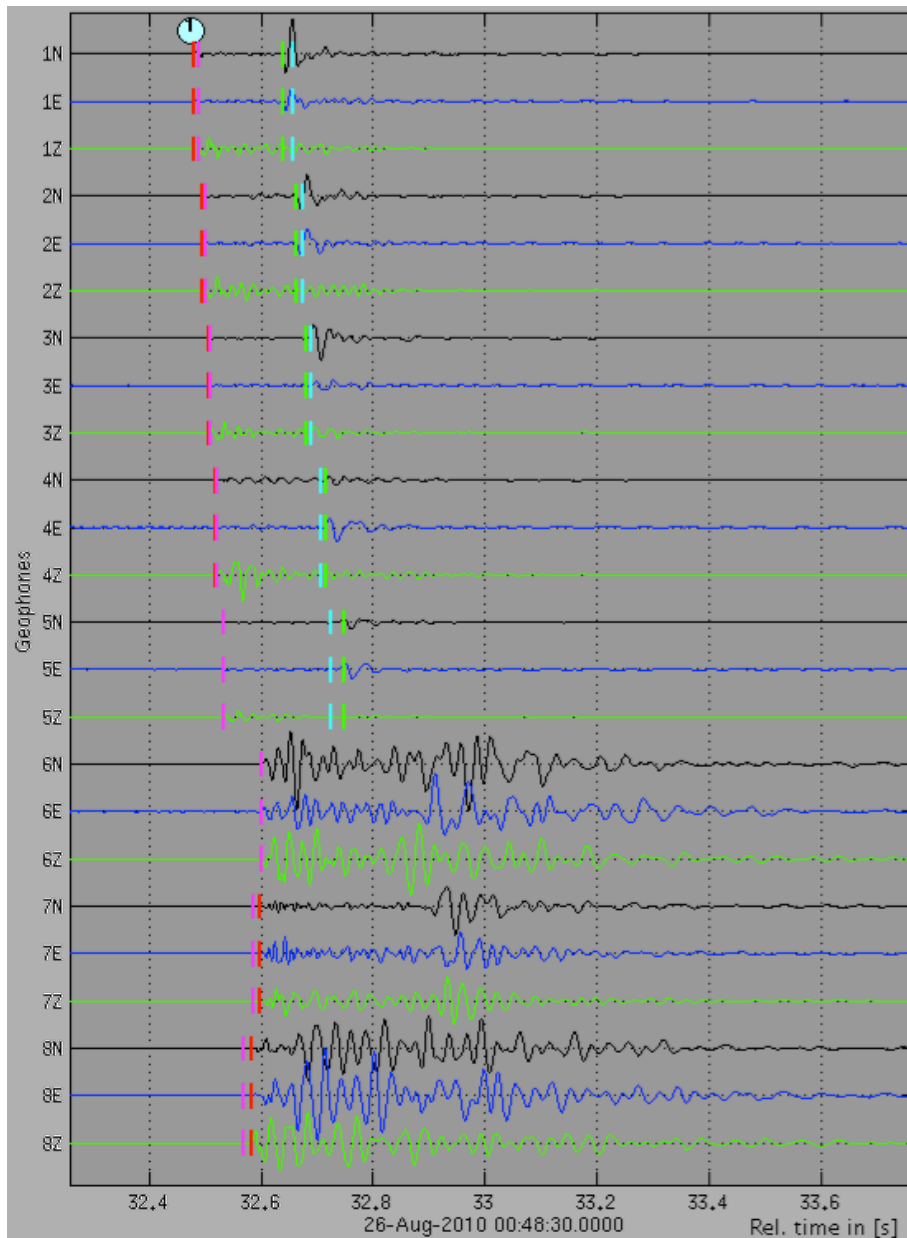


Figure 3: Seismograms of the seismic event that occurred after the injection shut-in phase. Geophones 1-5 are deployed in the deep borehole (1 deepest, 5 shallowest) with 50 m inter-station distance. Geophone 6 corresponds to SH3, 7 to SH2 and 8 to SH1. The red and green bars correspond to the picked P- and S-wave onsets, whereas the pink and the cyan bars correspond to the theoretical P- and S-wave onsets for the estimated location.

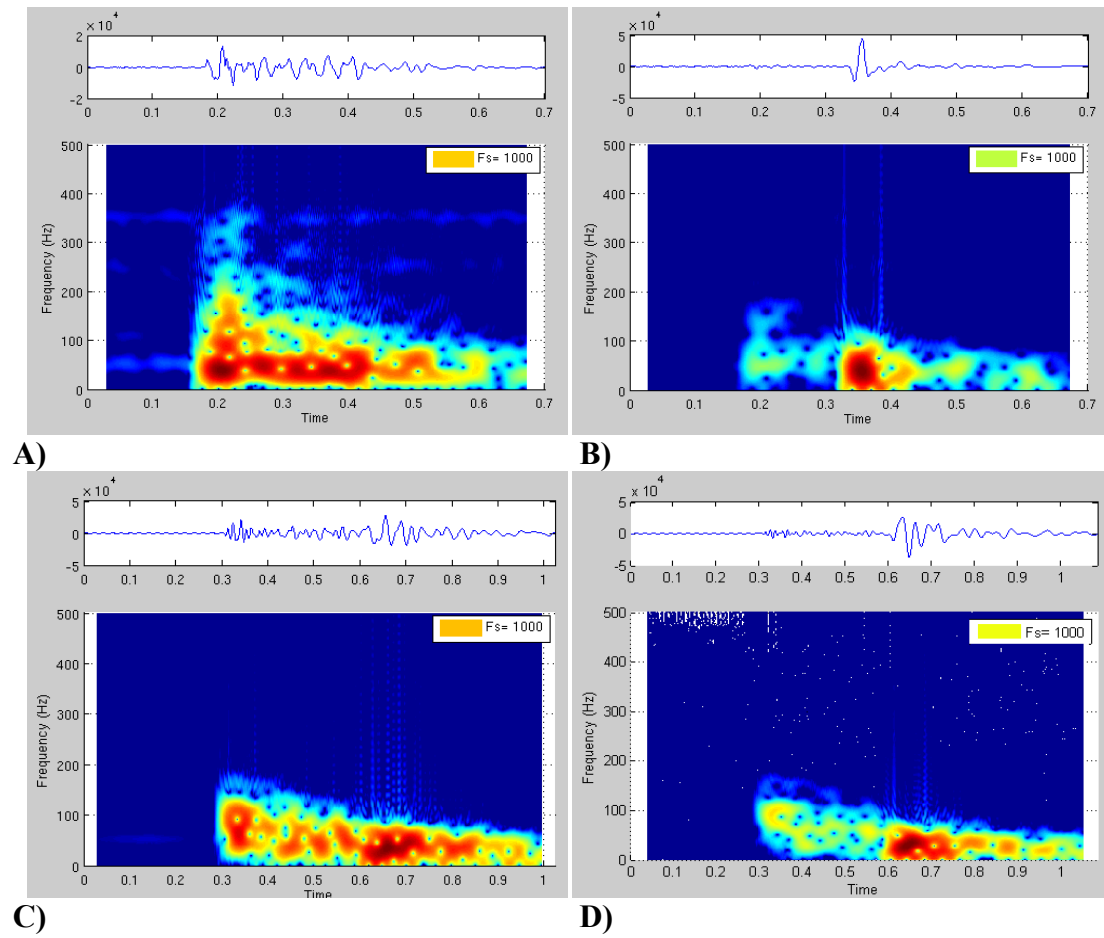


Figure 4: Spectrograms of seismic traces: A) vertical component of the deepest sensor at 294 m depth. Note the relatively high signal frequency reaching clearly above 200 Hz. This trace contains mainly P-wave energy. B) Horizontal component of the deepest sensor, containing mainly S-wave energy and with main signal frequency of about 100 Hz. C) spectrogram of vertical component of station SH2 and D) of a horizontal component of SH2. Note the lower signal frequencies caused by attenuation on the 12m deep boreholes as compared to the deeper borehole stations.

Discussion and Conclusions

Approximately 17 hours after the 5-days water injection test a microseismic event has been identified and located to the Northeast of the injection well (Figure 3). An accurate location of this seismic event was not possible yet, because of high uncertainties in the velocity model and uncertainties in the orientation of the horizontal sensor components. A more precise location estimate of the microearthquake will be important to investigate the link between the injection and the sudden stress release as a microearthquake. Therefore we also search the data for similar events at lower signal-to-noise ratios using e.g. cross-correlation techniques. In parallel, we will investigate stress field changes due to the injection (rate of ~ 400 m³/day at injection pressure of ~ 140 bar). This seems to be particular interesting since observations show that the measured pore pressure before injection is at 30 bar (absolute) and normal hydrostatic pressure would be at 82 bar (L. Larsen, pers. comm.). This corresponds to an underpressure of at least 50 bar in the formation.

Spectral analysis of the recorded waveforms confirms again the improved signal response comparing downhole sensors with surface or shallow borehole sensors (Figure 4). At first, the downhole recorded waveforms show less influence from high-frequency attenuation, and also the waveforms are significantly simpler, showing clear P- and S-wave phase onsets (Figure 3). One reason for the more complex waveforms at the shallow borehole sensors could be the fact of permafrost at shallow depths and no permafrost in the upper 1 to 5 meters. It will be interesting to compare the signal quality throughout different seasons of the year, setting up repeated and controlled small explosions.

We have also started to model potential temporal changes in migrated synthetic seismic sections, which might be due to large-scale CO₂ injection. For this task we introduce new functionalities within NORSAR's SeisRoX software that can perform 4D seismic modelling. We will then correlate the results from the microearthquake locations with the 4D seismic modelling results and potentially with real 4D seismic data, if available.

References

- Braathen, A., Gunnar Sand, Atle Mørk, Maria Jensen, Karoline Bælum, Harald Elvebakk, and Fred Hansen, 2010: Longyearbyen CO₂ lab – prospects after the pilot project. 29th Nordic Geological Winter Meeting, Oslo, 11-13 January. Abstract and Proceeding of the Geological Society of Norway 1-2010, p 28-29.
- Gharti, H. N., V. Oye, M. Roth, D. Kühn, (2010). Automated microearthquake location using envelope stacking and robust global optimization, *Geophysics* 75, MA27 (2010); doi:10.1190/1.3432784.
- Oye, V., Roth, M., (2003). Automated seismic event location for hydrocarbon reservoirs, *Computers & Geoscience*, 29, 851-863.
- Sand, G., and Braathen, A., 2006. CO₂-fritt Svalbard i 2025? *Svalbardposten*, 10 November.

Towards quantifying the seismogenesis of fluid injections in rocks

S. A. Shapiro¹, C. Dinske¹, C. Langenbruch¹, F. Haney¹, J. Kummerow¹, and F. Wenzel²

¹ Freie Universität Berlin, FR Geophysik, Malteserstr. 74-100, 12249 Berlin, Germany, shapiro@geophysik.fu-berlin.de

² Geophysical Institute, Karlsruhe Institute of Technology, Hertzstr. 16, 76187 Karlsruhe, Germany

Abstract

Recently we have found that under rather general conditions a number of fluid-injection induced earthquakes with a magnitude larger than a given one increases approximately proportionally to the injected fluid mass. This is the case in Enhanced Geothermal Systems as well as by hydraulic fracturing of hydrocarbon reservoirs. Here we show that using the seismicity rate of such events and the fluid injection rate a parameter (seismogenic index) can be derived, which quantifies the seismotectonic activity of an injection location. This index is independent of injection parameters. It is only a function of tectonic features of an injection site. The seismogenic index can be used to quantitatively compare different tectonic locations for a planned fluid injection (e.g., for geothermal or CO₂ injection) in terms of a potential risk to induce an event with a magnitude larger than a given one. Along with injection parameters, knowledge of the seismogenic index permits to estimate the occurrence probability of a given number of such events during a given time period. Moreover, this index can be used for feasibility studies of microseismic monitoring. A consideration of several case studies shows that the largest seismogenic index characterises the Basel geothermal site. The smallest ones are found for hydrocarbon reservoirs and the KTB (after a fluid-extraction experiment). It is already known that injections at geothermal sites are characterised by lower b-values than injections at hydrocarbon reservoirs. From our study it becomes clear that geothermal locations are also often characterised by a higher seismogenic index. These two factors explain the observation that geothermal injections have a tendency to induce significant events more frequently than hydrocarbon ones. On the other hand, this observation implies that microseismic monitoring of hydrocarbon reservoirs usually requires a higher level of sensitivity than such a monitoring of geothermal systems.

Introduction

An important characteristic of seismicity is the distribution of magnitudes of earthquakes. Fluid injections in rocks aimed to create Enhanced Geothermal Systems (EGS) can sometimes produce significant seismic events (see e.g., Majer et al., 2007). This is more seldom the case by hydraulic fracturing of hydrocarbon reservoirs. However, in both cases the spatial-temporal behavior of the seismicity triggering is controlled by a process of relaxation of stress and pore pressure perturbations initially created at the injection source. This relaxation process can be approximated by pressure diffusion (possibly a non-linear one) in the pore fluid of rocks (e.g., Shapiro and Dinske, 2009).

Shapiro et al. (2007) described the magnitude distribution for the condition of linear pressure diffusion and an injection source of constant strength. Later, Shapiro and Dinske (2009) extended this model to a general monotonously increasing type of the injection source. The process of fluid-rock interaction can be strongly non-linear in the sense of a strong impact of the injection on rock permeability. Such situations like a hydraulic fracturing or a shear-caused dilatational permeability enhancement are taken into account by their formalism. In spite of its simplicity and schematic character this formalism is able to well explain some observed phenomena and to indicate important factors which control magnitudes of fluid-induced seismicity. Since it is needed in the following, we briefly summarise this formalism.

We consider a point-like injection source in an infinite, homogeneous, permeable medium. Due to a fluid injection and the consequent process of pressure relaxation, the pore pressure p will change throughout the pore space. We assume that a random set of pre-existing cracks (defects) with a volume concentration N is statistically homogeneously distributed in the medium. We further assume that the cracks do not mutually interact. Each of the cracks is characterised by an individual critical value C of pore pressure necessary for occurrence of an earthquake along such a defect. The critical pressure C is randomly distributed on the pre-existing cracks and we assume that its statistical properties are independent of spatial locations. If at a given point \mathbf{r} of the medium (with a pre-existing crack) the pore pressure $p(t, \mathbf{r})$ increases with time, and at time t_0 it becomes equal to $C(\mathbf{r})$ then this point will be considered as a hypocentre of an earthquake occurring at time t_0 . For simplicity, no later earthquake will be possible at this point again. This is equivalent to an assumption that stress corrosion, tectonic load, tectonic deformation and other processes which lead to recharging of critical cracks are much slower than the process of pore pressure relaxation. Recently, Rothert and Shapiro (2007) found that C is approximately uniformly distributed between its minimum, C_{min} , and maximum, C_{max} . They are of the order of 10^2 and 10^6 Pa, respectively. We assume that generally C_{max} is larger than the injection-caused pressure perturbation (excluding maybe a small volume around the source) and C_{min} is vanishing small.

These assumptions result in the conclusion that the event probability is proportional to the pore pressure perturbation. This statement is valid for non-decreasing injection pressure. The total number of events induced from start of injection until time t is given by a spatial integral of pressure perturbations. Under rather general conditions including a strongly non-linear interaction between injected fluid and rock, this integral can be estimated from the fluid continuity equation. The continuity equation expresses the conservation of fluid mass, a principle, valid independently of any kind

of injection impact onto the rock permeability. Application of this principle yields for the cumulative number of induced seismic events:

$$N_{ev}(t) = N Q_c(t) / (C_{max} S), \quad (1)$$

with concentration of pre-existing cracks N , poroelastic uniaxial storage coefficient S , and cumulative injected fluid volume $Q_c(t)$. The quantity $F_t = C_{max}/N$ depends on the tectonic activity of an injection region only. Shapiro et al. (2007) introduced this quantity as tectonic potential. We see from equation (1) that the number of induced events is proportional to the injected fluid volume.

We now assume that the probability of a given event to have a magnitude larger than M , $W_{>M}$, is independent of the total event number. We further assume that fluid-induced seismicity obeys the Gutenberg-Richter statistics which means that the probability $W_{>M}$ of events with the magnitude larger than M is given by $\log W_{>M} = a - b M$, where a and b are seismotectonic constants. Multiplying equation (1) by the probability $W_{>M}$ we obtain that the expected number of events $N_{>M}$ with magnitude larger than M is given as:

$$\log N_{>M}(t) = \log Q_c(t) - b M + a - \log (F_t S). \quad (2)$$

In the following we will use equation (2) to introduce the seismogenic index which characterises the seismotectonic activity of an injection site, and to formulate the occurrence probability of a given number of events with magnitude larger than a given one.

Seismogenic index

Let us rearrange equation (2) to the following form:

$$\log N_{>M}(t) - \log Q_c(t) + b M = a - \log (F_t S). \quad (3)$$

Quantities on the left hand side of this equation are known or experimentally measurable. They depend on injection parameters and on induced seismicity. We now focus on the quantity Σ given by the right hand side of equation (3):

$$\Sigma = a - \log (F_t S). \quad (4)$$

This quantity neither depends on injection time nor on other injection characteristics. It is completely defined by seismotectonic features of a given location. We will address it as seismogenic index. The larger this index, the larger the probability of a significant magnitude event. Once the seismogenic index is measured for an injection site, it can be used together with the b -value of the Gutenberg-Richter distribution to forecast the number of events within a specific magnitude range:

$$\log N_{>M_1}(t) = \log Q_{c_1}(t) - b M_1 + \Sigma, \quad (5)$$

where Q_{c_1} and M_1 are cumulative injected volume respectively an arbitrary event magnitude for a new upcoming injection experiment at the same site. Note that such predictions will be valid only if b and Σ are not significantly changing with time.

The seismogenic index provides a convenient tool for a quantitative comparison of seismotectonic activity at different locations. We here consider four geothermal locations: Cooper Basin (Soma et al., 2004), Basel (Håring et al., 2008), Ogachi (Kaieda et al., 1993), and Soultz (Baria et al., 1999), and we include also non-geothermal sites in our study: KTB (Jost et al., 1998, Shapiro et al., 2006), Paradox Valley (Ake et al., 2005), Cotton Valley (Rutledge and Phillips, 2003), and Barnett Shale (Maxwell et al., 2006). The last two locations correspond to hydraulic fracturing of gas reservoirs. We compute the seismogenic index Σ for all locations according to equation (3). For our discussion we only use time periods that correspond to non-decreasing injection rates. In addition, we restrict our analysis to magnitude ranges that are not likely to be affected by observation, registration and processing. For our calculations, we attempt to include moment magnitudes. If moment magnitudes were not available, our estimates of the seismogenic index are biased by the order of difference between local and moment magnitudes in corresponding magnitude ranges. To our knowledge, this bias for the here presented locations is insignificant for our conclusions.

The values of the seismogenic index are illustrated in Figure 1. As assumed, they do not significantly fluctuate as function of time and therefore demonstrate reasonable stability. Statistical errors, magnitude dependence and temporal fluctuations of the estimates are less than ± 0.5 . We expect that the bias caused by differences between local and moment magnitudes is of similar size. We notice from Figure 1 following general tendency. The seismogenic index at hydraulic fracturing locations is smaller than at geothermal sites. In the considered examples of hydrocarbon reservoirs it is between -10 and -4 whereas it is larger than -4 for geothermal reservoirs as well as for KTB and Paradox Valley. The relatively low seismogenic index for KTB estimated from the 2004/05 injection is explained by the impact of the fluid extraction phase that took place before the injection. A significantly higher seismogenic index is obtained for Cooper Basin which is of the order of -1 . Soultz, Ogachi, the first KTB injection experiment and the Paradox Valley are characterized by slightly lower values of the index, from the range from -4 to -1 . The largest index in our examinations provides the Basel data set. Here we found for the seismogenic index a value of $0.2 \div 0.5$.

Occurrence probability of events with given magnitudes

Intuitively, a higher seismogenic index results in a higher probability of significant events. Let us assume a fluid injection at a constant injection rate Q_I . Then, the cumulative event number will be $N_{ev}(t) = NQ_I t / (SC_{max}) = vt$. It means that the cumulative event number is just proportional to time, where $v = NQ_I / (SC_{max})$ is a constant temporal event rate. Our model and assumptions imply that the events occur independently from each other. In other words, the induced seismicity follows a Poisson distribution (Langenbruch and Shapiro, 2009). In the case of an arbitrary non-decreasing injection rate the induced seismicity is an inhomogeneous Poisson process with non-constant temporal event rate. In the case of a constant injection rate the process reduces to a standard homogeneous Poisson process.

A sequence of events with a magnitude larger than M is also a Poisson process. The corresponding event rate v_M is equal to the product $v_M = vW_{>M}$. Using the Poisson distribution we can compute the occurrence probability $P(n, M, t)$ of n events of magnitude larger than M in the time interval $(0, t)$:

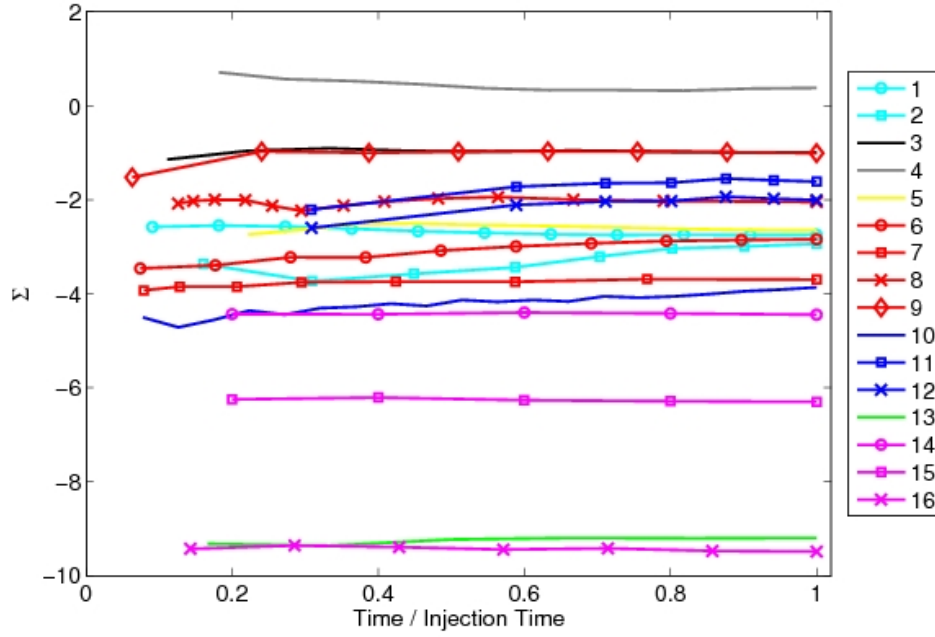


Figure 1: Averaged seismic index computed for different locations of Enhanced Geothermal Systems, hydraulic fracturing in hydrocarbon reservoirs, and other injection locations (injection times are given in brackets). 1: Ogachi 1991 (11 days), 2: Ogachi 1993 (16 days) 3: Cooper Basin 2003 (9 days), 4: Basel 2006 (5.5 days), 5: Paradox Valley (2500 days), 6-9: Soultz 1996 (48 hr), 1995 (11 days), 1993 (16 days) and 2000 (6 days), 10: KTB 2004/05 (194 days), 11-12: KTB 1994 (9 hr) [upper and lower bound, calculated for two b -values], 13: Barnett Shale (6 hr), 14-16: Cotton Valley stages A (2.5 hr), B (2.5 hr) and C(3.5 hr).

$$P(n, M, t) = ((vMt)^n / n!) \exp(-vMt) . \quad (6)$$

Of special practical interest is the probability of absence of an event with a magnitude larger than a given M in the time interval from $(0, t)$:

$$P(0, M, t) = \exp(-N_{>M}(t)) = \exp(-Q_c(t)10^{\Sigma - bM}), \quad (7)$$

where $N_{>M}(t)$ is given by equation (1) and in the last part of the equation we have substituted the Gutenberg-Richter magnitude distribution.

Let us assume that we want to exclude occurrence of events with magnitude larger than M with a probability 99 per cent. It means that $P(0, M, t) = 0.99$. Application of equation (7) now allows for computing a tolerable maximal cumulative injected volume or, by a given injection rate, the maximal possible injection time.

For a numerical demonstration we consider a fluid injection with parameters similar to the Basel stimulation. During about 5.5 days of the stimulation $11570m^3$ of fluid were injected into the rock. The seismicogenic index Σ is equal 0.25 and the b -value is 1.5. Equation (7) gives us a possibility to reply the following question: What is the probability that during such an injection events with a magnitude larger than $M=2.5$ will occur? This probability can be derived by substituting all parameters into equation (7) and computing $P(0, M, t)$. Next, we compute the value of $1 - P(0, M, t)$ and

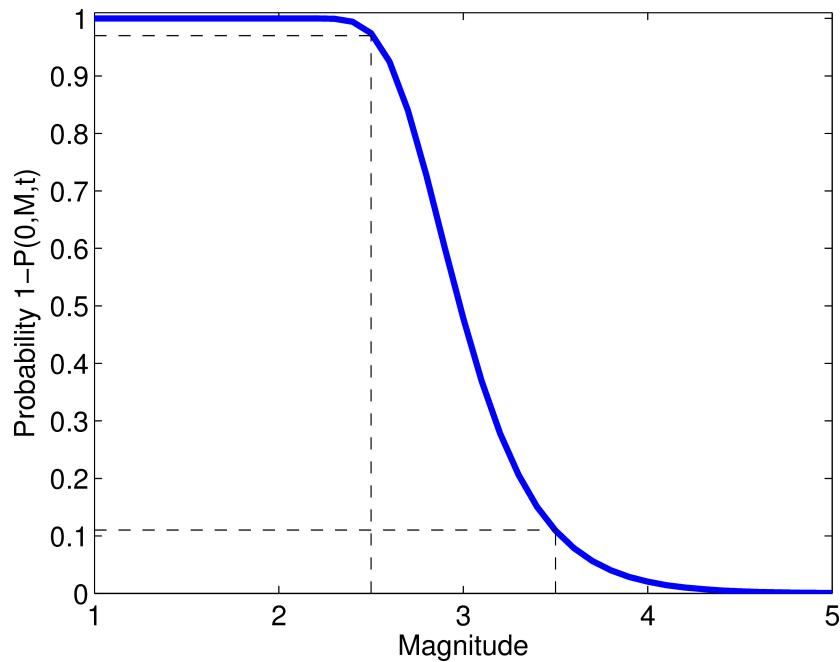


Figure 2. Probability that events with a magnitude larger than a given one would occur during a fluid injection into rocks. The parameters of the injection and of the seismotectonic state are given in the text. They are similar to the parameters of the Basel's injection.

then multiply the latter with 100 per cent. In such a way, we obtain approximately 97 per cent. The probability that events with a magnitude larger than 3.5 will occur is about 11 per cent only. Thus, the occurrence probability of events quickly decreases with increasing their magnitudes (compare with Figure 2).

In the Basel injection, the largest reported event with local magnitude of 3.4 occurred approximately 5 hours after shut-in of the 5.7 days continuous injection (Håring et al., 2008). Although this event happened outside of the time interval described by our model, our result, i.e. the derived probability values, seem to be realistic in the light of this event.

Conclusions

We have introduced a quantity, seismogenic index, which characterises the level of seismic activity one should expect from injecting fluid into rocks. An analysis of several case studies provides the largest seismogenic index for the geothermal sites in Basel and in Cooper Basin whereas the smallest ones are found at hydrocarbon reservoirs. This observation indicates that microseismic monitoring of hydrocarbon reservoirs requires a higher level of sensitivity compared to such monitoring of geothermal systems.

In addition to a larger seismogenic index, injection-induced seismicity at geothermal sites is also characterised by a lower b -value than at hydrocarbon reservoirs (Shapiro and Dinske, 2009). These two factors explain the phenomenon that injections at geothermal reservoirs have a tendency to occasionally induce significant events while not at hydrocarbon ones. This tendency is additionally enhanced by the multiple

amount of injected fluid volume by stimulations of geothermal systems compared to hydraulic fracturing of hydrocarbon reservoirs.

Fluid-induced seismicity follows a Poisson statistics. The seismogenic index and fluid injection rates are two key parameters controlling this statistics. We have provided explicit rules for estimation of occurrence probability for induced events of given magnitudes. All the results we discussed above apply to a time period of an active fluid injection.

Acknowledgements

We thank the sponsors of the PHASE consortium project and the Federal Ministry for the Environment, Nature Conservation and Nuclear Safety (BMU) as sponsor of the MAGS project for supporting the research presented in this paper. Microseismic data from Cooper Basin and Ogachi are courtesy of Dr. H. Kaieda (CRIEPI, Japan). Microseismic data from Basel are courtesy of Dr. M. O. Häring (Geothermal Explorers LTD). Microseismic data from Paradox Valley are courtesy of Dr. K. Mahrer (formerly, Bureau of Reclamation, presently, Waterford). Microseismic data from Cotton Valley are courtesy of Dr. J. Rutledge (LANL). Microseismic data from Barnett shale are courtesy of Dr. S. Maxwell (formerly, Pinnacle, presently Schlumberger). Microseismic data from Soultz experiments were kindly provided by Dr. A. Jupe and by the GEIE “Exploration Minière de la Chaleur”.

References

- Ake, J., K. Mahrer, D.O Connell, and L. Block (2005). Deep-Injection and closely monitored induced seismicity at Paradox Valley, Colorado, *Bulletin of the Seismological Society of America*, 95, 664–683.
- Baria, R., J. Baumgartner, A. Gerard, R. Jung, and J. Garnish (1999). European HDR research programme at Soultz-sous-Forets (France) 1987-1996, *Geothermics*, 28, 655-669, doi: 10.1016/S0375-6505(99)00036-X.
- Häring, M. O., U. Schanz, F. Ladner, and B. Dyer (2008). Characterization of the Basel 1 enhanced geothermal system, *Geothermics*, 37, 469-495.
- Jost, M. L., T. Busselberg, O. Jost, and H.P. Harjes, (1998). Source parameters of injection-induced microearthquakes at 9 km depth at the KTB Deep Drilling site, Germany *Bulletin of the Seismological Society of America*, 88, 815-832
- Kaieda, H., K. Kiho, and I. Motojima (1993). Multiple fracture creation for hot dry rock development, *Trends in Geophysical Research*, 2,127–139.
- Langenbruch, C., and S. A. Shapiro (2009). Inter event times of fluid induced seismicity, 72 EAGE Conference and Exhibition, Barcelona, paper F022.
- Majer, E. L., R. Baria, M. Stark, S. Oates, J. Bommer, B. Smith, and H. Asanuma (2007). Induced seismicity associated with Enhanced Geothermal Systems, *Geothermics*, 36,185–222.

- Maxwell, S., C. Waltman, N. R. Warpinski, M. Mayerhofer, and N. Boroumand (2006). Imaging seismic deformation induced by hydraulic fracture complexity, paper SPE 102801.
- Rothert, E., and S. A. Shapiro (2007). Statistics of fracture strength and fluid -induced microseismicity, *Journal of Geophysical Research*, 112, B04,309, doi:10.1029/2005JB003,959.
- Rutledge, J. T., and W. S. Phillips (2003). Hydraulic stimulation of natural fractures as revealed by induced microearthquakes, carthage cotton valley gas field, east texas, *Geophysics*, 68,441–452.
- Shapiro, S. A., and C. Dinske (2009). Scaling of seismicity induced by nonlinear fluid-rock interaction, *Journal of Geophysical Research*, 114, B09, 307, doi:10.1029/2008JB006,145.
- Shapiro, S. A., J. Kummerow, C. Dinske, G. Asch, E. Rothert, J. Erzinger, H.-J. Kämpel, and R. Kind (2006). Fluid induced seismicity guided by a continental fault: Injection experiment of 2004/2005 at the German Deep Drilling Site (KTB), *Geophys. Res. Lett.*, 33, L01309, doi:10.1029/2005GL024659.
- Shapiro, S. A., C. Dinske, and J. Kummerow (2007). Probability of a given-magnitude earthquake induced by a fluid injection, *Geophysical Research Letters*, 34, L22,314, doi:10.1029/2007GL031,615.
- Soma, N., H. Asanuma, H. Kaieda, K. Tezuka, D. Wyborn, and H. Niitsuma (2004). Onsite mapping of microseismicity at Cooper Basin, Australia HDR project by the Japanese team, in *Proceedings 29th Workshop on Geothermal Reservoir Engineering*, Stanford, California.

Laboratory study of temporal-spatial peculiarities of microseismicity spreading due to pore pressure change

S. B. Turuntaev, E. I. Ereemeeva, and E. V. Zenchenko

Institute of Geosphere Dynamics, Russian Academy of Sciences, Leninsky prosp., d.38, k.1, Moscow, Russia, turunt@postman.ru

Abstract

A possibility to use data on microseismicity variations in space and time due to pore pressure change for estimation of the permeability is considered. The analysis is based on laboratory experiments made for study of relation between acoustic emission (which corresponds to microseismic events in real scale) and pore pressure change due to water injection/release into/from a porous sample under load. The study showed a possibility to resolve an inverse problem of defining local permeability by registering microseismic activity variation in particular volume of the porous medium.

Introduction

Microseismic events are related with variations of rock stresses and reflect rock deformations and fluid migration in porous rocks. The change of pore pressure due to oil production and water flooding for oil recovery often leads to seismic events with magnitudes varied from negligible values to significant and catastrophic events (Adushkin and Turuntaev, 2005). It was shown by (Shapiro et al., 2002, 2005, Rothert and Shapiro, 2007) that it is possible to use data on microseismic event «cloud» propagations due to fluid injection in permeable rocks for estimation of the rock permeability. It was suggested, that in poro-elastic approximation a critical pore pressure propagation in isotropic porous medium can be estimated by simple relation:

$$r = \sqrt{4\pi Dt} \quad (1)$$

where r – distance from injection point, D – hydraulic diffusion coefficient, t – time from injection beginning. Formula (1) can be obtained from a solution of piezo conductivity equation, which describes an evolution of pore pressure in porous medium with elastic matrix. Actually, the equation of piezo conductivity looks like common diffusion equation (or equation of thermal conductivity) (Stchelkachev, 1995):

$$\frac{\partial p}{\partial t} = \frac{\partial}{\partial x_i} \left(D_{ij} \frac{\partial p}{\partial x_j} \right) = \frac{\partial D_{ij}}{\partial x_i} \frac{\partial p}{\partial x_j} + D_{ij} \frac{\partial^2 p}{\partial x_i \partial x_j}, \quad (2)$$

where D_{ij} is a tensor of hydraulic diffusivity. For homogenous isotropic medium

$$\frac{\partial p}{\partial t} = D \nabla^2 p. \quad (3)$$

In case of step-like increase of the pore pressure at the point of the fluid injection in isotropic homogeneous infinite medium, the equation (3) has the solution (1) (Shapiro et al, 2002). If one plots r - t diagram of microseismic events spreading and fits the

envelope curve of the type (1), it will be possible to estimate hydraulic diffusivity coefficient D from this fitting and, hence, to estimate the permeability k from the relation

$$D = \frac{k}{\mu_0 \beta m_0},$$

where μ_0 – fluid viscosity, m_0 – initial porosity, β – medium compressibility $\beta = (1 - m_0)\beta^{(s)} + m_0\beta^{(f)}$, $\beta^{(f)} = \alpha\beta^{(g)} + (1 - \alpha)\beta^{(w)}$ (compressibility of solid matrix, fluid, water and gas are denoted by upper indexes s, f, w, g); α is gas to fluid volume ratio.

In the presented paper, the variations of permeability were estimated by analyzing laboratory experiment data. In the experiments, pore pressure as well as acoustic emission AE (which corresponds to microseismic emission in real scale) were measured. Permeability variation was estimated with the help of experimental data on pore pressure variations in space and time; the results were compared with permeability evaluation from data on AE activity change in time.

The proposed approach is aimed to expand ideas suggested by Shapiro et al. (2002, 2005) for estimation of the permeability of inhomogeneous medium by using not only an information on microseismic event cloud propagations but also data on microseismicity variation in time.

The study showed a possibility to resolve an inverse problem of defining local permeability by registering microseismic activity variation in particular volume of the porous medium, and significant change of permeability on non-stationary stage of fluid flow during both pore pressure increase and decrease.

Experimental procedure

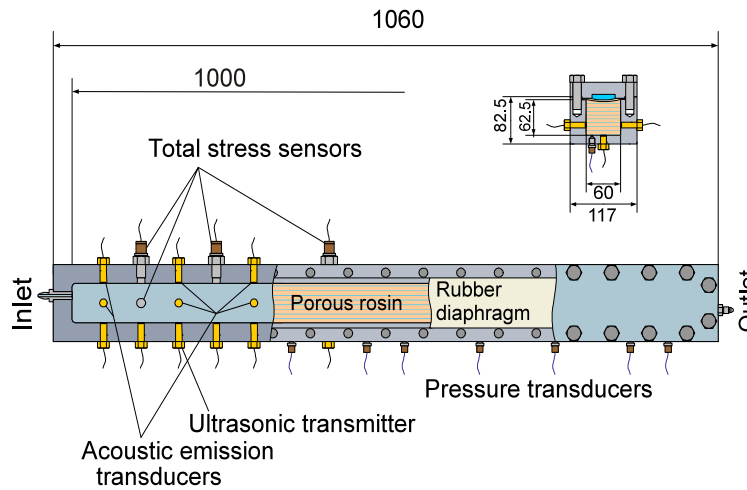
Experiments were made by means of laboratory setup shown in Fig.1. The setup (the cell) includes long stainless steel rod (1060 mm in length) with rectangular cross-section (117×82.5 mm). A rectangular channel (cross-section 65×62.5 mm) was milled in the rod. The channel was covered by a thick rectangular lid; a rubber diaphragm was placed between the rod and the lid. Time-size-flow rate and stress-strength dimensionless simulation criteria were used to choose the modelling material. It was found, that a mixture of pebbles with grain sizes from 2.5 to 5 mm and crashed rosin with grain sizes from 1 to 5 mm in proportion 3 to 1 is suitable for the research. The channel was filled with the mixture, then it was loaded by water injection into the gap between the lid and the diaphragm. Depending on the load, we got porous permeable samples with permeability shown in Table 1. A number of holes were made in both lateral and bottom sides of the rod for sensors. Valves at both tips of the box were used for fluid injection (through inlet) and pore pressure release (through outlet). The lateral interior of the cell was cover by 3.5 mm rubber band to reduce lateral rigidity. Assembled setup was vacuumized and filled by distilled water to prevent air bubbles formation.

Table 1. Experiment parameters

Experiment	1(Inject)	2(Drop)	3(Inject)	4(Drop)	5(Inject)	6(Drop)
Permeability, mD	20	20	14	14	10	10
Number of AE pulses	5 671	2 987	2 731	1 825	1 822	491

In one set of the experiments, water was injected into the cell with constant flow rate $0.35 \text{ cm}^3/\text{s}$. Vertical load was maintained constant, it was about 10-11 MPa, maximum pore pressure was less by 0.5 – 1.0 MPa than the vertical load. In another set of the experiments, the pore pressure was increased by water injection in undrained cell up to 10-11 MPa, then, after 3 hours from the pore pressure increase, the pressure was released through the outlet.

Ten pressure transducers were placed at 50, 110, 170, 230, 350, 410, 530, 650, 830 and 950 mm from inlet. Pore pressure data were registered by PC-based AD converter with sampling frequency 10 Hz.



12 piezoceramic acoustic emission transducers were placed in the sidewalls of the cell at 50, 110, 170, 230, 290 and 410 mm from inlet. There were groups of three sensors at positions 50, 170 and 290 mm placed at both sides and at the bottom of the cell. The AE signals were digitized by high speed AD converter with sampling frequency 800 kHz. The acoustic emission record was

Figure 1: Layout of the laboratory setup.

synchronized with the pressure record. Typical duration of the AE pulses record was 100 seconds.

After each experiment, the permeability was estimated under stationary flow conditions using measurements of pore pressure at several points of the cell. It was found, that the sample was inhomogeneous, which resulted in permeability distribution along the cell shown in Fig.2. The permeability distribution changed after each experiment.

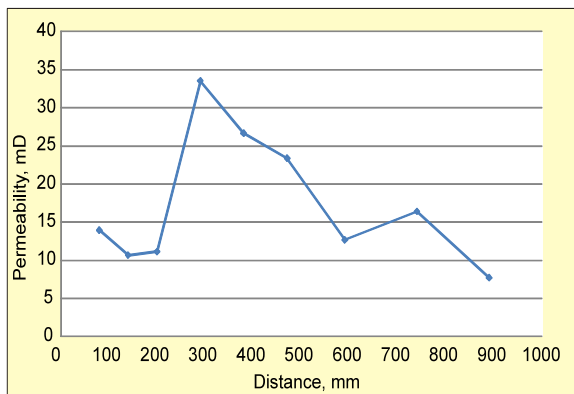


Figure 2: Variation of the permeability along the sample.

AE records processing includes filtration, discrimination of acoustic events from background, localization of acoustic events, composition of acoustic pulses catalogue, which includes time of event registration, amplitude of event, event coordinate.

To compare AE with pore pressure changes, the data on positions and times of occurrence of AE pulses were transformed into the form of “acoustic emission activity”. Acoustic emission activity is defined here as a number of acoustic events which appeared on a given area at a given time interval:

$$A(t) = \sum_{\substack{i \in (t, t+\Delta t) \\ j \in (x-\Delta x, x+\Delta x)}} N_{i,j},$$

where $A(t)$ – AE activity, $N_{i,j}$ – number of pulses, Δt and Δx was taken as 1 sec and 10 mm consequently.

Results and discussion

In case of homogeneous and isotropic medium the diffusion equation has form (3). For the described experiments the initial condition can be written as:

$$p(x, 0) = p_0$$

A constant fluid rate Q at the inlet end of the cell and constant pressure at the outlet end are taken as boundary conditions:

$$\frac{\partial p(0,t)}{\partial x} = -a, \quad p(1,t) = p_0$$

In that case, the solution of the one-dimensional diffusion equation can be written as:

$$p(x,t) = p_0 + a(1-x) - 2a \sum_{i=0}^{\infty} \frac{e^{-\mu_i^2 Dt}}{\mu_i^2} \cos \mu_i x \quad (4)$$

where $\mu_i = \frac{\pi}{2} + \pi i$, $i \in \{0\} \cup N$, $D = \frac{k}{\mu_0 \beta m_0}$ and $a = \frac{Q \mu_0}{Sk}$.

The solution is plotted in Figure 3 as a variation of the pressure with time at one point in comparison with experimental data. The significant discrepancy between analytical and experimental results can be diminished by taking into account higher compressibility of the saturated porous sample due to presence of small amount of residual gas (not more than 0.1%) and permeability inhomogeneity along the cell (Fig. 2).

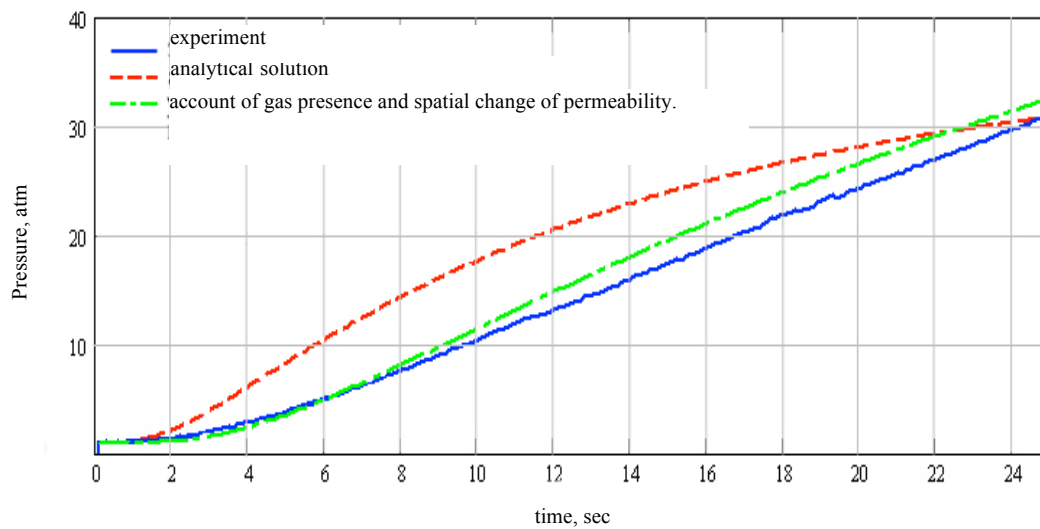


Figure 3: Comparison of analytical and experimental curves of pore pressure vs. time during water injection.

Pore pressure change leads to an increase of effective stresses, which results in fracturing and acoustic pulses. The model of the fracturing process can be based on two suggestions (Shapiro et al. 2002, Delépine et al., 2004):

- a fracture appears when the pore pressure reaches critical threshold value;
- the critical value spatial distribution can be described by some distribution.

In case of pore pressure decrease in the sample under external load, a difference between the external load and the pore pressure is considered as the critical value.

One can suggest that critical pore pressure distribution has one of the following forms:

normal distribution
$$N(p^*) = \frac{1}{\sigma\sqrt{2\pi}} e^{-\frac{(p^*-M)^2}{2\sigma^2}};$$

Weibull distribution, which is used for description of fractured rock fragment size

distributions
$$N(p^*) = ba^{-b} (p^*)^{b-1} e^{-\left(\frac{p^*}{a}\right)^b};$$

Log-normal distribution, which can be used to describe repeatedly crashed rock

fragments distribution
$$N(p^*) = \frac{1}{p^* \sigma \sqrt{2\pi}} e^{-\frac{(\ln p^* - \mu)^2}{2\sigma^2}},$$

where M, σ, a, b, μ are the distribution parameters.

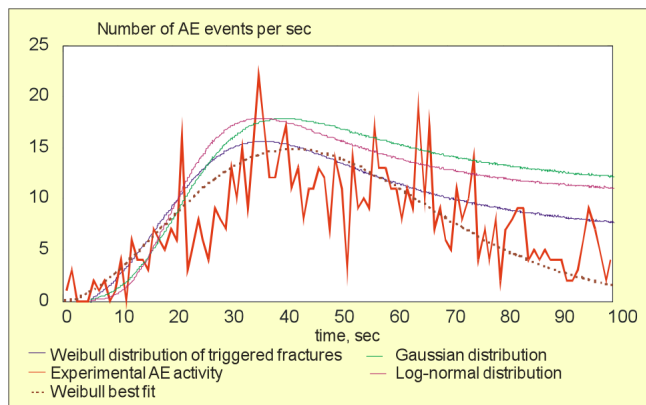


Figure 4: Comparison of experimental data on AE activity variations during pore pressure increase with mean AE activity calculated in accordance with several distributions of critical pore pressure.

At a particular distance from the injection point for each time interval the pore pressure range was taken from solution (4), and the number of the sample points for which the critical pressure values fall in this pore pressure range was calculated in accordance with one of the above distributions. The number of such points was taken as mean AE activity. Parameters of distributions were calculated to provide the best correspondence between experimental and analytical AE variations. The mean value of Gaussian error

function was found to be equal to 7-9 MPa, which is less by 1-2 MPa than the external vertical load. The standard deviation of Gaussian distribution was found to be 3 MPa. Parameters of Weibull distribution a and b were found to be equal to 7-9 MPa and 3.4, parameters of Log-normal distribution were 4.5 and 0.2.

The example of experimental AE activity change in time and its mean value variations calculated as described above are shown in Fig. 4. The comparison of experimental and theoretical curves shows that the Weibull distribution looks to be the best one among considered critical pore pressure distributions.

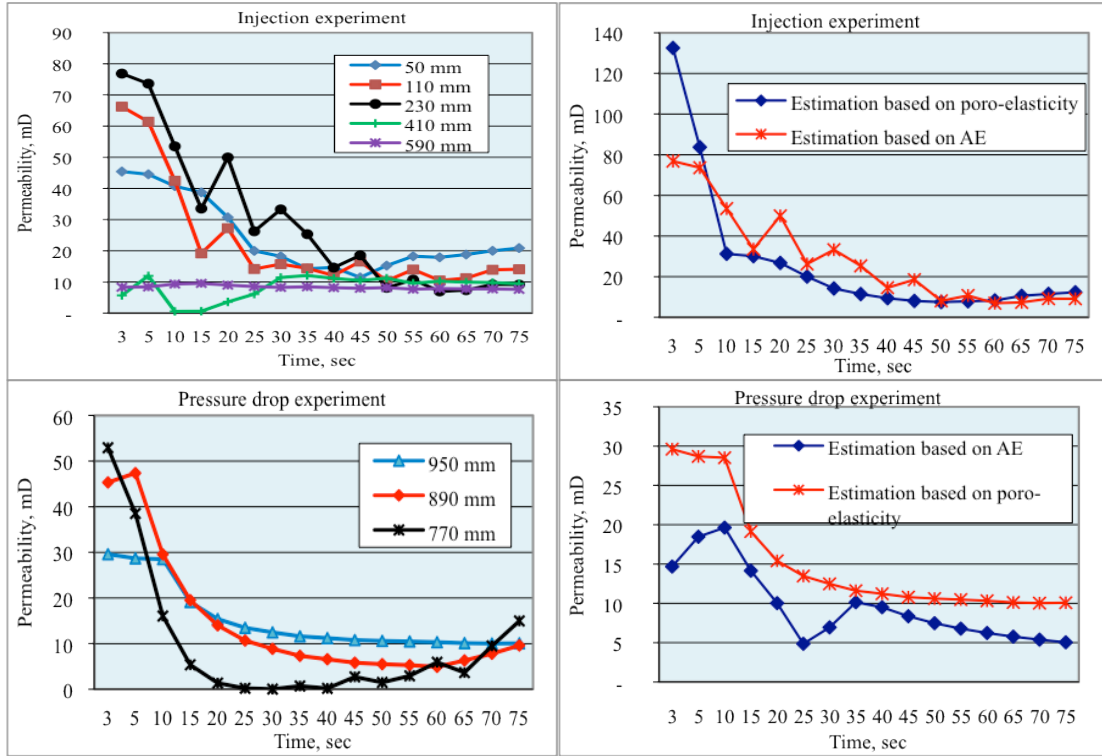


Figure 5: Permeability variations calculated at several points along the sample using poro-elastic equation (left graphs); comparison of permeability calculation based on poro-elastic equation with estimation by AE activity (right graphs) in injection and pressure drop experiments. The distance from injection point is shown.

If we use scaled Weibull distribution in probability density form

$$N(t) = N^* b t^{-1} \left(\frac{t}{t_0} \right)^b e^{-\left(\frac{t}{t_0} \right)^b} \quad (5)$$

to fit directly the experimental data shown in Fig. 4, we will get very good agreement between mean experimental data and Weibull distribution.

From poro-elastic equation we know relation between pressure p and time t , permeability can be considered as a parameter of the relation. From the other hand we know the relation between pore pressure and the number of triggered fractures, which means AE activity. So one can numerically estimate permeability k for each time, provided that the pore pressure and the number of triggered events are known. The procedure was the following:

1. AE activity variation in time was measured for each position of the AE sensors along the cell, as it was described above.
2. It was suggested, that critical pore pressure was distributed under Weibull distribution, so the number of triggered AE pulses could be estimated as

$$N(t) = b a^{-b} p^{b-1} e^{-\left(\frac{p}{a} \right)^b},$$

where $p=p(t)$ is the pore pressure variation measured at point of AE sensor location. Coefficients a and b were chosen to best fit experimental data on AE activity variation. It was found that value of coefficient a is approximately equal to

mean value of pore pressure, coefficient b is near 3.5 in injection experiments and near 6 in pressure drop experiments.

3. Then we use theoretical dependence of pore pressure on time (4) to re-calculate mean value of $N(t)$.
4. After that, we set re-calculated $N(t)$ equal to best fit (5) and calculated permeability from obtained equation for each time.

From the other hand, one can estimate the permeability from data on pore pressure gradient and pore pressure time derivative from diffusion equation (2) in one-dimensional form.

The results of the permeability change estimations based on diffusion equation and on AE mean value variations are shown in Fig. 5. It is interesting that an increase of the pore pressure leads to a significant increase of the permeability, but then the permeability diminishes to a value that is characteristic for stationary flow. The time of relaxation is near one minute. One can see that permeability calculation based on diffusion equation and estimation based on AE variations gives close results.

Conclusions

It was found, that if one calculates pore pressure change in accordance with diffusion equation, the results will be in good agreement with experimental data, provided that one takes into account real compressibility and unhomogeneity of the medium.

The mean AE activity variation can be described as triggering process controlled by pore pressure change and change of the number of potential fractures, which can be activated by the pore pressure change. It was found, that distribution of these “potential fractures” can be approximated by Weibull distribution.

It was shown that it is principally possible to resolve an inverse problem of defining local permeability by registering microseismic activity change in particular volume of porous medium.

Acknowledgements

The authors wish to acknowledge the generous support of Russian Foundation for Basic Research (RFBR project # 10-05-00638).

References

- Adushkin V.V., and Turuntaev, S.B. (2005). Man-made processes in the Earth Crust (dangerous and catastrophic events). Moscow, INEK-IDG RAS (in Russian).
- Delépine N., Cuenot N., Rothert E., Parotidis M., Rentsch, S., and Shapiro, S. (2004). Characterization of fluid transport properties of the Hot Dry Rock reservoir Soultz-2000 using induced microseismicity: *Journal of Geophysics and Engineering*, **1**, 77-83.

Articles

- Rothert, E. and Shapiro, S. A. (2007). Statistics of fracture strength and fluid-induced microseismicity, *Journal of Geophysical Research*, 112, B04309, doi:10.1029/2005JB003959.
- Schelkatchev, V.N. (1995). *Fundamentals and applications of nonstationary filtration theory*: Moscow, Neft i gaz (in Russian).
- Shapiro, S. A., Rentsch, S., and Rothert, E. (2005). Characterization of hydraulic properties of rocks using probability of fluid-induced microearthquakes: *Geophysics*, **70**, F27-F34.
- Shapiro, S. A., Rothert, E., Rath, V., and Rindschwentner, J. (2002). Characterization of fluid transport properties of reservoirs using induced microseismicity: *Geophysics*, **67**, 212–220.

Occurrence probability and earthquake size of post shut-in events in geothermal projects

Friedemann Wenzel¹, Andreas Barth¹, Cornelius Langenbruch², and Serge A. Shapiro²

¹ Karlsruhe Institute of Technology, Geophysical Institute, Hertzstr. 16, 76187 Karlsruhe, Germany, friedemann.wenzel@kit.edu, a.barth@kit.edu

² Freie Universität Berlin, Fachrichtung Geophysik, Malteserstr. 74-100, 12249 Berlin, Germany, cornelius@geophysik.fu-berlin.de, shapiro@geophysik.fu-berlin.de

Abstract

In recent geothermal projects that were associated with induced seismicity it has been observed that the largest earthquake or earthquakes occurred after shut-in, the moment when the pressurised fluid injection in the borehole is stopped. We use a probabilistic approach based on Omori's law and a Gutenberg-Richter magnitude distribution to demonstrate that the probability of exceeding a certain maximum magnitude after shut-in is as high or higher than before stopping the fluid injection. The amount of this increase is dependent on the exponent of Omori's law q . For the reference case of $q=2$ and a 10% probability at shut-in time t_s we obtain an increase to 14.6% for $t = 2t_s$. If we consider a constant probability level of occurrence for an event larger than a given magnitude at shut-in time, this maximum magnitude increases by 0.12 units for $t = 2t_s$. For the Fenton Hill experiment recent studies reveal $q=7.5$ that corresponds to only a small amount of probability increase for the post-injection phase.

Introduction

It is known that fluid injections at geothermal sites, which are performed to develop the reservoirs, can induce low magnitude earthquakes in critically stressed zones of the surrounding rock. Even after shut-in, that is, after the pressurised fluid injection into the borehole is stopped, a significant number of seismic events can occur. The understanding, characterisation, and forecasting of post-injection events is particularly important, because during recent geothermal projects such as Soultz-sous-Forêts (Charl  ty et al., 2007), Basel (H  ring et al., 2008), and Landau it has been observed that the largest earthquakes tend to occur after shut-in. This makes it still more difficult to control such events. Those earthquakes have had a large impact in society and understanding their temporal occurrence was identified as one major goal of geothermal research (Mayer et al., 2007). There is speculation that the largest earthquakes are therefore causally related to the shut-in as if the stop of injection would lead to the larger earthquake. However, recent findings from Langenbruch & Shapiro (2010a) suggest that the presence of unstable pre-existing fractures may increase the seismicity rate and thus the probability of exceeding a certain magnitude even after stopping injection.

We demonstrate in this paper (a) that the largest earthquakes should occur after the shut-in of injection in the context of the ‘‘Seismicity Based Reservoir Characterization Theory (SBRC)’’; (b) that even larger earthquakes have to be expected, if injection would be continued; (c) that the largest expected magnitude can be estimated. All three statements apply in a probabilistic sense only.

Theory

There are two fundamental laws in statistical seismology, namely the Omori law, which describes the decay rate of aftershock activity after tectonically driven earthquakes, and the Gutenberg-Richter relation describing the frequency magnitude distribution of earthquakes. It was observed and verified in recent works that both fundamental laws are also valid in the context of injection-induced seismicity (Shapiro et al., 2007; Langenbruch & Shapiro, 2010a).

We describe the fluid injection by a point source in a permeable fluid-saturated medium with pre-existing fractures and assume that the fluid is liberated from this source with constant strength until the shut-in time t_s .

According to Shapiro et al. (2007) this leads to a constant seismicity rate \bar{v}_1 for earthquakes with magnitudes larger than some lower threshold value m_1 . For another magnitude M the Gutenberg-Richter earthquake size distribution suggests a constant seismicity rate \bar{v}_M :

$$\bar{v}_M = \bar{v}_1 \cdot 10^{-b(M-m_1)}. \quad (1)$$

In general, the behaviour of seismicity triggering in space and time is controlled by the relaxation process of stress and pore pressure perturbation that was initially created at the injection source. This relaxation process can be approximated by linear pressure diffusion in the pore fluid of rocks. Following the Mohr-Coulomb failure criterion the resulting increase in pore pressure can lead to rock failure along pre-existing, sub-critically stressed cracks. If critical pore pressures leading to reactivation of individual pre-existing fractures are equally distributed between a lower bound $C_{min}=0$ Pa and a maximum value C_{max} larger than the overpressure between source and reservoir, Omori's law can be utilised to describe the decay rate of seismic activity after shut-in of injection in the following modified form (Langenbruch & Shapiro, 2010a):

$$v_1(t) = \bar{v}_1 \cdot \left(\frac{t_s}{t} \right)^q, \quad (2)$$

with the constant seismicity rate \bar{v}_1 during injection, time $t \geq 0$ from injection start, the shut-in time t_s , and the exponent q between 1 and 2. Recently the analysis of seismicity data from geothermal projects suggests even higher values for q (Langenbruch & Shapiro, 2010a; see below).

We assume that the induced earthquakes represent a Poisson process (Shapiro et al., 2010; Langenbruch & Shapiro, 2010b). If the seismicity rate is constant the Poisson process is called homogeneous. The probability that no earthquake in excess of M occurs between the initiation of injection and some time t can be written as

$$P_0(M, t) = \exp(-\bar{v}_M \cdot t) = \exp\left(-\bar{v}_1 \cdot 10^{-b(M-m_1)}\right) = \exp\left(-\bar{v}_1 \cdot \exp^{-\beta(M-m_1)}\right), \quad (3)$$

with $\beta = b \cdot \ln 10 \approx 2.3 \cdot b$. The distribution is of Gumbel type, which is not surprising as we look for the extreme value of $\bar{v}_M \cdot t$ earthquakes.

If the Poisson process varies with time it becomes inhomogeneous. The probability that no earthquake in excess of M occurs between the initiation of injection and some time t can be written as

$$P_0(M, t) = \exp\left(-\int_0^t v_M(\tau) d\tau\right). \quad (4)$$

For the shut-in time we get for the probability that magnitude M is not exceeded between time 0 and t_s :

$$\ln \frac{1}{P_0(M, t_s)} = \bar{v}_M \cdot t_s. \quad (5)$$

Using the decaying seismicity rate for the time after shut-in $t \geq t_s$ we get

$$\ln \frac{1}{P_0(M, t)} = \bar{v}_M \cdot t_s + \int_{t_s}^t v_M(\tau) d\tau = \bar{v}_M \cdot t_s \cdot \left(1 + \frac{1}{q-1} - \frac{1}{(q-1) \cdot (t/t_s)^{q-1}}\right). \quad (6)$$

Thus it is clear that the probability P_0 of not exceeding magnitude M is still decreasing after shut-in. If the injection is not shut off but continues some time beyond ($t \geq t_s$) we have the trivial relation

$$\ln \frac{1}{P_0(M, t)} = \bar{v}_M \cdot t_s \cdot \left(1 + \frac{t-t_s}{t_s}\right) = \bar{v}_M \cdot t. \quad (7)$$

Hence the probability to exceed magnitude M (that is $1 - P_0$) still increases after shut-in. Let us give an example (Fig. 1): If the probability to exceed magnitude M at the time of the shut-in is given by $1 - P_0 = 10\%$, this probability increases to $1 - P_0 = 14.6\%$ considering all events occurring until $t = 2t_s$ and an exponent of $q=2$ (eq. 6). For $q=1.5$ the above probability changes to $1 - P_0 = 15.4\%$. The corresponding value for a on-going injection is: $1 - P_0 = 19\%$ (eq. 7).

For $q=1$, first the limit of $q-1$ decreasing to zero has to be evaluated (see appendix):

$$\lim_{q \rightarrow 1} P_0(M, t \geq t_s) = \exp\left(-\bar{v}_M t_s \cdot (1 + \ln(t/t_s))\right). \quad (8)$$

For $t = 2t_s$ it follows that $1 - P_0 = 16.3\%$. However, this theoretical limit of q is not expected in nature.

Next we study how the probabilistically determined largest earthquake changes in magnitude given a constant probability level of occurrence. We assume a 50% chance that no earthquake larger than M_s occurs:

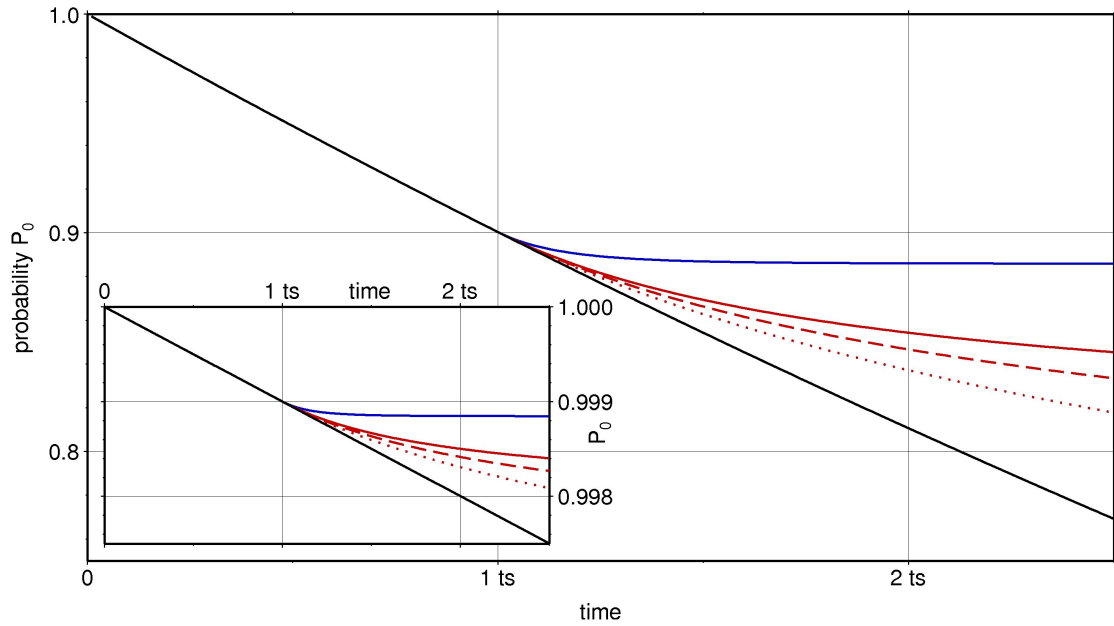


Figure 1. Probability P_0 of not exceeding a maximum magnitude M with time (shut-in time t_s). The solid black line corresponds to continued injection. Other lines show P_0 after shut-in for different q -values: $q=1$ (dotted red), $q=1.5$ (dashed red), $q=2$ (solid red), and as obtained for the Fenton Hill dataset $q=7.5$ (solid blue). Main graph: $P_0(t_s)=90\%$, inset $P_0(t_s)=99.9\%$.

$$\ln \frac{1}{P_0(M_s, t_s)} = \bar{v}_{M_s} \cdot t_s = \bar{v}_1 \cdot 10^{-b(M_s - m_1)} \cdot t_s = \ln \frac{1}{0.5} \approx 0.7. \quad (9)$$

From this M_s can be calculated if \bar{v}_1 and b are known. Keeping the probability level constant – in our example 50% – we can ask how would the maximum magnitude increase beyond M_s if we (a) continue injection until $t \geq t_s$ and (b) stop injection and wait until $t \geq t_s$.

The general implicit formula for both cases is

$$P_0(M_s, t_s) = P_0(M_s + \Delta M, t). \quad (10)$$

In case (a) we get after some manipulations:

$$\Delta M = \frac{1}{b} \log(t/t_s). \quad (11)$$

Thus we have a 50% chance that no earthquake larger than M_s occurs until t_s and if we then extend the injection time from t_s to $t = 2t_s$ we have a 50% chance to get no earthquake larger than

$$M_s + \Delta M = M_s + \frac{1}{b} \log(2) \approx M_s + \frac{0.3}{b} \approx M_s + 0.2, \quad (12)$$

assuming a b -value of 1.5. The general shut-in case leads to

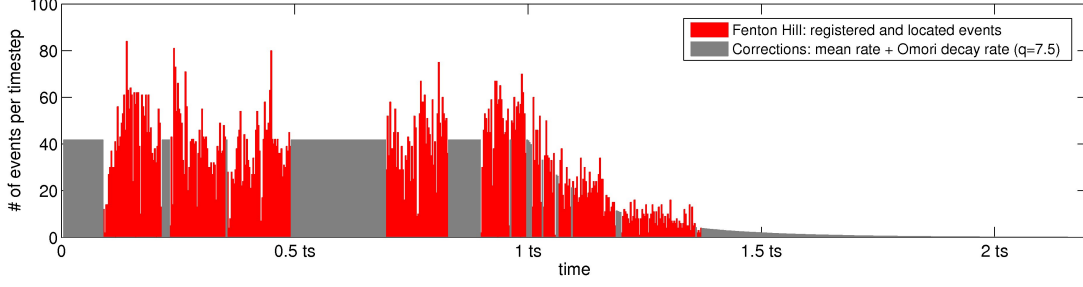


Figure 2. Temporal development of seismicity in the Fenton Hill geothermal project. Grey areas show the mean rate before shut-in time t_s for gaps in the observation due to a not operating monitoring system. After shut-in grey areas show the best fit for Omori's law with $q=7.5$.

$$\Delta M = \frac{1}{b} \log \left(1 + \frac{1}{q-1} - \frac{1}{(q-1) \cdot (t/t_s)^{q-1}} \right). \quad (13)$$

For the reference value of $q=2$ and again $t = 2t_s$, we find

$$\Delta M = \frac{\log 1.5}{b} \approx 0.12. \quad (14)$$

With $q=1.5$ this changes to

$$\Delta M = \frac{\log 1.6}{b} \approx 0.14. \quad (15)$$

For the lower value of $q=1$ the limit of equation 13 has to be evaluated:

$$\lim_{q \rightarrow 1} \Delta M = \frac{1}{b} \log \left(\lim_{q \rightarrow 1} \left(1 + \frac{1}{q-1} - \frac{1}{(q-1) \cdot (t/t_s)^{q-1}} \right) \right). \quad (16)$$

With the results from above it follows:

$$\lim_{q \rightarrow 1} \Delta M = \frac{1}{b} \log \left(1 + \ln(t/t_s) \right). \quad (17)$$

For the $b=1.5$ and $t = 2t_s$ given above that is

$$\lim_{q \rightarrow 1} \Delta M \approx 0.152. \quad (18)$$

Fenton Hill

We apply the above theory to real data that was recorded during the Fenton Hill (New Mexico, USA) Hot Dry Rock injection experiment in 1983 (House, 1987). After 62 h the injection was stopped and the seismic monitoring went on for 23 h, i.e. $t/t_s = 1.4$. Figure 2 shows the temporal evolution of the observed seismicity. Gaps in the monitoring are filled in with the mean seismicity rate before shut-in. The decay of seismicity for the post-injection phase can be well approximated by the modified Omori law. A value of $q=7.5$ results in the best fit to the observed post-injection

seismicity. Highly unstable fracture systems result in low q -values and a high seismicity rate close before and after the shut-in. This may also be the reason for large magnitude events close before or after shut-in. With increasing stability of the fracture system the q -value increases (Langenbruch & Shapiro, 2010a). We use the value of $q=7.5$ to calculate the probability P_0 of not exceeding magnitude M_S . Assuming $P_0 = 99.9\%$ at shut-in time, P_0 becomes 99.88% for $t = 2t_s$ (eq. 6, see Fig. 1).

Conclusion

We have shown that based on a modified Omori law and a Gutenberg-Richter distribution the probability P_0 of not exceeding a maximum magnitude during injection and after its termination can be determined. The decay of seismicity after shut-in and thus P_0 strongly depends on the exponent q of the modified Omori law. Two characteristic values have been calculated for the post-injection phase and the case of an on-going injection: (a) the continuing decrease of P_0 and (b) the increase of the maximum magnitude given a constant probability level of occurrence. For (a) we find an increase of $1 - P_0$, i.e. the probability of exceeding a maximum magnitude, from a given value of 10% at shut-in time t_s to 14.6% for time $t = 2t_s$ ($q=2$). At the same time a continued injection would result in $1 - P_0 = 19\%$. The maximum magnitude (b) thus increases for $t = 2t_s$ by 0.2 for continued injection and 0.12 for the shut-in case (that corresponds to an increase of seismic energy by a factor of 1.5). Thus for low probabilities to exceed the maximum magnitude at shut-in time and a high q -value only a small increase in the risk is to be expected, while higher probabilities in combination with lower q -values result in a significant enlargement of the probability of exceeding the magnitude threshold.

Acknowledgements

We thank Adrien Oth for his constructive and detailed remarks to improve the manuscript.

Appendix

For the evaluation P_0 for $q=1$, we substitute $r=q-1$:

$$\lim_{r \rightarrow 0} P_0(M, t \geq t_s) = \exp \left(-\bar{v}_M t_s \cdot \left(1 + \lim_{r \rightarrow 0} \left(\frac{1}{r} - \frac{1}{r \cdot (t/t_s)^r} \right) \right) \right). \quad (\text{A1})$$

With

$$\lim_{r \rightarrow 0} \left(\frac{1}{r} - \frac{1}{r \cdot (t/t_s)^r} \right) = \lim_{r \rightarrow 0} \frac{1 - (t/t_s)^{-r}}{r} \quad (\text{A2})$$

and applying L'Hôpital's rule

$$\lim_{x \rightarrow 0} \frac{f(x)}{g(x)} = \lim_{x \rightarrow 0} \frac{f'(x)}{g'(x)}, \quad (\text{A3})$$

it follows:

$$\lim_{r \rightarrow 0} \frac{1 - (t/t_s)^{-r}}{r} = \lim_{r \rightarrow 0} (t/t_s)^{-r} \cdot \ln(t/t_s) = \ln(t/t_s) \quad (\text{A4})$$

and

$$\lim_{r \rightarrow 0} P_0(M, t \geq t_s) = \exp(-\bar{v}_M t_s \cdot (1 + \ln(t/t_s))). \quad (\text{A5})$$

References

- Charl ty, J., Cuenot, N., Dorbath, L., Dorbath, C., Haessler, H. & Frogneux, M. (2007). Large earthquakes during hydraulic stimulations at the geothermal site of Soultz-sous-For ts. *Int. J. Rock Mech. Min.*, 44, 1091-1105.
- H ring, M. O., Schanz, U., Ladner, F. & Dyer, B. C. (2008). Characterisation of the Basel 1 enhanced geothermal system, *Geothermics* 37, 5, Pages 469-495, doi: 10.1016/j.geothermics.2008.06.002.
- House, L. (1987). Locating microearthquakes induced by hydraulic fracturing in crystalline rocks. *Geophys. Res. Lett.*, 14, 919–921.
- Langenbruch, C. & Shapiro, S. A. (2010a). Decay Rate of Fluid Induced Seismicity after Termination of Reservoir Stimulations. *Geophysics*, Geo-2009-0404 (accepted).
- Langenbruch, C. & Shapiro, S. A. (2010b). Inter Event Times of Fluid Induced Seismicity. Extended abstract F022, 72nd EAGE Conference & Exhibition
- Majer, E. L., Baria, R., Stark, M., Oates, S., Bommer, J., Smith, B. & Asanuma, H. (2007). Induced seismicity associated with Enhanced Geothermal Systems. *Geothermics*, 36, 185-222.
- Shapiro, S. A., Dinske, C. & Kummerow, J. (2007). Probability of a given-magnitude earthquake induced by a fluid injection. *Geophys. Res. Lett.*, 34. doi:10.1029/2007GL031615.
- Shapiro, S. A., Dinske, C., Langenbruch, C. & Wenzel, F. (2010). Seismogenic index and magnitude probability of earthquakes induced during reservoir fluid stimulations. *The Leading Edge*; March 2010, 29/3, 304-309, doi: 10.1190/1.3353727

Table of Contents

FOREWORD		III
PROGRAM		V
LIST OF PARTICIPANTS		XI
SECTION I – ABSTRACTS		1
SECTION II – ARTICLES		61
1	Braun, T., J. Heinicke, and T. Dahm <i>The difficulty to distinguish natural and human related seismicity in a complex tectonically active area</i>	63
2	Dahm, T., S. Hainzl, D. Becker, and the FKPE DINSeis group <i>How to discriminate induced, triggered, and natural seismicity</i>	69
3	Fischer, T., and A. Guest <i>Tensile earthquakes: view of seismology and geomechanics</i>	77
4	Groos, J., and J. Ritter <i>Seismic noise: A challenge and opportunity for seismological monitoring in densely populated areas</i>	87
5	Moldoveanu, T., K.-P. Bonjer, and M. Pecingine <i>Aspects concerning seismicity analyses of the Vidraru-Arges (Romania) dam area</i>	99
6	Oye, V., H. N. Gharti, D. Kühn, and A. Braathen <i>Microseismic monitoring of fluid injection at the Longyearbyen CO₂-Lab, Svalbard</i>	109
7	Shapiro, S. A., C. Dinske, C. Langenbruch, F. Haney, J. Kummerow, and F. Wenzel <i>Towards quantifying the seismogenesis of fluid injections in rocks</i>	115
8	Turuntaev, S. B., E. I. Eremeeva, and E. V. Zenchenko <i>Laboratory study of temporal-spatial peculiarities of microseismicity spreading due to pore pressure change</i>	123
9	Wenzel, F., A. Barth, C. Langenbruch, and S. A. Shapiro <i>Occurrence probability and earthquake size of post shut-in events in geothermal projects</i>	131

Déjà parus

- Vol 1:** Seismic Networks and Rapid Digital Data Transmission and Exchange (1990)
- Vol 2:** GPS for Geodesy and Geodynamics (1990)
- Vol 3:** Non Tidal Gravity Changes: Intercomparison between Absolute and Superconducting Gravimeters (1991)
- Vol 4:** Geodynamical Instrumentation Applied to Volcanic Areas (1991)
- Vol 5:** Local and National Seismic Networks: On Line Data Processing with Microcomputer Facilities (1992)
- Vol 6:** Application of Artificial Intelligence Techniques in Seismology and Engineering Seismology (1992)
- Vol 7:** European Macroseismic Scale 1992 (1993)
- Vol 8:** New Challenges for Geodesy in Volcanoes Monitoring (1995)
- Vol 9:** Dynamical Systems and Artificial Intelligence Applied to Data Banks in Geophysics (1995)
- Vol 10:** Accurate Orbit Determination and Observations of High Earth Satellites for Geodynamics (1995)
- Vol 11:** Non Tidal Gravity Changes: Intercomparison between Absolute and Superconducting Gravimeters (1995)
- Vol 12:** Application of Artificial Intelligence Techniques in Seismology and Engineering Seismology (1996)
- Vol 13:** Historical Seismic Instruments and Documents: a Heritage of Great Scientific and Cultural Value (1997)
- Vol 14:** Short Term Thermal and Hydrological Signatures Related to Tectonic Activities (1997)
- Vol 15:** European Macroseismic Scale (1998)
- Vol 16:** Geodynamical Hazards Associated with Large Dams (1998)
- Vol 17:** High Precision Gravity Measurements with Application to Geodynamics and Second GGP Workshop (2000)
- Vol 18:** Evaluation of the Potential For Large Earthquakes in Regions of Present Day Low Seismic Activity in Europe (2001)
- Vol 19:** L'Echelle Macrosismique Européenne 1998 New (version française) (2001)
- Vol 20:** Analytical Representation of Potential Field Anomalies for Europe (2003)
- Vol 21:** Escala Macrosismica Europea 1998 (spanish version) (2003)
- Vol 22:** IMG 2002- Instrumentation and Metrology in Gravimetry (2003)
- Vol 23:** The State of GPS Vertical Positioning Precision: Separation of Earth Processes by Space Geodesy (2004)
- Vol 24:** Forcing of Polar Motion in the Chandler Frequency Band: A Contribution to Understanding Interannual Climate Variations (2005)
- Vol 25:** GOCINA: Improving Modeling of Ocean Transport and Climate Prediction in the North Atlantic Region Using GOCE Gravimetry (2006)
- Vol 26:** International Comparison of Absolute Gravimeters in Walferdange (Luxembourg) of November 2003 (2006)
- Vol 27:** Escala Macrosismica Europea 1998 (updated spanish version) (2009)
- Vol 28:** Seismicity Patterns in the Euro-Med Region (2009)
- Vol 29:** Active Volcanism and Continental Rifting (2010)

